Dynamic analysis of tapered circular discs made of isotropic and orthotropic materials using Rayleigh-Ritz method and ANSYS

Chirag Delvadiya

A thesis

in

the Department

of

Mechanical and Industrial Engineering

Presented in Partial Fulfillment of the Requirements

For the Degree of

Master of Applied Science (Mechanical Engineering) at

Concordia University

Montreal, Quebec, Canada

Sept 30

CONCORDIA UNIVERSITY
School of Graduate Studies

This is to certify that the thesis prepared

By: Chirag Kantilal Delvadiya

Entitled: Dynamic analysis of tapered circular discs made of isotropic and orthotropic materials using Rayleigh-Ritz method and ANSYS

and submitted in partial fulfillment of the requirements for the degree of

Master of Applied Science (Mechanical Engineering)

complies with the regulations of the University and meets the accepted standards with respect to originality and quality.

Signed by the final examining committee:

Dr. W.Ghaly Chair

Dr. J. Dargahi Examiner

Dr. L. Lin Examiner

Dr. R. Ganesan Supervisor

Approved by
Chair of Department or Graduate Program Director

Dean of Faculty

Date November 4, 2016

ABSTRACT

Dynamic analysis of tapered circular discs made of isotropic and orthotropic materials using Rayleigh-Ritz method and ANSYS

Tapered rotating circular disc provides advantages of preferred stress state compared to the uniform-thickness circular disc rotating at the same speed. Hence, linearly-tapered circular disc and circular disc with hyperbolic profile along radial direction, often known as Stodola's disc, are increasingly being used in many engineering applications such as in automobiles, turbomachinery, steam turbines, flywheels, and space structures. It is important to study the in-plane dynamics and out-of-plane dynamics of such circular discs as they play a vital role in causing vibration and noise. Design of circular disc for such applications also requires the knowledge of three-dimensional bending vibration characteristics of the disc. The present thesis aims at developing a generalized formulation and then to investigate the three-dimensional in-plane and out-of-plane vibration characteristics of uniform-thickness circular annular disc, linearly-tapered circular annular disc, and Stodola's disc with clamped-free boundary condition.

The trigonometric functions in circumferential coordinate are employed in all the three displacement components in Rayleigh-Ritz method to calculate the natural frequencies. The numerical approach based on Rayleigh-Ritz method with finite-element-like modification has been developed to study the free vibration behaviour of the tapered circular discs made of isotropic and orthotropic materials and of clamped-free boundary condition. Numerical and symbolic computations have been performed using MATLAB and MAPLE software. The results for natural frequencies have been validated using Finite Element Method using ANSYS and results from previous literature wherever available. A comprehensive parametric study is conducted to study the effects of various design parameters.

ACKNOWLEDGEMENTS

Firstly, I would like to dedicate this accomplishment to my parents, Mr. Kantilal Delvadiya and Mrs. Lalitaben Delvadiya. I want thank my brother Hardik for providing continuous moral support and my fiancée Krishna for her love, care, understanding and patience. I am blessed because you all love me.

Then, I am grateful to my thesis supervisor Professor Rajamohan Ganesan for his time, continuous support and valuable guidance provided during my research. I am grateful to receive the valuable suggestions from my supervisor during thesis writing period. His perfectionism has self-realized me lifelong learning. I gratefully acknowledge the funding sources for my research provided by NSERC and Concordia University.

Finally, I am thankful to my friends, Jignesh and Reynaldo, for the time we spent together.

Table of Contents

List of Figures

List of Tables

Nomenclature

Symbol	Description
Π	Total strain energy of disc
T	Total kinetic energy of disc
Π_{max}	Maximum strain energy of uniform thickness disc
T_{max}	Maximum kinetic energy of uniform thickness disc
ζ	Non-dimensional radius
ξ	Non-dimensional thickness
β	Radius ratio of disc
ς	Damping ratio
Ω	Non-dimensional frequency parameter of disc
Ω_{LT}	Frequency parameter of linearly-tapered disc
Ω_{LTo}	Frequency parameter of linearly-tapered orthotropic disc
ω	Circular natural frequency of disc
α	Mass-proportional damping coefficient
β_k	Stiffness-proportional damping coefficient
a	Ratio of outer radius to thickness
A_{ij}, B_{kl}, C_{pq}	Constant coefficients in assumed displacement polynomials in in r, θ and z directions respectively

u_r, u_θ, u_z	Displacements in r, θ and z directions respectively
U, V, W	Amplitudes of deformation in r, θ and z directions respectively
n	Nodal diameter number
C_{ij}	Elements of stiffness matrix
c_c	Critical damping
R_i	Inner radius of disc
R_o	Outer radius of disc
E	Modulus of elasticity
G	Modulus of rigidity
n_r, n_θ, n_z	Constraint functions in r, θ and z directions respectively
N	Numerator of equation of Rayleigh's quotient
D	Denominator of equation of Rayleigh's quotient
E_1	Modulus of elasticity in radial direction
E_2	Modulus of elasticity in circumferential direction
G_{12}	In-plane shear modulus
ρ	Density of isotropic material
ρ_o	Density of orthotropic material
v_{12}	Major Poisson's ratio
v_{21}	Minor Poisson's ratio

I, J	Upper limit of polynomial of radial direction
K, L	Upper limit of polynomial of circumferential direction
P, Q	Upper limit of polynomial of transverse direction
$(\Pi_{max})_{LT}$	Maximum strain energy of linearly tapered disc
$(\mathrm{T}_{max})_{LT}$	Maximum kinetic energy of linearly tapered disc
h_{mid}	Mid-point thickness of tapered disc
h_o	Outer thickness of tapered disc
h_i	Inner thickness of tapered disc
s	Taper parameter of Stodola's disc
$(\Pi)_{rot}$	Strain energy of rotating Stodola's disc
$(\mathrm{T})_{rot}$	Kinetic energy of rotating Stodola's disc
$\bar{n}$	Degree of orthotropy

Chapter 1

Introduction

1.1 General

Rotating and non-rotating circular discs of uniform thickness and/or with linear and non-linear thickness variations have many engineering applications such as automobiles, turbomachinery, planetary gear box, steam turbines, flywheels, space structures, etc. Moreover, in some of the applications, the circular discs of non-linear thickness variations provide certain advantages compared to the uniform thickness or linearly-tapered profiles. The rotating discs of non-linear thickness variations are well studied in terms of the stresses generated due to rotational effect and proved to be advantageous compared to the stressed state of rotating discs of uniform thickness.

Modal analysis of any structural component is performed in order to determine the natural frequencies and associated mode shapes at the design stage. Moreover, the modal analysis provides the basis for further detailed dynamic analysis such as transient analysis, harmonic analysis, etc. For designing the circular disc for specified application, knowledge of in-plane mode vibrations and out-of-plane mode vibrations is essential.

In the automotive application of thick circular disc as a disk brake, it is observed that sound radiates from disc effectively when the disc is vibrating at lowest bending mode natural frequency [1]. Hence, it is important to study the bending mode vibration. Moreover, frictional stresses over the disc serve as external forces and excite in-plane, out-of-plane and coupled modes of vibrations. Due to the friction between rotor and braking pads, the upper surface of the rotor (i.e. circular disc) wears out with the passage

of time due to friction between them, which indeed depends on the material capabilities of the rotor (i.e. wear resistance and heat resistance). As a result, slight taper is observed at the top rotor side, which can be dealt as tapered circular disc and as a consequence dynamic response of the same is changed (in most cases, natural frequency of the structure is increased because of the taper), which disturbs the initially investigated design parameters of the uniform thickness rotor and results in higher vibration of car at higher speed. This is the reason behind the to-and-fro motion of an old car when one applies the brake or one drives it at higher speed. Hence, out-of-plane vibration response of the thick tapered circular clamped-free disc with respect to rotational speed should be studied well in advance in order to increase the robustness in design. In any application, if this aspect isn't studied properly, severe vibrations occur which result in the fatigue failure. Therefore, studying the dynamic behaviour of the thick discs is one of the major research interests of the researchers.

Consider the application of the thick circular disc in railway wheels, where the lowest in-plane mode and the lowest out-of-plane mode vibrations are to be studied at the preliminary design stage. Although there are many factors responsible for the noise generation during operation of rail-wheel, a significant reduction in the noise can be achieved by minimizing bending mode vibration frequency of the disc [2] (if the rail-wheel is modelled as circular tapered clamped-free disc).

The following Figures 1.1 and 1.2 show the application of circular discs of clamped-free boundary condition in turbomachinery and automobile.

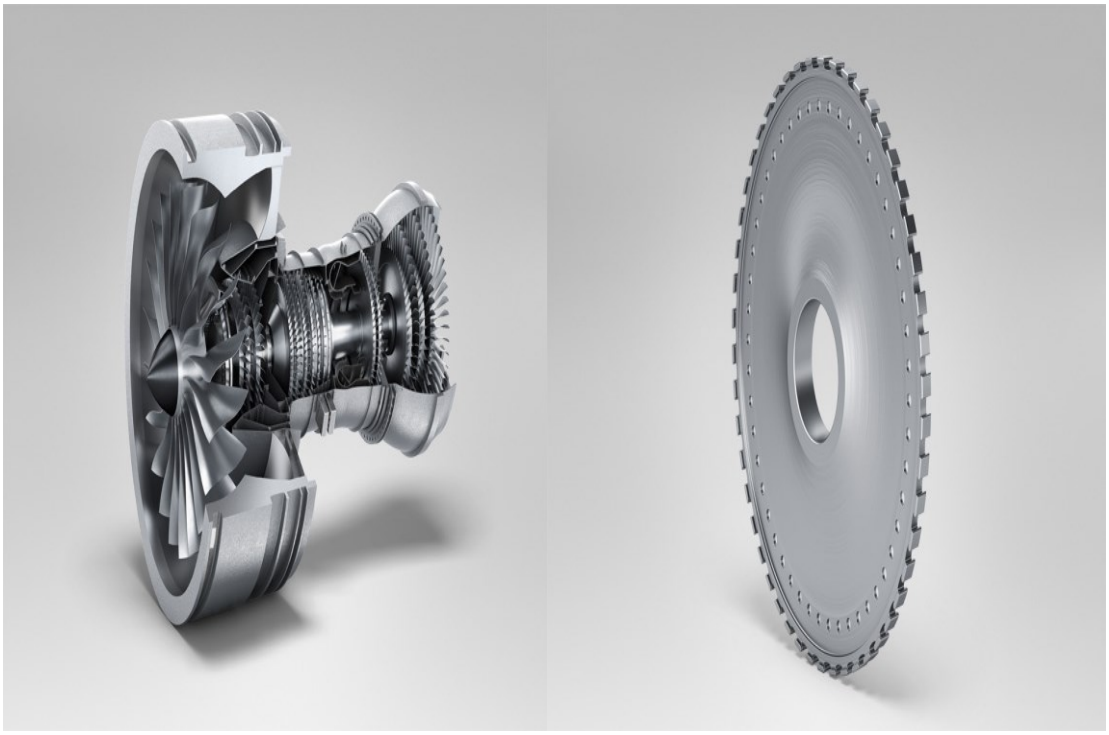

Figure 1.1: Application of non-linearly tapered circular disc in turbomachinery [3]

Figure 1.2: Application of uniform thickness circular disc in automobile [4]

1.2 Three-dimensional vibration analysis in mechanical design

In actual practice, the critical structural components used for various industrial applications may be modelled as specific structural elements such as bar, rod, beam, plate or shell, based on their size/shape characteristics. Researchers have developed various theories with suitable initial assumptions to study the dynamic behaviour of such structural elements. For the realistic dynamic analysis of certain problems like thick beams, thick pressure vessels, thick circular discs in turbomachinery or in automotive applications, one should go for three-dimensional analysis. Further, the advantage of developing three-dimensional elasticity problem is that it can be applied to any structural element irrespective of the size/shape of the structural element.

Furthermore, in many cases, the exact or closed-form solutions to such problems are not available. Nowadays, modern three-dimensional finite element solutions are available but to achieve accurate results they can't justify the time and computational costs involved in the project. Therefore, researchers always seek accurate and efficient three-dimensional Rayleigh-Ritz approximate solutions or two-dimensional approximate solutions based on the criticality of the problem. In the three-dimensional dynamic analysis, there are no kinematic constraints imposed upon the displacements of middle surface unlike the case of classical one-dimensional or two-dimensional plate theories. To solve such three-dimensional elasticity problem, various approximate methods are widely used which are discussed in the following Section 1.3.

It is possible to solve the structural dynamics problem with the breakdown of the assemblies and subassemblies partially and applying the structural dynamic analysis and testing procedures. Modal analysis is one of them and of course the root of all the advanced dynamic analysis procedures. Modal analysis can be performed with the

analytical techniques or experimental techniques. By carrying out analysis, we describe the structure in terms of its natural characteristics such as natural frequencies and associated mode shapes and damping.

1.3 Hamilton's principle and approximate methods

In many cases, it is cumbersome to describe the physical system by applying Newton's law, especially when the forces acting on the system are uncertain. Trying to describe such a system in terms of Newton's equations of motion requires the estimation of the total force, which does not seem feasible always. In such cases, the system can be easily described by equations of motion derived by applying Hamilton's principle.

Hamilton's principle can be stated as follows:

$$\delta \int_{t_1}^{t_2} L \, dt = 0 \tag{1.1}$$

where $L = T - W$ is the Lagrangian function. Here, T is the kinetic energy of the system and W is the strain energy of the system under consideration. The above integral is often known as "action integral". It states that the variation of integral of Lagrangian from time t_1 to t_2 is zero provided that variations of displacements are zero at t_1 and t_2.

1.3.1 Rayleigh-Ritz method

Walter Ritz has developed the method that is an extension of Rayleigh's method, known as Rayleigh-Ritz method. It provides a better approximation for the fundamental natural frequency. To use this method, it is necessary to represent the deformed shape of the structure by series of shape functions multiplied by the constant coefficients. We know that by taking a finite number of terms in a polynomial, we impose a certain limitation on the possible shapes of the deflection of the structure. Therefore, the

frequencies calculated using a finite number of terms in Rayleigh-Ritz polynomial often overestimate the values of natural frequencies compared to their exact solutions.

Let $\Phi_1(x), \Phi_2(x), ..$ be a series of functions $\Phi_j(x)$ that suitably represent X, the deformed shape of the structure under consideration and also satisfy the boundary conditions. Then we have,

$$X = \mathrm{a}_1\Phi_1(x) + \mathrm{a}_2\Phi_2(x) + \cdots + \mathrm{a}_j\Phi_j(x) \tag{1.2}$$

where, $\mathrm{a}_1, \mathrm{a}_2..$ are constant coefficients.

From the principle of conservation of energy, Rayleigh's quotient can be derived as follows:

$$\omega^2 = \frac{U_{max}}{T^*_{max}} \tag{1.3}$$

Here, maximum kinetic energy is expressed as $\omega^2 T^*_{max}$. The accuracy of results also depends on the selection of the polynomial i.e. how good the polynomial represents the deformed shape of vibrating body.

In order to have the approximation as close as possible to the exact value, Ritz proposed to choose the coefficients $\mathrm{a}_1, \mathrm{a}_2..$ such that the result of Equation (1.3) be minimum [5]. Hence, a system of equations are obtained as follows:

$$\frac{\partial \omega^2}{\partial a_j} = 0 \tag{1.4}$$

Upon simplification,

$$\frac{\partial U_{max}}{\partial a_j} - \omega^2 \frac{\partial T^*_{max}}{\partial a_j} = 0 \tag{1.5}$$

The number of such equations will be the number of coefficients in Equation (1.2). This system of equation can yield non-zero solution if the determinant of the coefficients of $\mathrm{a}_1, \mathrm{a}_2..$ is equal to zero. A system of Equation (1.5) can be rewritten as follows:

$$[[K] - \omega^2[M]]\left[\{a_j\}\right] = 0 \tag{1.6}$$

where, $\left[\{a_j\}\right] = [\mathrm{a}_1\ \mathrm{a}_2\ \ldots]^T$ is the column matrix consisting of coefficients. The determinant of augmented matrix in Equation (1.6) yields the frequency equation and the roots of this equation represent the circular natural frequencies of vibrations.

1.4 Literature survey

A comprehensive literature review is presented on in-plane and out-of-plane vibrations of linearly-tapered and non-linearly tapered circular discs. Research work on vibration analysis of circular discs using Ritz method and finite element method have been chronicled. The majority of work done in the past is limited to the vibration analysis of linearly-tapered disc and the non-linearly tapered disc of parabolic profiles (i.e. convex shape profiles) considering Classical plate theory or Mindlin plate theory.

At the end of this section, the research work conducted on vibration analysis of rotating discs is presented. From that, it can be concluded that the work on the transverse vibration of rotating disc with hyperbolic thickness variation is very rare or limited. The following is the up to date survey categorized based on the subject:

1.4.1 Review of vibration analysis of uniform thickness circular discs

At first, vibration problem of a circular disc of free-free boundary conditions was tackled by Love [6] who derived the equations of motion from the concepts of elasticity and provided the general solutions. Deresiewicz and Mindlin [7] studied the axially symmetric transverse vibrations of a circular disc. The frequency responses for the circular disc of free-free boundary condition obtained using both the classical thin plate theory and the Mindlin plate theory were presented.

Venkatesan and Kunukkasseril [8] studied the free vibration response of layered circular plates using shear deformation theory. Guruswamy and Yang [9] developed an element of 24 DOFs (Degrees Of Freedom) to study the static and dynamic behaviour of thick circular plates. Irie et al. [10] conducted free vibration analysis based on the Mindlin plate theory considering nine different boundary conditions. Liew et al. [11] studied the free flexural vibration of circular and annular Mindlin plates using Rayleigh-Ritz method. So and Leissa [12] have proposed the three-dimensional Rayleigh-Ritz solution to study the three-dimensional in-plane and out-of-plane vibration response of thick circular annular plates. They used the admissible functions in all three directions by employing trigonometric function in circumferential coordinate and algebraic polynomials in radial and axial coordinates. The scope of their formulation was limited to the thick circular discs made of isotropic materials. Kang [13] applied this three-dimensional Ritz solution to conduct free vibration analysis of shallow spherical dome. Zhou et al. [14] developed the three-dimensional solution for circular and annular plates using the Chebyshev-Ritz method. Park [15] introduced 2D exact solution for in-plane vibration of a clamped circular plate. He used Helmholtz decomposition to derive uncoupled equations of motion from highly coupled equations of motion, which were obtained by applying Hamilton's principle. Recently, Bashmal

et al. [16] used the boundary characteristic orthogonal polynomials in the Rayleigh-Ritz method to obtain the frequency parameters of the annular disc with point elastic support. Moreover, Bashmal et al. [17] also conducted in-plane free vibration of circular annular disks considering characteristic orthogonal polynomials in Rayleigh-Ritz method. The material properties considered in their model were isotropic. Huang and Chen [18] estimated natural frequency of circular discs with V-notches using Ritz method. Sridhar and Rao [19] developed a four noded 48 DOF sector element to conduct large deformation Finite Element Analysis of laminated circular composite plates. They employed Newton-Raphson method as the nonlinear solution technique. Recently, Gupta et al [20] studied dynamic behaviour of fiber reinforced composite discs considering SHELL 181 element using ANSYS. Wang et al. [21] have developed modified Fourier-Ritz approach to study free in-plane vibration of orthotropic annular plates with general boundary conditions. They studied the effect of different fiber reinforcement configurations and rotational speed on natural frequency.

Kim and Dickinson [22] studied flexural vibration of thin, flat annular circular plates using Rayleigh-Ritz method. They have used a series comprising of orthogonally generated polynomial functions in Rayleigh-Ritz method. Comparison is made between natural frequency results obtained using three-dimensional Rayleigh-Ritz approach (presented in Chapter-2) with results obtained by Kim and Dickinson [22]. This validation is presented in Appendix B.

1.4.2 Review of vibration analysis of linearly-tapered and non-linearly tapered circular discs

The effect of taper on the dynamic behaviour of the circular disc is an important parameter to investigate. Early works on analysing the effect of taper were that of Chandrika Prasad et al. [23] and Gupta and Lal [24], who conducted a dynamic analysis of linearly-tapered circular discs and parabolically-tapered circular discs respectively.

Soni and Amba Rao's [25] paper contains the analysis for free axisymmetric vibrations of orthotropic circular plates of linear thickness variation. Their study doesn't account for the non-linear thickness variation. Kirkhope and Wilson [26] have used the annular finite element method to study the stress and vibration behaviour of thin rotating discs. Moreover, their element allows the specific thickness variation in the radius direction. They presented numerical data for free vibration response of linearly-tapered circular discs and parabolically-tapered circular discs. Mota and Petyt [27] developed the semi-analytical finite element based on Mindlin theory for the dynamic analysis of circular disc of varying thickness in the radial direction. Their formulation was limited to the discs made of isotropic materials.

Lenox and Conway [28] developed an exact, closed-form solution for transverse vibrations of a thin plate having a parabolic thickness variation. Their proposed solution involves only the power of radius and constant coefficients which are way simpler than that for the case of uniform thickness solution with the involvement of Bessel functions. Reddy and Huang [29] presented the finite element formulation for the non-linear axisymmetric bending of annular plates considering Reissner-Mindlin plate theory and Von Karman non-linearity. Singh and Saxena [30] used the Rayleigh-Ritz method to study the axisymmetric transverse vibration of a circular plate of linear thickness

variation and made of isotropic materials. In their study, radial direction deformation is not accounted in axisymmetric transverse vibration analysis unlike the three-dimensional formulation presented in this thesis.

Recently, Duan et al. [31] introduced the transformation of variables to translate the governing equation for the free vibration of the thin annular plate into a fourth-order generalized hypergeometric equation. Gupta et al. [32] employed the differential quadrature method to analyse the free vibration response of non-linearly tapered isotropic discs considering classical plate theory assumption. Vishwanathan and Sheen [33] used the point collocation method to study free vibration of a circular plate of variable thickness.

To validate the results of linearly-tapered disc of clamped-free boundary condition, natural frequencies of linearly-tapered disc of small taper angle are calculated and compared with that of uniform-thickness circular disc with comparable thickness. This comparison is given in Appendix B.

1.4.3 Review of vibration analysis of rotating circular discs

The above literature survey is limited to the free vibration analysis of non-rotating circular discs. The modelling of such discs with the inclusion of rotational effects makes the problem more relevant to their actual applications. In that case, a problem of rotating disc involves the gyroscopic effect and the centrifugal forces generated due to the rotation.

At first, Lamb and Southwell [34] tackled the problem of spinning disc of uniform thickness using Rayleigh's method. Nowinski [35] conducted the non-linear transverse vibration analysis of spinning circular discs rotating at constant angular speed and of uniform thickness using two-term polynomial in Ritz method. Barasch and Chen [36]

have reduced the fourth-order equation of motion to a set of four first-order equations. They used the modified Adam's method to study the variation of transverse mode natural frequency of rotating disc of uniform thickness with rotational speed.

Recently, Baddour [37] derived non-linear equations of motion accounting for the rotary and in-plane inertia terms for spinning circular disc using Hamilton's principle for the first time. She proposed the solution of Helmholtz equations via separation of variables and further considering the classical Bessel functions. This study was limited to thin rotating circular disc of uniform thickness. Khoshnood and Jalali [38] conducted the transverse vibration analysis of rotating orthotropic discs of uniform thickness by expanding the transverse deformation in Fourier series. Hamidzadeh [39] conducted in-plane free vibration analysis and stability analysis of rotating annular discs on the basis of two-dimensional linear plane stress theory of elasticity. He proposed the time independent solution and time dependent solution of governing equations of motion to study the influence of rotational speed and radios ratio on the natural frequency of the disc. Dousti and Jalali [40] calculated the eigenmodes of linearized questions using collocation method and compared the mode shapes of composite disc and isotropic disc.

The above work is limited to free vibration analysis of the circular rotating discs of uniform thickness or the linearly-tapered rotating discs.

1.5 Objective of thesis

The main objectives of the present study are as follow:

1) To calculate the Rayleigh's damping coefficients based on modal mass participation factor to obtain the realistic damping natural frequencies of in-plane mode and out-of-plane mode vibration of uniform thickness disc, linearly-tapered disc and Stodola's disc.
2) To investigate the three-dimensional free vibration response of uniform thickness circular discs, and linearly-tapered and non-linearly tapered circular discs using Rayleigh-Ritz method and finite element method using ANSYS.
3) To conduct a comprehensive parametric study to study the effects of taper angles, taper shapes, radius ratios, material properties, and the degree of orthotropy on free vibration frequency response of circular disc considering clamped-free boundary condition.
4) To study the effect of rotational speed on the lowest bending mode natural frequency of Stodola's disc considering Kirchhoff hypothesis and linear strain-displacement relationship. Equations of motion are proposed for a hyperbolic profile for the first time for further future investigations.
5) The accuracy of proposed Rayleigh-Ritz solutions and Rayleigh-Ritz solutions with finite-element-like modification is verified by comparing them to finite element solutions using ANSYS.

1.6 Layout of thesis

The present chapter provides a brief introduction, overview of applications and literature review on free vibrations of uniform thickness and tapered circular discs.

In Chapter 2, the modelling of three-dimensional vibration problem is articulated considering the theory of elasticity. Then the application of Rayleigh-Ritz method to free vibration problem of the uniform thickness discs is presented. The selection procedure is proposed to determine the order of polynomials in Rayleigh-Ritz method. The procedure for estimation of Rayleigh's damping coefficients based on modal mass participation factor is presented. At the end of the Chapter, strain energy and kinetic energy equations are determined for orthotropic discs. Rayleigh-Ritz solutions are validated by comparing them with ANSYS solutions.

Chapter 3 contains the proposed analytical approach to investigate the three-dimensional vibration response of linearly-tapered circular discs which is developed based on the classical Rayleigh-Ritz method with finite-element-like modification. The complete mathematical formulation is presented and explained along with the numerical data of the lowest in-plane and the lowest out-of-plane modes natural frequencies for the linearly-tapered circular disc. Considering clamped-free boundary condition, the parametric study is conducted based on taper angles and radius ratios.

In Chapter 4, the analytical method derived in Chapter 3 is re-employed to study the free vibration behaviour of Stodola's disc. The parametric study is conducted based on the taper parameters of the Stodola's disc.

Chapter 5 is devoted to the bending mode vibrations of Stodala's disc rotating at constant speed. The effect of rotation on the lowest bending mode natural frequency of Stodola's disc is studied by considering the Kirchhoff's hypothesis and linear strain-

displacement relationship. Here, Rayleigh-Ritz method is employed for the first time for the rotating Stodola's discs. Moreover, the parametric study on the effects of constant rotational speeds and degree of orthotropy on free vibration bending mode natural frequency is conducted.

Finally, major contributions of the present thesis and recommendations for future work are presented in Chapter 6.

Chapter 2

Three-dimensional in-plane and out-of-plane vibrations of annular clamped-free disc of uniform thickness

2.1 Introduction

This chapter describes the generalized formulation for in-plane and out-of-plane vibration analyses of a thick circular disc of clamped-free boundary condition and made of isotropic or orthotropic material. The clamped-free boundary condition is taken into consideration since this has a wide range of applications. Rayleigh-Ritz method is employed to obtain the natural frequencies and mode shapes. To study the free vibration response of the circular disc of uniform thickness, trigonometric functions are employed in the circumferential coordinate for all the three displacement components in Rayleigh-Ritz method. The formulation for the three-dimensional vibration analysis is first developed for the isotropic disc and then extended for the orthotropic disc. The material chosen for the isotropic disc is Structural Steel having Young's modulus of 200 GPa and Poisson's ratio of 0.3. For the orthotropic disc, Graphite-Polymer Composite material are considered. The material properties for the Graphite-Polymer Composite material is given in Table 2.6. Rayleigh-Ritz solutions are compared with the finite element solutions obtained using ANSYS.

A three-dimensional vibration model can reveal more comprehensive and accurate vibration characteristics of the circular disc involving both in-plane and out-of-plane modes and coupling between in-plane and out-of-plane motions. For thick discs, this coupling between in-plane mode and the out-of-plane mode is strong and this fact necessitates the requirement for the development of efficient three-dimensional

Rayleigh-Ritz solutions. In many applications, it is required to know the in-plane and the out-of-plane response of the disc at the design stage.

2.2 Modelling

In order to use Rayleigh-Ritz method, expressions for total kinetic energy and total strain energy must be formulated. Here, kinetic energy and strain energy of the element of the infinitesimal volume are calculated and later integrated over the entire volume (non-deformed or initial volume) of the disc to derive the expressions for the total strain energy and total kinetic energy. This approach holds true for the continuous systems.

2.2.1 Formulation for strain energy

Strain energy is the energy stored in a body due to deformation. It is difficult to keep track of the displacements (deformations), which are usually unknown if it is to be measured with respect to the Eulerian frame of reference. Hence, it is advantageous to consider the Lagrangian coordinates and they can be employed by fixing a coordinate frame on the body. The motion of this body-fixed frame indicates the rigid body motion of the body. Displacements (deformations) measured from this frame of reference contribute to the strain energy. Hence, it is clear that the strain energy of stationary disc and rotating disc are the same if they are derived from this approach.

As discussed earlier, consider the infinitesimal volume element of the disc. Strain energy of such an element can be written as follows:

$$\Pi_{element} = \frac{1}{2}\sigma_{ij}\epsilon_{ij} \tag{2.1}$$

where, σ_{ij} and ϵ_{ij} are the stress and strain tensors respectively.

By integrating the Equation (2.1) over the entire domain of the disc, total strain energy of the disc can be calculated.

This way total strain energy of the uniform disc is given by:

$$\Pi = \frac{1}{2}\int_{-\frac{h}{2}}^{\frac{h}{2}}\int_{0}^{2\pi}\int_{R_i}^{R_o}[\sigma_{rr} \quad \sigma_{\theta\theta} \quad \sigma_{zz} \quad \sigma_{r\theta} \quad \sigma_{\theta z} \quad \sigma_{zr}]\begin{bmatrix}\varepsilon_{rr}\\ \varepsilon_{\theta\theta}\\ \varepsilon_{zz}\\ 2\varepsilon_{r\theta}\\ 2\varepsilon_{\theta z}\\ 2\varepsilon_{zr}\end{bmatrix} r\,dr\,d\theta\,dz \tag{2.2}$$

where, h is the total thickness of the disc and R_i and R_o are the inner radius and the outer radius of the circular disc respectively. Note that the engineering strains are considered in Equation (2.2).

Assuming small strains, the stress-strain relations follow the Hooke's law and hence the relationship is linear. Again, this doesn't mean that the deformations in r, θ, and z directions are small. To derive the expression for strain energy of the disc in terms of displacements, the first step is to write the stresses in terms of strains and the strains in terms of displacements. In cylindrical coordinate system, they are as follow:

$$\sigma_{rr} = \lambda(\varepsilon_{rr} + \varepsilon_{\theta\theta} + \varepsilon_{zz}) + 2G\varepsilon_{rr} \tag{2.3}$$

$$\sigma_{\theta\theta} = \lambda(\varepsilon_{rr} + \varepsilon_{\theta\theta} + \varepsilon_{zz}) + 2G\varepsilon_{\theta\theta} \tag{2.4}$$

$$\sigma_{zz} = \lambda(\varepsilon_{rr} + \varepsilon_{\theta\theta} + \varepsilon_{zz}) + 2G\varepsilon_{zz} \tag{2.5}$$

$$\sigma_{r\theta} = 2G\varepsilon_{r\theta} \tag{2.6}$$

$$\sigma_{\theta z} = 2G\varepsilon_{\theta z} \tag{2.7}$$

$$\sigma_{zr} = 2G\varepsilon_{zr} \tag{2.8}$$

$$\varepsilon_{rr} = \frac{\partial u_r}{\partial r} \tag{2.9}$$

$$\varepsilon_{\theta\theta} = \frac{\mathrm{u_r}}{\mathrm{r}} + \frac{1}{\mathrm{r}}\frac{\partial \mathrm{u_\theta}}{\partial \theta} \tag{2.10}$$

$$\varepsilon_{zz} = \frac{\partial \mathrm{u_z}}{\partial \mathrm{z}} \tag{2.11}$$

$$\varepsilon_{\mathrm{r}\theta} = \frac{1}{2}\left(\frac{1}{\mathrm{r}}\frac{\partial \mathrm{u_r}}{\partial \theta} + \frac{\partial \mathrm{u_\theta}}{\partial \mathrm{r}} - \frac{\mathrm{u_\theta}}{\mathrm{r}}\right) \tag{2.12}$$

$$\varepsilon_{\mathrm{zr}} = \frac{1}{2}\left(\frac{\partial \mathrm{u_r}}{\partial \mathrm{z}} + \frac{\partial \mathrm{u_z}}{\partial \mathrm{r}}\right) \tag{2.13}$$

$$\varepsilon_{\theta\mathrm{z}} = \frac{1}{2}\left(\frac{1}{\mathrm{r}}\frac{\partial \mathrm{u_z}}{\partial \theta} + \frac{\partial \mathrm{u_\theta}}{\partial \mathrm{z}}\right) \tag{2.14}$$

Substituting Equations (2.3) to (2.14) into Equation (2.2), total strain energy as a function of displacements (i.e. $u_r, \mathrm{u_\theta}$ and $\mathrm{u_z}$) can be derived. Upon simplification, it can be written as below:

$$\begin{aligned}\Pi = \frac{E}{4(1+v)}\int_{\frac{-h}{2}}^{\frac{h}{2}}\int_0^{2\pi}\int_{R_i}^{R_o}\frac{2v}{(1-2v)}\left(\frac{\partial u_r}{\partial r} + \frac{\mathrm{u_r}}{\mathrm{r}} + \frac{1}{r}\frac{\partial \mathrm{u_\theta}}{\partial \theta} + \frac{\partial \mathrm{u_z}}{\partial \mathrm{z}}\right)^2 \\ + 2\left(\frac{\partial u_r}{\partial r}\right)^2 + 2\left(\frac{\mathrm{u_r}}{\mathrm{r}} + \frac{1}{r}\frac{\partial \mathrm{u_\theta}}{\partial \theta}\right)^2 + 2\left(\frac{\partial \mathrm{u_z}}{\partial \mathrm{z}}\right)^2 \\ + \left(\frac{1}{\mathrm{r}}\frac{\partial \mathrm{u_r}}{\partial \theta} + \frac{\partial \mathrm{u_\theta}}{\partial \mathrm{r}} - \frac{\mathrm{u_\theta}}{\mathrm{r}}\right)^2 + \left(\frac{\partial \mathrm{u_r}}{\partial \mathrm{z}} + \frac{\partial \mathrm{u_z}}{\partial \mathrm{r}}\right)^2 \\ + \left(\frac{1}{\mathrm{r}}\frac{\partial \mathrm{u_z}}{\partial \theta} + \frac{\partial \mathrm{u_\theta}}{\partial \mathrm{z}}\right)^2 r\,dr\,d\theta\,dz\end{aligned} \tag{2.15}$$

In Equation (2.15), E and v are the Young's modulus and Poisson's ratio of the material respectively. Moreover, $u_r, \mathrm{u_\theta}$ and $\mathrm{u_z}$ are the displacements in r, θ and z directions respectively.

To simplify the mathematical calculations, the Equation (2.15) can be reduced to the non-dimensional form in r and z coordinates by letting ζ and ξ as non-dimensional parameters respectively.

Let, $\zeta = \frac{r}{R_o}$ and $\xi = \frac{z}{\mathrm{h}}$

Recall that h is the total thickness of the disc.

Let's introduce β as a radius ratio in the lower limit of integration in Equation (2.15).

Rewriting the Equation (2.15) in terms of newly introduced non-dimensional parameters, one gets:

$$\Pi = \frac{E\,h}{4(1+v)}\int_{\frac{-1}{2}}^{\frac{1}{2}}\int_{\beta}^{1}\int_{0}^{2\pi}\frac{2v}{(1-2v)}\left(\frac{\partial u_r}{\partial \zeta}+\frac{\mathrm{u_r}}{\zeta}+\frac{1}{\zeta}\frac{\partial \mathrm{u_\theta}}{\partial \theta}+\frac{R_o}{h}\frac{\partial \mathrm{u_z}}{\partial \xi}\right)^2$$
$$+2\left(\frac{\partial u_r}{\partial \zeta}\right)^2+2\left(\frac{\mathrm{u_r}}{\zeta}+\frac{1}{\zeta}\frac{\partial \mathrm{u_\theta}}{\partial \theta}\right)^2+2\left(\frac{R_o}{h}\frac{\partial \mathrm{u_z}}{\partial \xi}\right)^2$$
$$+\left(\frac{1}{\zeta}\frac{\partial \mathrm{u_r}}{\partial \theta}+\frac{\partial \mathrm{u_\theta}}{\partial \zeta}-\frac{\mathrm{u_\theta}}{\zeta}\right)^2+\left(\frac{R_o}{h}\frac{\partial \mathrm{u_r}}{\partial \xi}+\frac{\partial \mathrm{u_z}}{\partial \zeta}\right)^2 \tag{2.16}$$
$$+\left(\frac{1}{\zeta}\frac{\partial \mathrm{u_z}}{\partial \theta}+\frac{R_o}{h}\frac{\partial \mathrm{u_\theta}}{\partial \xi}\right)^2\zeta d\theta\, d\zeta\, d\xi$$

where, β is the radius ratio defined by $\frac{R_i}{R_o}$. The above Equation (2.16) describes the strain energy of the disc in terms of displacements $u_r, \mathrm{u_\theta}$ and $\mathrm{u_z}$ of an arbitrary point of the disc.

2.2.2 Formulation for kinetic energy

It is confirmed from the formulation developed in sub-section 2.2.1 that the strain energy of a stationary disc and that of a rotating disc are the same. It is the kinetic energy that is not the same and hence the corresponding two vibration models are different based on the kinetic energy.

The kinetic energy of an infinitesimal volume element of stationary disc is given by:

$$T_{element} = \frac{1}{2}\rho v^2 dV \tag{2.17}$$

where, ρ is the density of the material and dV is the volume of an element. Equation (2.17) can be re-written as follows:

$$T_{element} = \frac{1}{2}\rho\left[\left(\frac{\partial u_r}{\partial t}\right)^2 + \left(\frac{\partial u_\theta}{\partial t}\right)^2 + \left(\frac{\partial u_z}{\partial t}\right)^2\right] dV \tag{2.18}$$

This kinetic energy of an infinitesimal volume element is integrated over the un-deformed domain of the disc to determine the total kinetic energy of the non-rotating disc. This way one gets:

$$T = \frac{1}{2}\rho h R_o^2 \int_{\frac{-1}{2}}^{\frac{1}{2}} \int_{\beta}^{1} \int_{0}^{2\pi} \left[\left(\frac{\partial u_r}{\partial t}\right)^2 + \left(\frac{\partial u_\theta}{\partial t}\right)^2 + \left(\frac{\partial u_z}{\partial t}\right)^2\right] \zeta d\theta \, d\zeta \, d\xi \tag{2.19}$$

The above Equation (2.19) describes the total kinetic energy of the disc in terms of displacements u_r, $\mathrm{u_\theta}$ and $\mathrm{u_z}$ of an arbitrary point on the disc.

2.3 Solution by Rayleigh-Ritz method

The equations of motion could have been derived for the uniform thickness disc by applying Hamilton's principle. Hamilton's principle states that the variation of the integral of the Lagrangian function over time t_1 to t_2 is zero provided that variations of displacements are zero at time t_1 and t_2. Lagrangian function can be calculated by assembling strain energy and kinetic energy, which are derived in Section 2.2. Variation can be performed with respect to each generalized coordinate to generate equations of motion i.e. to get the first equation of motion, one should perform the variation of Langrangian function with respect to u_r. For deriving second equation of motion, perform the variation of Langrangian function with respect to u_θ and so on. This approach is handy only for the uniform thickness discs but for non-linearly tapered discs, exact or closed-form solutions for the partial differential equations are not available.

To overcome such difficulty, many approximate methods have drawn the attention of researchers such as Ritz method, Rayleigh-Ritz method and Galerkin method and are extensively used to solve the structural dynamic problems. In the present work, Rayleigh-Ritz method is employed to calculate the approximate natural frequencies of the uniform-thickness disc.

Rayleigh-Ritz method is the extension of the Ritz's method. To use this method, it is necessary to make some assumption of the deflected shape of the vibrating elastic body. The frequency of vibration will then be found by employing the conservation of energy principle [5]. In Rayleigh-Ritz method, a number of assumed functions are taken into consideration to have the closest approximation to the exact solution. Hence, this method provides not only the lowest approximate frequency but also higher mode approximate frequencies. The accuracy of this method depends on the choice of assumed approximation functions that one should select to represent the configuration of the system during vibration, which also should satisfy the geometric boundary conditions of structural dynamics problem. It is necessary to find the maximum strain energy and the maximum kinetic energy of the system in order to derive the Rayleigh's quotient, which is the ratio of maximum strain energy to maximum kinetic energy.

Let the displacements in r, θ and z directions be expressed as the following assumed sinusoidal variation of vibration response:

$$u_r = U \sin n\theta \ \sin \omega t \tag{2.20}$$

$$u_\theta = V \cos n\theta \ \sin \omega t \tag{2.21}$$

$$u_z = W \sin n\theta \ \sin \omega t \tag{2.22}$$

where, n is the circumferential wave number (i.e. nodal diameter number). It is taken into consideration in order to distinguish between different mode shapes. Here, U, V

and $W$are the amplitudes of vibration in r, θ and z directions respectively. ω is the circular natural frequency of vibration.

Furthermore, amplitudes U, V and W can be expressed in terms of the combination of the arbitrary coefficients and algebraic polynomials [12].

$$U = n_r \sum_{i=0}^{I} \sum_{j=0}^{J} A_{ij}\ \zeta^{i}\ \xi^{j} \tag{2.23}$$

$$V = n_\theta \sum_{k=0}^{K} \sum_{l=0}^{L} B_{kl}\ \zeta^{k}\ \xi^{l} \tag{2.24}$$

$$W = n_z \sum_{p=0}^{P} \sum_{q=0}^{Q} C_{pq}\ \zeta^{p}\ \xi^{q} \tag{2.25}$$

where, $n_r,\ n_\theta\ and\ n_z$ are the constraint functions that depend on geometric boundary conditions. The functions $n_r,\ n_\theta\ and\ n_z$ are used to impose the necessary boundary conditions to the model.

Let $n_r = n_\theta = n_z = \frac{\zeta(\zeta-\beta)}{(1-\beta)}$ for the clamped-free disc.

For example,

At inner edge ($r = R_i$), $n_r = n_\theta = n_z = 0$. Hence, displacements at inner radius are restricted to zero.

At outer edge ($r = R_o$), $n_r = n_\theta = n_z = 1$. Hence, there are no constraints for displacements at outer radius.

Consider the Equation (2.23). It expresses the amplitude of vibration in r-direction which is again the function of combination of arbitrary coefficients, non-dimensional radius and non-dimensional thickness terms. Here, I and J indicate the maximum

number of non-dimensional radius and thickness terms respectively. For example, for $I = J = 2$, the amplitude in r direction consists of 9 terms, which is given by:

$$U = n_r \left(A_{22}\zeta^2\xi^2 + A_{21}\zeta^2\xi^1 + A_{12}\zeta^1\xi^2 + A_{20}\zeta^2 + A_{11}\zeta^1\xi^1 + A_{02}\xi^2 + A_{10}\zeta^1 + A_{01}\xi^1 + A_{00}\right) \tag{2.26}$$

As a rule of thumb, Equation (2.23) yields $(I+1)(J+1)$ number of terms for the specific values of I and J.

2.3.1 Maximum Strain energy

As discussed in earlier Sections, maximum strain energy and maximum kinetic energy are the building blocks for the Rayleigh's quotient. After substitution of the assumed displacements expressed by Equations (2.23), (2.24) and (2.25) into Equation (2.16), the following maximum strain energy is obtained using MAPLE:

$$\begin{aligned}\Pi_{max} = \frac{E\,h}{4(1+v)}\int_{-\frac{1}{2}}^{\frac{1}{2}}\int_{\beta}^{1}\int_{0}^{2\pi}\Bigg(&\frac{2v}{1-2v}\left(\left(\frac{\partial U}{\partial\zeta}\right)\sin n\theta - \frac{n\,V\sin n\theta}{\zeta} + \frac{U\sin n\theta}{\zeta} + a\left(\frac{\partial \mathrm{W}}{\partial\xi}\sin n\theta\right)^2\right) + 2\left(\frac{\partial U}{\partial\zeta}\sin n\theta\right)^2 \\ &+ 2\left(\frac{U\sin n\theta}{\zeta} - \frac{n\,V\sin n\theta}{\zeta}\right)^2 + 2a^2\left(\frac{\partial \mathrm{W}}{\partial\xi}\sin n\theta\right)^2 \\ &+ \left(\frac{n\,U\cos n\theta}{\zeta} + \frac{\partial V}{\partial\zeta}\cos n\theta - \frac{V\cos n\theta}{\zeta}\right)^2 \\ &+ \left(a\frac{\partial \mathrm{V}}{\partial\xi}\cos n\theta + \frac{n\,W\cos n\theta}{\zeta}\right)^2 \\ &+ \left(a\frac{\partial \mathrm{U}}{\partial\xi}\sin n\theta + \frac{\partial W}{\partial\zeta}\sin n\theta\right)^2\Bigg)\zeta\,d\theta\,d\zeta\,d\xi\end{aligned} \tag{2.27}$$

In above Equation (2.27), the maximum value of $sin^2\,\omega t$ is considered in order to derive the maximum strain energy.

2.3.2 Maximum kinetic energy

After substitution of the assumed displacements expressed by Equations (2.23), (2.24) and (2.25) into Equation (2.19), the following total kinetic energy expression is obtained using MAPLE:

$$T = \frac{1}{2}R_o^2 h\rho\,\omega^2 \int_{-\frac{1}{2}}^{\frac{1}{2}}\int_{\beta}^{1}\int_{0}^{2\pi}(U^2\sin^2 n\theta + V^2\cos^2 n\theta + W^2\sin^2 n\theta)\cos^2\omega t\,\zeta\,d\theta\,d\zeta\,d\xi \tag{2.28}$$

To calculate maximum kinetic energy of the disc, consider the maximum value of $\cos^2\omega t$ in the Equation (2.28). This way one gets:

$$T_{max} = \frac{1}{2}R_o^2 h\rho\,\omega^2 \int_{-\frac{1}{2}}^{\frac{1}{2}}\int_{\beta}^{1}\int_{0}^{2\pi}(U^2\sin^2 n\theta + V^2\cos^2 n\theta + W^2\sin^2 n\theta)\,\zeta\,d\theta\,d\zeta\,d\xi \tag{2.29}$$

Later, complementary displacement functions are used to derive different mode shapes, which are discussed in the following sub-section 2.4.1. Formulations for maximum kinetic energy and maximum strain energy hold true for the complementary set of displacement functions too.

2.3.3 Rayleigh's quotient

The law of conservation of energy implies that the total energy of the isolated system is constant. Hence, comparing the maximum kinetic energy and the maximum strain energy, neglecting damping, Rayleigh's quotient can be derived as follows:

$$\Pi_{max} = \omega^2 T^*{}_{max} \tag{2.30}$$

where, $T^*{}_{max} = \frac{1}{2}\,\rho h R_o^2 \int_{-\frac{1}{2}}^{\frac{1}{2}} \int_{\beta}^{1} \int_{0}^{2\pi} (U^2 \sin^2 n\theta + V^2 \cos^2 n\theta + W^2 \sin^2 n\theta)\,\zeta\, d\theta\, d\zeta\, d\xi$

Therefore,

$$\begin{aligned} &\frac{Eh}{4(1+v)} \int_{-\frac{1}{2}}^{\frac{1}{2}} \int_{\beta}^{1} \int_{0}^{2\pi} (\Pi_{uni}\ terms)\ \zeta d\theta\, d\zeta\, d\xi \\ &\qquad = \frac{1}{2}\omega^2 \rho h R_o^2 \int_{-\frac{1}{2}}^{\frac{1}{2}} \int_{\beta}^{1} \int_{0}^{2\pi} (T^*{}_{uni} terms)\,\zeta d\theta\, d\zeta\, d\xi \end{aligned} \tag{2.31}$$

Here,

$$\begin{aligned} (\Pi_{uni}\ terms) = \frac{2v}{1-2v} \Bigg(&\left(\frac{\partial U}{\partial \zeta}\right) \sin n\theta - \frac{n\, V \sin n\theta}{\zeta} + \frac{U \sin n\theta}{\zeta} \\ &+ a \left(\frac{\partial \mathrm{W}}{\partial \xi} \sin n\theta\right)^2 \Bigg) + 2 \left(\frac{\partial U}{\partial \zeta} \sin n\theta\right)^2 \\ &+ 2 \left(\frac{U \sin n\theta}{\zeta} - \frac{n\, V \sin n\theta}{\zeta}\right)^2 + 2a^2 \left(\frac{\partial \mathrm{W}}{\partial \xi} \sin n\theta\right)^2 \\ &+ \left(\frac{n\, U \cos n\theta}{\zeta} + \frac{\partial V}{\partial \zeta} \cos n\theta - \frac{V \cos n\theta}{\zeta}\right)^2 \\ &+ \left(a \frac{\partial \mathrm{V}}{\partial \xi} \cos n\theta + \frac{n\, W \cos n\theta}{\zeta}\right)^2 \\ &+ \left(a \frac{\partial \mathrm{U}}{\partial \xi} \sin n\theta + \frac{\partial W}{\partial \zeta} \sin n\theta\right)^2 \end{aligned} \tag{2.32}$$

and

$$(T^*{}_{uni} terms) = U^2 \sin^2 n\theta + V^2 \cos^2 n\theta + W^2 \sin^2 n\theta \tag{2.33}$$

Hence, Rayleigh's quotient (Ω^2) becomes:

$$\Omega^2 = \frac{\int_{-\frac{1}{2}}^{\frac{1}{2}} \int_{\beta}^{1} \int_{0}^{2\pi} (\Pi_{uni}\ terms)\ \zeta d\theta\, d\zeta\, d\xi}{\int_{-\frac{1}{2}}^{\frac{1}{2}} \int_{\beta}^{1} \int_{0}^{2\pi} (T^*_{uni} terms)\, \zeta d\theta\, d\zeta\, d\xi} = \frac{N}{D} \tag{2.34}$$

Note that N and D are the numerator and the denominator of the Rayleigh's quotient respectively. In above Equations (2.32), (2.33) and (2.34), subscript 'uni'refers to the vibration model of uniform thickness circular disc.

Upon simplifying the Equations (2.31) and (2.34),

$$\Omega = \sqrt{2\omega^2 R_0^2 \frac{\rho(1+v)}{E}} \tag{2.35}$$

Equation (2.35) represents the non-dimensional frequency parameter of the uniform disc.

2.3.4 Formulation of eigenvalue problem

To obtain the best possible approximation of natural frequencies for the assumed shape functions, arbitrary coefficients are adjusted and natural frequency is made stationary. Minimizing the Rayleigh's quotient with respect to arbitrary constants considered in Equations (2.23), (2.24) and (2.25), one gets:

$$\frac{\partial \Omega^2}{\partial A_{ij}} = 0 \tag{2.36}$$

$$\frac{\partial \Omega^2}{\partial B_{kl}} = 0 \tag{2.37}$$

$$\frac{\partial \Omega^2}{\partial C_{pq}} = 0 \tag{2.38}$$

These give the set of $(I+1)(J+1)+(K+1)(L+1)+(P+1)(Q+1)$ linear algebraic equations in terms of arbitrary coefficients (i.e. $A_{ij}, B_{kl}\ and\ C_{pq}$). These equations are given as follow:

$$\frac{\partial N}{\partial A_{ij}} - \Omega^2 \frac{\partial D}{\partial A_{ij}} = 0 \tag{2.39}$$

$$\frac{\partial N}{\partial B_{kl}} - \Omega^2 \frac{\partial D}{\partial B_{kl}} = 0 \tag{2.40}$$

$$\frac{\partial N}{\partial C_{pq}} - \Omega^2 \frac{\partial D}{\partial C_{pq}} = 0 \tag{2.41}$$

The above equations can be rewritten and represented as the eigenvalue problem,

$$[[K] - \Omega^2[M]] \begin{bmatrix} \{A_{ij}\} \\ \{B_{kl}\} \\ \{C_{pq}\} \end{bmatrix} = 0 \tag{2.42}$$

where, $\{A_{ij}\}, \{B_{kl}\}\ and\ \{C_{pq}\}$ are column matrices. The dimensions of these matrices depend on the number of terms considered in Equations (2.23), (2.24) and (2.25).

To have a non-trivial solution, in Equation (2.42) let the determinant of the augmented matrix be zero. MAPLE code is developed to determine this determinant and solve for unknowns and, as a result, non-dimensional frequency parameters ($\Omega_i, i = 1, 2, 3$ ...) are calculated for the assumed nodal diameter numbers.

To study three-dimensional vibrations of the tapered disc, the presented approach is useful after suitable modifications. For this purpose, the modified Rayleigh-Ritz procedure is developed and explained in Chapter 3.

2.4 Results and Discussion

It is very clear by now that the number of natural frequencies that can be obtained from solving the augmented matrix of Equation (2.42) is equal to the number of terms considered in the assumed shape functions. At this point, it is advisable to conduct convergence study to determine the exact number of terms to be used in the assumed

polynomials, which gives the closest approximation to the exact solution. In Rayleigh-Ritz method, frequencies should converge to their exact solutions in the upper bound manner. This study is conducted and explained in the following section.

2.4.1 Pure circumferential mode and pure transverse mode

For the stationary uniform-thickness disc case, the in-plane mode is the pure circumferential mode, in which there are no radial and transverse deformations present. If there is no circumferential deformation, the mode shape can be described as a pure transverse mode. In this formulation, assumed displacement functions and their complimentary sets are considered to investigate pure transverse mode frequencies and pure circumferential mode frequencies of the disc.

Assumed set (A):

$$u_r = U \cos n\theta \ \sin \omega t \tag{2.43}$$

$$u_\theta = V \sin n\theta \ \sin \omega t \tag{2.44}$$

$$u_z = W \cos n\theta \ \sin \omega t \tag{2.45}$$

For $n = 0$, Set (A) describes the lowest transverse mode (i.e. the lowest out-of-plane mode or the lowest bending mode) and the displacements for this mode are as follows,

$$u_r = U \sin \omega t \tag{2.46}$$

$$u_\theta = 0 \tag{2.47}$$

$$u_z = W \sin \omega t \tag{2.48}$$

Complimentary set (B):

$$u_r = U \sin n\theta \ \sin \omega t \tag{2.49}$$

$$u_\theta = V \cos n\theta \ \sin \omega t \tag{2.50}$$

$$u_z = W \sin n\theta \ \sin \omega t \tag{2.51}$$

For $n = 0$, Set (B) yields pure circumferential mode (i.e. the lowest in-plane mode) and the displacements for this mode are as follows,

$$u_r = 0 \tag{2.52}$$

$$u_\theta = V \sin \omega t \tag{2.53}$$

$$u_z = 0 \tag{2.54}$$

2.4.2 Coupled mode shapes

In the lowest bending mode vibrations, there exist 'small' radial deformation and the transverse component of displacement as the present study is based on a three-dimensional analysis and is not limited to plane stress or plane strain assumptions.

For $n \geq 1$, Set (A) functions are considered. Hence, there exist all the three displacement components and hence named as coupled mode shapes, which can be identified based on the nodal diameter numbers. If Set (B) functions are chosen to investigate the coupled mode shapes, it can be inferred that mode shapes may be rotated by 90 degrees due to the nature of assumed trigonometric functions but they should have the same frequencies as reported by Set (A).

2.5 Example

A uniform thickness disc made of a structural steel material is considered. Let the inner radius and the outer radius of the disc be 0.4 m and 2 m. The thickness of the disc is 0.15 m. For the structural steel material, the values of modulus of elasticity and Poisson's ratio are 200 GPa and 0.3 respectively.

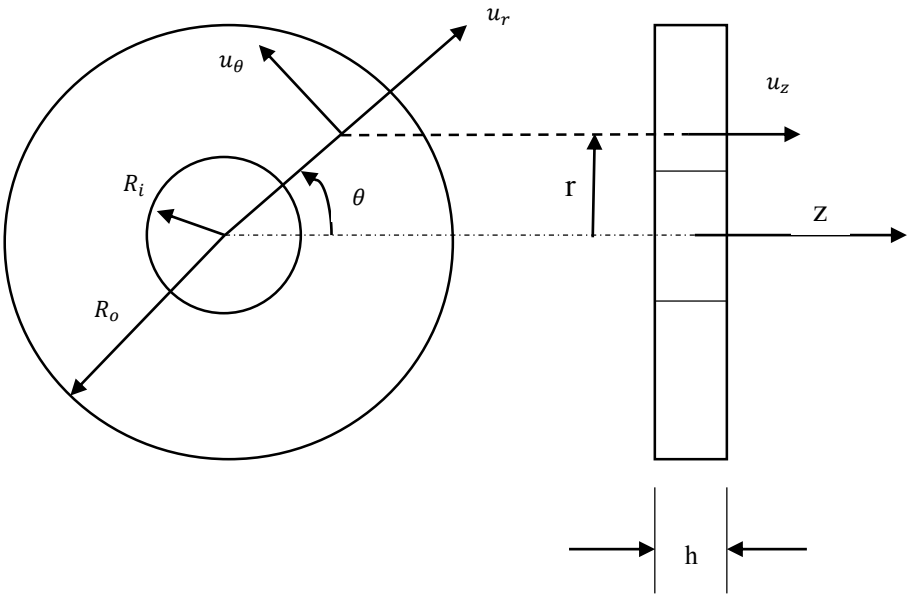

Figure 2.1: Geometry and coordinate system for uniform-thickness disc

Note that in Rayleigh-Ritz method, if the upper limit of summation is set to 1(which gives four constants coupled with four displacement terms), it generates 12x12 matrix. Just to start with, an equal number of polynomial terms are taken for the ease of calculations, though these results may not be closest to their exact solutions. These results are given in the following Table 2.1. Non-dimensional frequency parameters obtained using MAPLE for $I = J = K = L = P = Q = 1$ are given in the third column.

Mode set	Non-dimensional frequency without convergence study $\Omega = \sqrt{2\omega^2 R_0^2 \frac{\rho(1+v)}{E}}$	Non-dimensional frequency parameter after convergence study
Set A $n = 0$ out-of-plane	0.3639 2.6783 3.9915	0.2025 - -
Set B $n = 0$ in-plane	0.8248 9.0738 46.1847	0.5945 - -
Set A $n = 1$ coupled	0.3469 1.7524 2.7464	0.1856 - -
Set A $n = 2$ coupled	0.3526 2.8408 2.9564	0.2406 - -
Set A $n = 3$ coupled	0.5042 3.3160 -	0.4565 - -
Set A $n = 4$ coupled	0.8155 3.7955 -	0.7829 - -
Set A $n = 5$ coupled	1.2383 4.1983 -	1.0818 - -

Table 2.1: Lowest non-dimensional frequencies grouped according to corresponding mode shapes

In above Table 2.1, frequencies of the lowest in-plane mode, the lowest out-of-plane mode and the coupled modes for the stated example are demonstrated. For three-dimensional vibrations of the stationary uniform disc case, the lowest out-of-plane mode has deformations in transverse as well as in radial directions.

At this point, convergence study is necessary to get the frequencies approximation closest to the exact frequencies. This can be achieved by the following procedure. Here, convergence procedure is only explained for the lowest bending mode.

The natural frequencies and mode shapes are calculated for the above-stated example using ANSYS. In the modal analysis in ANSYS, mode 3 represents pure transverse mode. In the simulation, SOLID 186 elements are used for the analysis and later results are compared with that obtained using SHELL 281.

The following Figure 2.2 and Figure 2.3 show the geometry of SOLID 186 and SHELL 281 elements. The brief descriptions of these elements are given next:

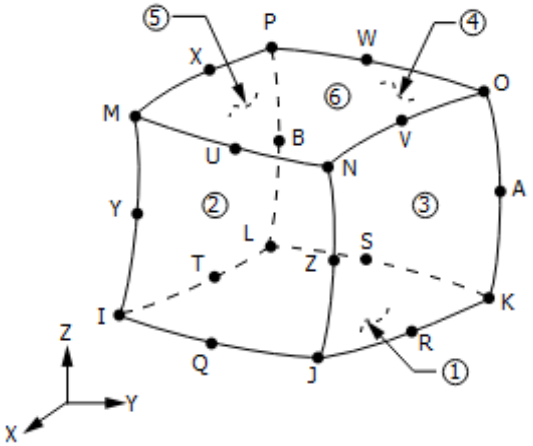

Figure 2.2 : SOLID186 homogeneous structural solid element geometry [41]

SOLID 186 is a higher-order 3-D element that consists of 20 nodes and it exhibits quadratic displacement behaviour. This element has three degrees of freedom per node (translations in the nodal X, Y, and Z directions). It supports plasticity, creep, stress

stiffening, large deflection and large strain capabilities. The SOLID 186 homogeneous structural solid element is well suited to modelling irregular meshes that can be produced by various CAD/CAM systems.

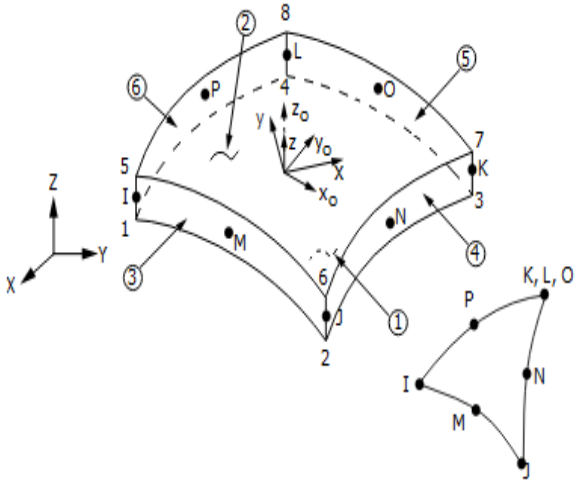

Figure 2.3: SHELL 281 element geometry [41]

The above Figure 2.3 describes the geometry and coordinate system for SHELL 281 element. Furthermore, a triangular-shaped element option is available by defining the same node number for nodes K, L and O. This element has eight nodes with six degrees of freedom at each node (three translations in the X, Y and Z axes and rotations about X, Y and Z axes). SHELL 281 is well suited for analysing thin to moderately thick shell structures. It is well suited for linear, and large rotation and large strain nonlinear applications.

Consider the lowest transverse mode. Now it is possible to extract the deformation values of each point, which are deformed in the transverse direction. Later, these can be represented as a plot of transverse deformation versus radial coordinate. This procedure helps to develop more accurate polynomial that can be fed into the above Rayleigh-Ritz formulation. This results in deriving approximate in-plane and out-of-plane frequencies which are closer to the exact solutions.

A total of 49 points are selected in the radial direction lying on the face of the circular disc and their respective z-direction deformations are calculated using ANSYS. The numerical values of transverse deformation are presented in Table 2.2.

	Radial Coordinate (m)	Transverse Displacement (m)
1	-2	1.33E-02
2	-1.9167	1.25E-02
3	-1.8333	1.17E-02
4	-1.75	1.09E-02
5	-1.6667	1.01E-02
6	-1.5833	9.34E-03
7	-1.5	8.52E-03
8	-1.4167	7.70E-03
9	-1.3333	6.88E-03
10	-1.25	6.06E-03
11	-1.1667	5.25E-03
12	-1.0833	4.46E-03
13	-1	3.70E-03
14	-0.9167	2.96E-03
15	-0.8333	2.28E-03
16	-0.75	1.65E-03
17	-0.6667	1.10E-03
18	-0.5833	6.44E-04
19	-0.5	3.00E-04
20	-0.4166	5.09E-05
21	-0.3333	0.00E+00
22	-0.25	0.00E+00
23	-1.6667	0.00E+00
24	-0.0083	0.00E+00
25	0	0.00E+00
26	0.0083	0.00E+00
27	1.6667	0.00E+00
28	0.25	0.00E+00
29	0.3333	0.00E+00
30	0.4166	4.91E-05
31	0.5	3.00E-04
32	0.5833	6.45E-04
33	0.6667	1.10E-03
34	0.75	1.65E-03
35	0.8333	2.28E-03
36	0.9167	2.97E-03
37	1	3.70E-03
38	1.0833	4.47E-03
39	1.1667	5.26E-03
40	1.25	6.07E-03
41	1.3333	6.89E-03
42	1.4167	7.71E-03
43	1.5	8.54E-03
44	1.5833	9.35E-03
45	1.6667	1.02E-02
46	1.75	1.10E-02
47	1.8333	1.18E-02
48	1.9167	1.25E-02
49	2	1.33E-02

Table 2.2: Transverse displacement values for different radial coordinate values in the lowest out-of-plane mode

It is obvious and clear from Table 2.2 that there is no transverse deformation at the center of the disc and at the inner radius.

The comparison between deformation data of the lowest out-of-plane mode with different degrees of a polynomial function is given next.

It is clear from the following Figure 2.4 that second-degree polynomial doesn't represent accurately the deformation that was obtained using ANSYS. This concludes the requirement of higher degree polynomial in Rayleigh-Ritz procedure to represent the actual deformation shape.

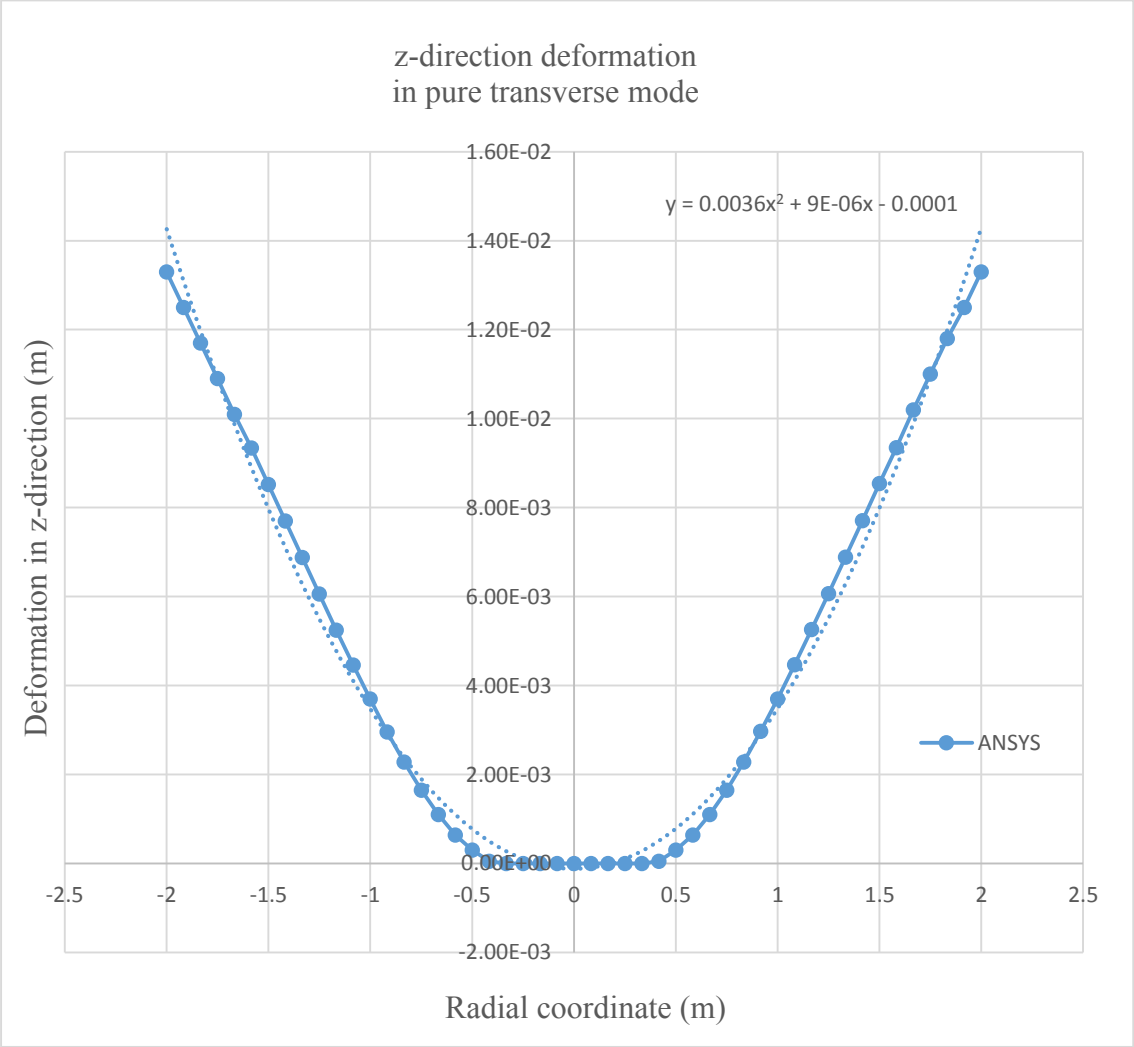

Figure 2.4: Comparison of transverse deformations in the lowest out-of-plane mode obtained using ANSYS and second-degree polynomial

In the following Figure 2.5, the comparison is made between transverse deformations in the lowest out-of-plane mode obtained using ANSYS and third-degree polynomial.

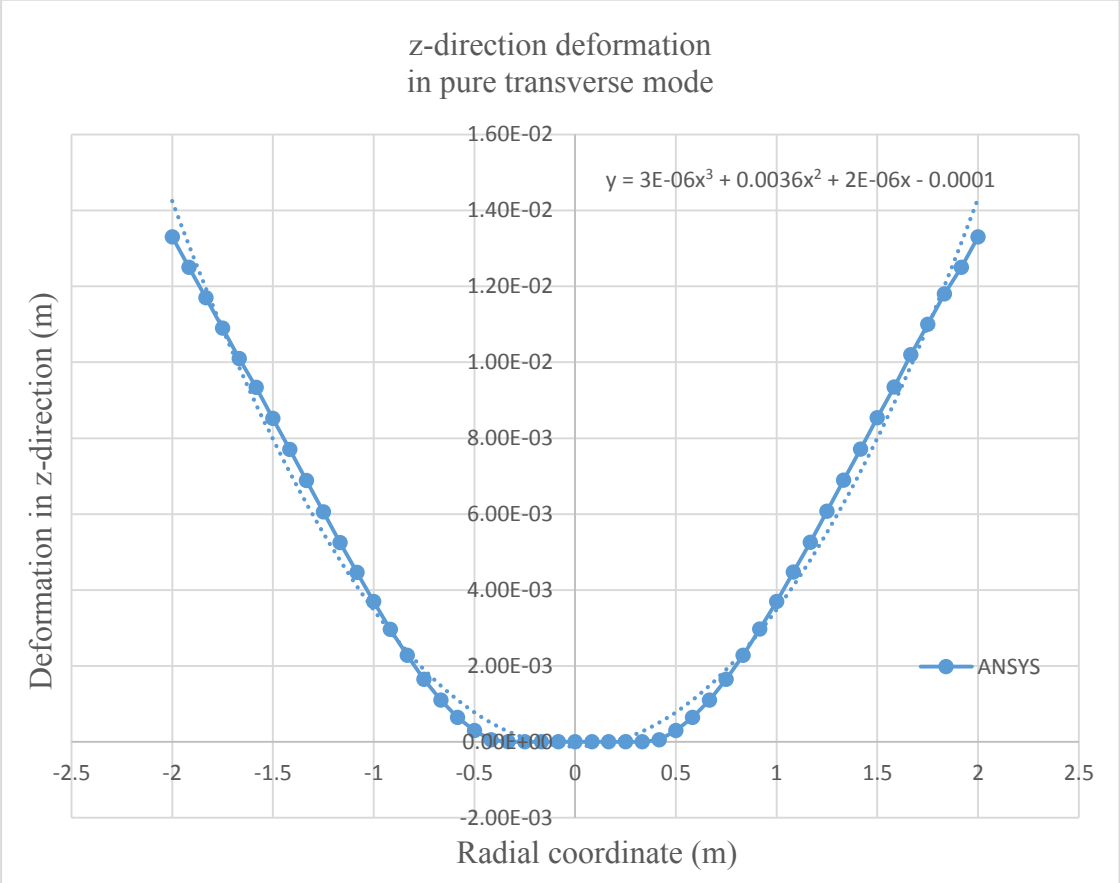

Figure 2.5: Comparison of transverse deformations in the lowest out-of-plane mode obtained using ANSYS and third-degree polynomial

It is concluded from the following Figure 2.6 that 4^{th}-degree polynomial best fits the z-direction deformation obtained using ANSYS. Both curves coincide in Figure 2.6, where the 4^{th}-degree polynomial equation is used. It means that to represent the transverse mode shape, one needs higher degree polynomial terms for W.

In Figure 2.4 to Figure 2.6, the dark dotted line represents the transverse deformation curve plotted using the transverse deformation data obtained using ANSYS. The light dotted line represents the curve obtained using the equation with assumed degree of the polynomial.

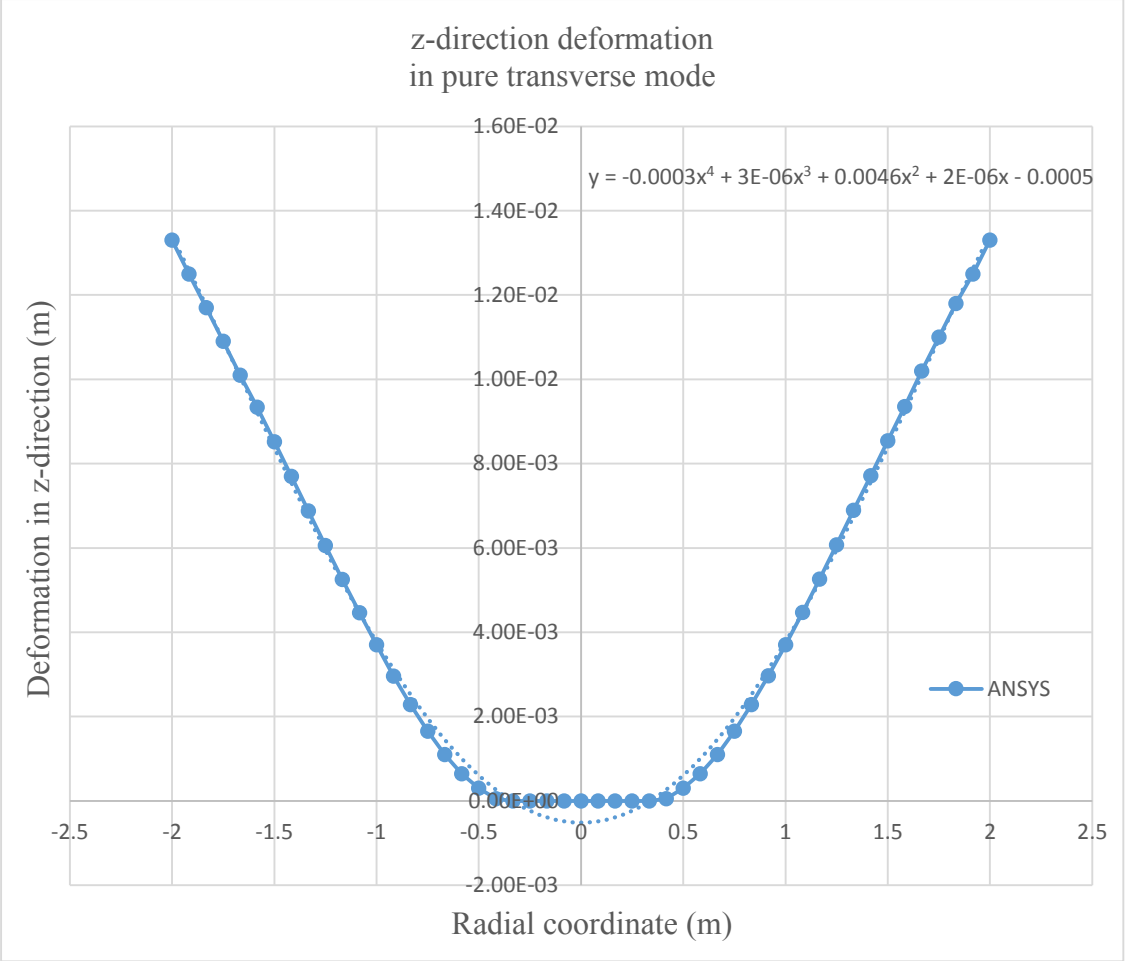

Figure 2.6: Comparison of transverse deformations in the lowest out-of-plane mode obtained using ANSYS and fourth-degree polynomial

There exists a small radial deformation in the lowest out-of-plane mode, which should be taken into account in Rayleigh-Ritz procedure. As it is 'small' radial deformation in the lowest out-of-plane mode, a number of deformation points are considered from ANSYS.

A total of 491 points are selected in the whole circumference of the disc and radial deformations are noted at each point. These deformations are shown in Table 2.3. In Table 2.3, the first column indicates the circumferential position of the point and the second column indicates the respective radial deformation.

	Circumferential Coordinate (m)	Radial deformation (m)
1	0	0.013274
2	2.56E-02	0.013274
3	5.12E-02	0.013274
4	7.69E-02	0.013274
5	0.10253	0.013274
6	0.1282	0.013274
7	0.15387	0.013274
8	0.17953	0.013274
9	0.20519	0.013274
10	0.23092	0.013274
11	0.25665	0.013274
12	0.28253	0.013274
13	0.30841	0.013274
14	0.33406	0.013274
15	0.35971	0.013274
85	2.1545	0.013277
86	2.18	0.013278
87	2.2055	0.013278
88	2.2312	0.013278
89	2.2569	0.013278
90	2.2824	0.013278
470	12.029	0.013274
471	12.055	0.013274
472	12.08	0.013274
473	12.106	0.013274
474	12.131	0.013274
475	12.157	0.013274
476	12.182	0.013274
477	12.207	0.013274
478	12.233	0.013274
479	12.259	0.013274
480	12.285	0.013274
481	12.31	0.013274
482	12.336	0.013274
483	12.362	0.013274
484	12.388	0.013274
485	12.413	0.013274
486	12.439	0.013274
487	12.465	0.013274
488	12.49	0.013274
489	12.516	0.013274
490	12.541	0.013274
491	12.566	0.013274

Table 2.3: Radial deformation values for circumferential coordinate values in the lowest out-of-plane mode

In the following Figure 2.7 to Figure 2.11, the dark dotted line represents the radial deformation curve in pure transverse mode, plotted using the r-deformation data obtained using ANSYS. The light dotted line represents the curve represented by the

equation with assumed degree of the polynomial.

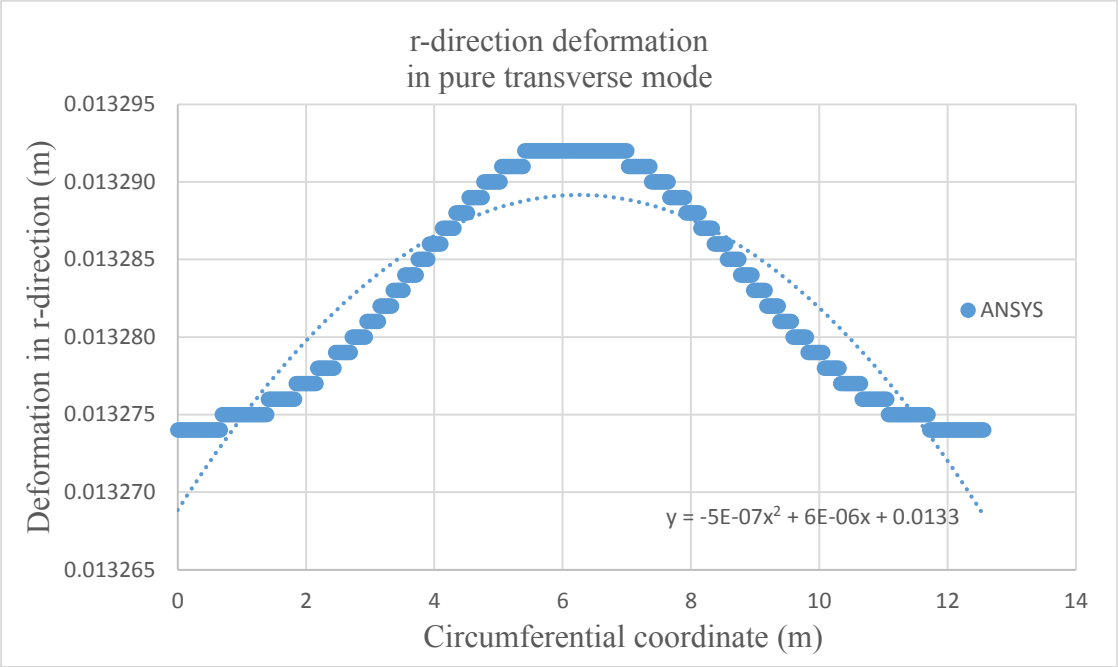

Figure 2.7: Comparison of radial deformations in the lowest out-of-plane mode obtained using ANSYS and second-degree polynomial

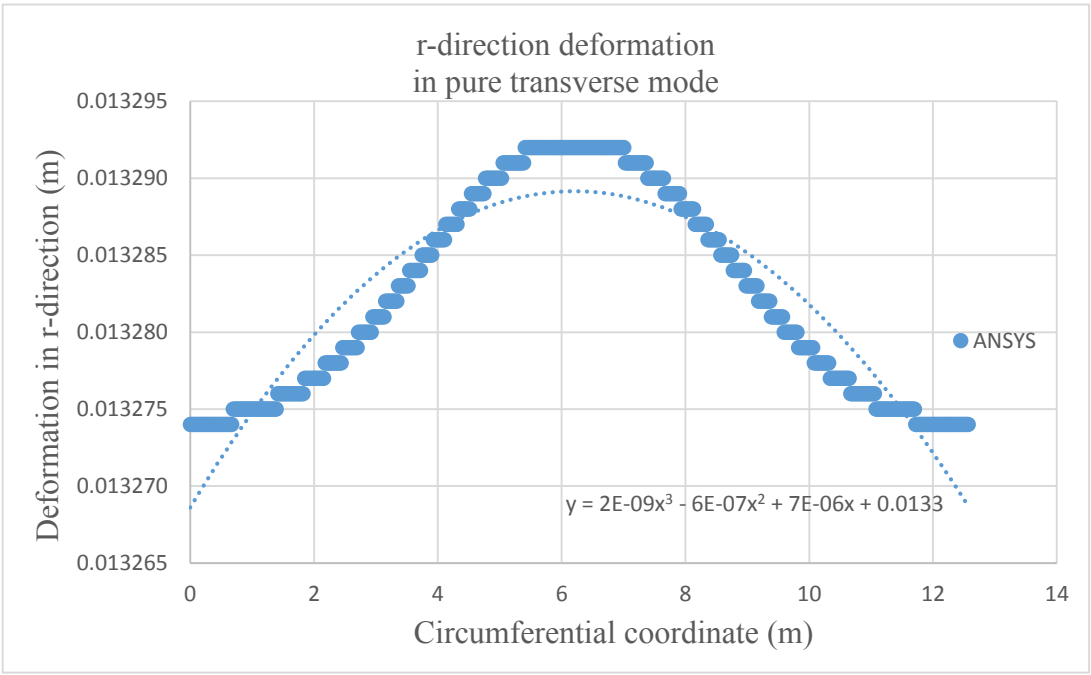

Figure 2.8: Comparison of radial deformations in the lowest out-of-plane mode obtained using ANSYS and third-degree polynomial

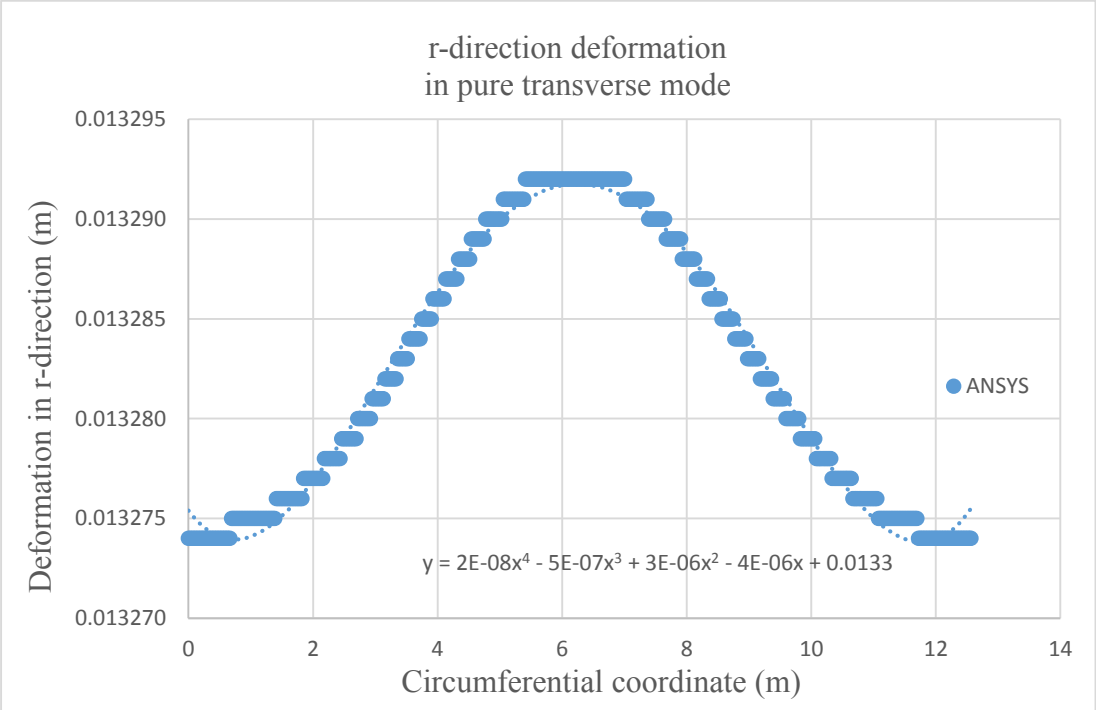

Figure 2.9: Comparison of radial deformations in the lowest out-of-plane mode obtained using ANSYS and fourth-degree polynomial

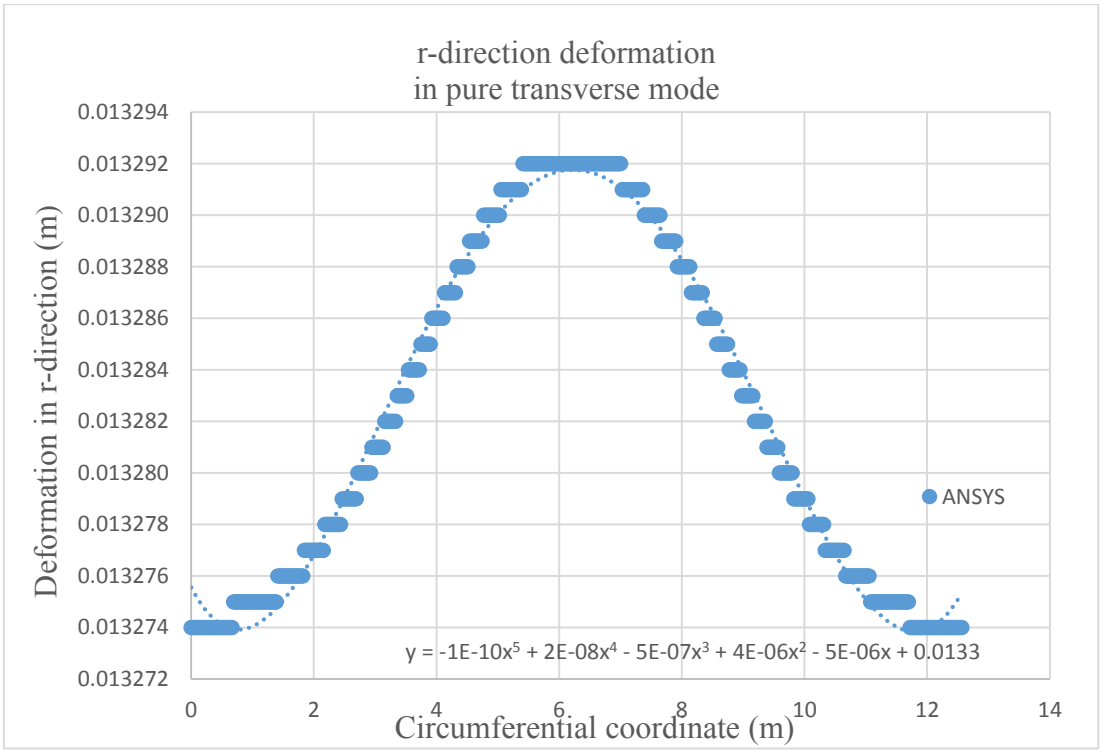

Figure 2.10: Comparison of radial deformations in the lowest out-of-plane mode obtained using ANSYS and fifth-degree polynomial

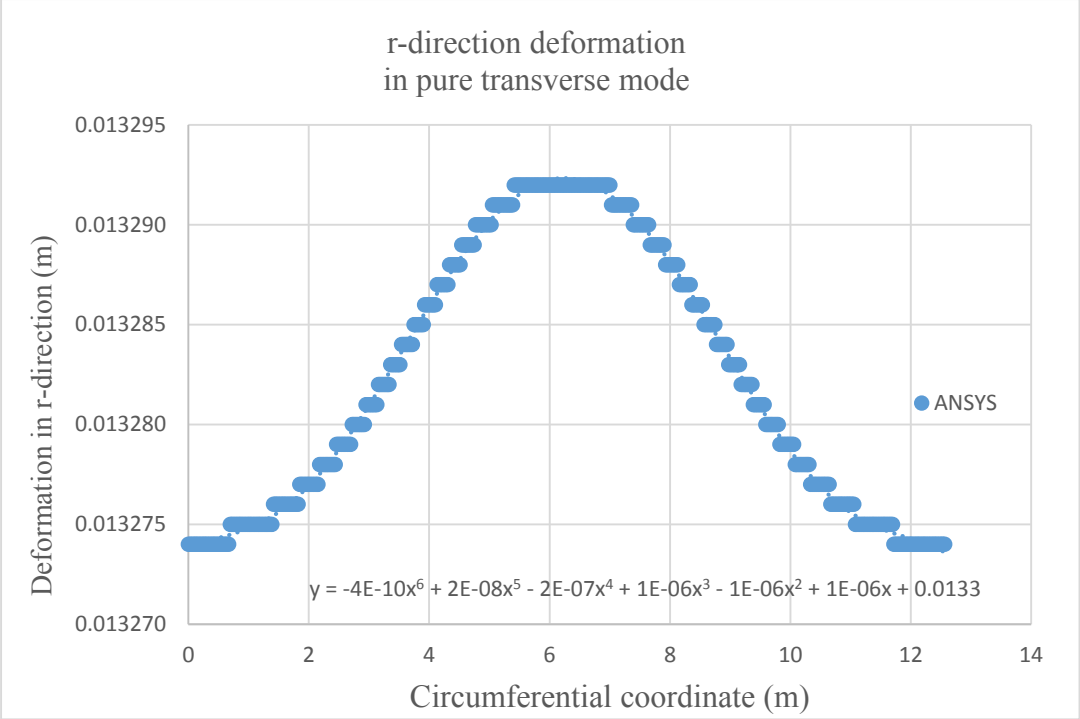

Figure 2.11: Comparison of radial deformations in the lowest out-of-plane mode obtained using ANSYS and sixth-degree polynomial

It is interpreted from Figure 2.7 to Figure 2.11 that, a 6^{th}-degree polynomial best fits the radial deformation graph obtained from the ANSYS. Hence, a higher degree of z-direction terms is needed in 'U' to have a closer approximation of the out-of-plane mode natural frequency.

The above convergence study is strictly for the lowest out-of-plane mode vibration analysis. The same methodology can be repeated to study the lowest in-plane mode and the coupled modes.

Comparison of Rayleigh-Ritz solutions obtained after convergence study is made with Finite Element solutions for natural frequencies of the lowest in-plane mode, the lowest out-of-plane mode, and the coupled modes. The comparison is shown in the following Table 2.4.

Nodal diameter number	Degree of Polynomial	Size of augmented matrix	Rayleigh-Ritz solution		ANSYS solution	
			Non-dimensional frequency	Natural Frequency (in Hz)	Natural frequency (in Hz)	
					SOLID 186	SHELL 281
$n = 0$ bending mode	$J = P = 4$ and $I = Q = 2$	30x30	0.2025	50.44	47.45	46.74
$n = 0$ in-plane mode	$K = L = 4$	25x25	0.5945	148.09	148.65	148.49
$n = 1$ coupled mode	$J = P = L = 4$ and $I = K = Q = 2$	45x45	0.1856	46.23	43.67	42.08
$n = 2$ coupled mode			0.2406	59.93	57.78	57.05
$n = 3$ coupled mode			0.4565	113.72	112.81	112.39
$n = 4$ coupled mode			0.7829	195.02	193.88	193.39

Table 2.4: Comparison of Rayleigh-Ritz solution with ANSYS solution

Recall that I, J, K, L, P and Q denote the upper limit of summation in Equations (2.23), (2.24) and (2.25).

The mode shapes of the uniform thickness disc in the lowest bending mode vibration, the lowest circumferential mode vibration, and for nodal diameter values of one, two, three and four are presented in the following Figure 2.12 to Figure 2.14:

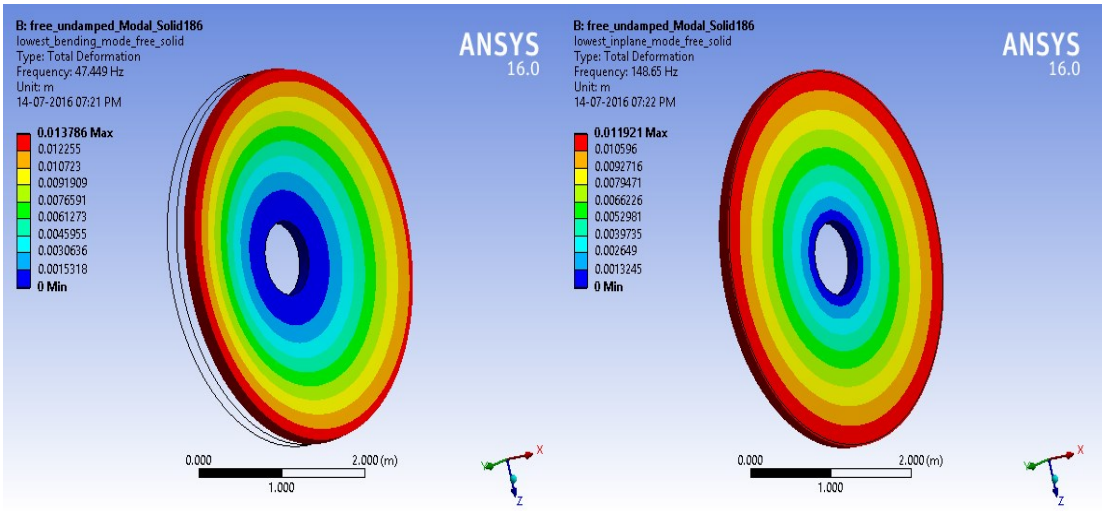

Figure 2.12: The $n = 0$ bending mode vibration and circumferential mode vibration

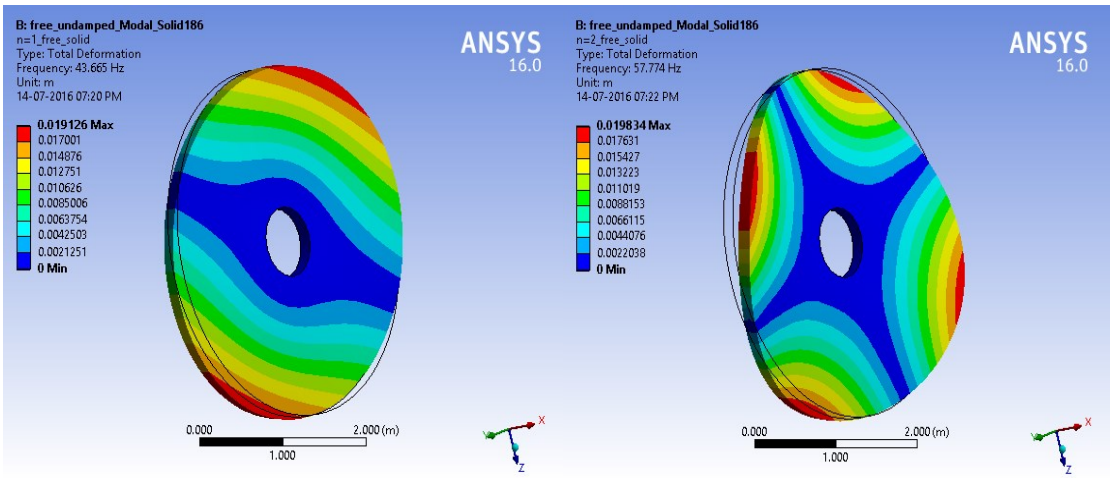

Figure 2.13:The $n = 1$ mode vibration and $n = 2$ mode vibration

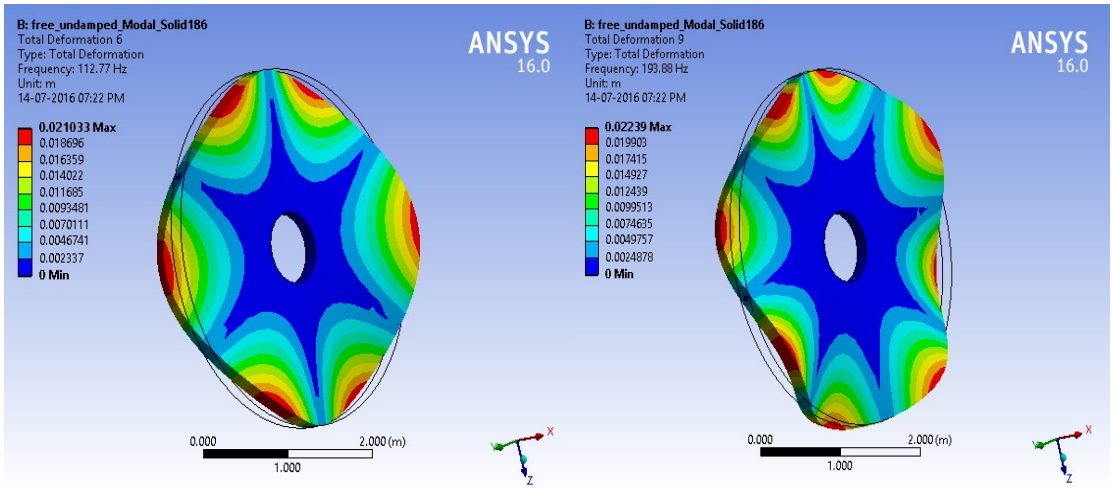

Figure 2.14: The $n = 3$ mode vibration and $n = 4$ mode vibration

2.6 Rayleigh's damping

Rayleigh's damping is proportional to a linear combination of mass and stiffness. The damping matrix can be written as follows:

$$[C] = \alpha[M] + \beta_k[K] \tag{2.55}$$

One may assume a constant damping ratio for all significant modes. That's indeed unrealistic. It is observed that modal mass participation decreases as mode number increases. From this, it is clear that as mode number increases, frequency increases according to the formula, $\omega_n = \sqrt{\frac{K}{M}}$. Considering critical damping formula, $c_c = 2\sqrt{KM}$ it can be concluded that as mode number increases, critical damping should decrease. Damping ratio can be defined as $\varsigma = \frac{C}{C_c}$. Hence, with an increase in mode number damping ratio should increase and this fact violates if one assumes a constant damping ratio for all the modes that are taken into consideration.

Hence, for the system where higher mode contribution is significant, which are pure transverse mode and pure circumferential mode in the present analysis, it is unrealistic to consider the constant damping ratio for all the modes. The main objective of the method followed here is to derive the values of α and β_k such that they should respect the variation of mass participation.

It is desirable to consider the first few modes that have significant mass participation. It is observed from the FEA of above example that 90% mass participation occurs within the 11^{th} mode. Hence, instead of assigning 5% constant damping ratio to all modes, let's define for the structural steel, minimum damping of 2% for the first mode and 5% damping for the 11^{th} mode. Now, the primary question is to determine damping ratios for the intermediate modes, and they can be best estimated

by using few techniques such as the linear interpolation, 11th significant mode approximation, full range approximation and damping ratio based on average data. These techniques are explained in the following paragraphs [42].

Dataset based on linear interpolation can be obtained by,

$$\varsigma_i = \frac{\varsigma_m - \varsigma_1}{\omega_m - \omega_1}(\omega_i - \omega_1) + \varsigma_1 \tag{2.56}$$

where, m is the 11th (significant) mode within which 90% of mass participation is observed from FEA.

For the second data set, recall that 90% mass participation factor is found at 11th mode from ANSYS. Let's rename 11th mode as the significant mode.

For the first mode,

$$2\omega_1\varsigma_1 = \alpha + \beta_k\omega_1^2 \tag{2.57}$$

For the significant mode (i.e. 11th mode),

$$2\omega_{11}\varsigma_{11} = \alpha + \beta_k\omega_{11}^2 \tag{2.58}$$

Damping coefficients α and β can be calculated from Equations (2.57) and (2.58).

$$\beta_k = \frac{2\omega_1\varsigma_1 - 2\omega_{11}\varsigma_{11}}{\omega_1^2 - \omega_{11}^2} \tag{2.59}$$

$$\alpha = 2\omega_1\varsigma_1 - \beta_k\omega_1^2 \tag{2.60}$$

For this example, $\beta_k = 0.000054$ and $\alpha = 7.1$. Therefore, the subsequent modal damping ratio can be calculated by $\varsigma_i = \frac{\alpha}{2\omega_i} + \frac{\beta_k\omega_i}{2}$.

For the third data set, consider generating the second data set using the above procedure but for $\varsigma_1, \omega_1, \varsigma_{2.5m}$ and $\omega_{2.5m}$. Here, 2.5m is considered to have full range

approximation. This way we have Rayleigh's damping coefficients $\beta_k = 0.0000465$ and $\alpha = 7.9$.

The fourth data set is based on the average of the second and the third data sets. Results of all four data sets are given in Table 2.5.

Estimation of Rayleigh's damping coefficients						
Mode number	Natural Frequency from ANSYS (Hz)	Circular natural frequency from ANSYS (rad/sec)	Damping ratio based on linear interpolation	Damping ratio based on 11^{th} mode approximation	Damping ratio based on full range approximation	Damping ratio based on average data
1	43.436	273.0263	0.0200	0.0200	0.0208	0.0204
2	43.487	273.3469	0.0200	0.0204	0.0208	0.0206
3	47.216	296.7863	0.0205	0.0200	0.0202	0.0201
4	57.635	362.2771	0.0218	0.0196	0.0193	0.0195
5	57.659	362.4280	0.0218	0.0196	0.0193	0.0195
6	112.75	708.7143	0.0287	0.0241	0.0221	0.0231
7	112.76	708.7771	0.0287	0.0241	0.0221	0.0231
8	148.61	934.1200	0.0332	0.0290	0.0259	0.0275
9	193.9	1218.8000	0.0388	0.0358	0.0316	0.0337
10	193.91	1218.8629	0.0388	0.0358	0.0316	0.0337
11	283.15	1779.8000	0.0500	0.0500	0.0436	0.0468
12	294.04	1848.2514	0.0514	0.0518	0.0451	0.0485
13	294.07	1848.4400	0.0514	0.0518	0.0451	0.0485
14	301.26	1893.6343	0.0523	0.0530	0.0461	0.0496
15	301.66	1896.1486	0.0523	0.0531	0.0462	0.0496
16	363.51	2284.9200	0.0601	0.0632	0.0549	0.0590
17	363.72	2286.2400	0.0601	0.0633	0.0549	0.0591
18	387.35	2434.7714	0.0630	0.0672	0.0582	0.0627
19	387.35	2434.7714	0.0630	0.0672	0.0582	0.0627
20	411	2583.4286	0.0660	0.0711	0.0616	0.0664
21	411.04	2583.6800	0.0660	0.0711	0.0616	0.0664
22	476.76	2996.7771	0.0742	0.0821	0.0710	0.0765
23	476.89	2997.5943	0.0742	0.0821	0.0710	0.0766
24	543.47	3416.0971	0.0826	0.0933	0.0806	0.0869
25	543.52	3416.4114	0.0826	0.0933	0.0806	0.0869
26	631.91	3972.0057	0.0936	0.1081	0.0933	0.1007
27	632.02	3972.6971	0.0937	0.1082	0.0934	0.1008
28	649.57	4083.0114	0.0959	0.1111	0.0959	0.1035

Table 2.5: Estimation of Rayleigh's damping coefficients

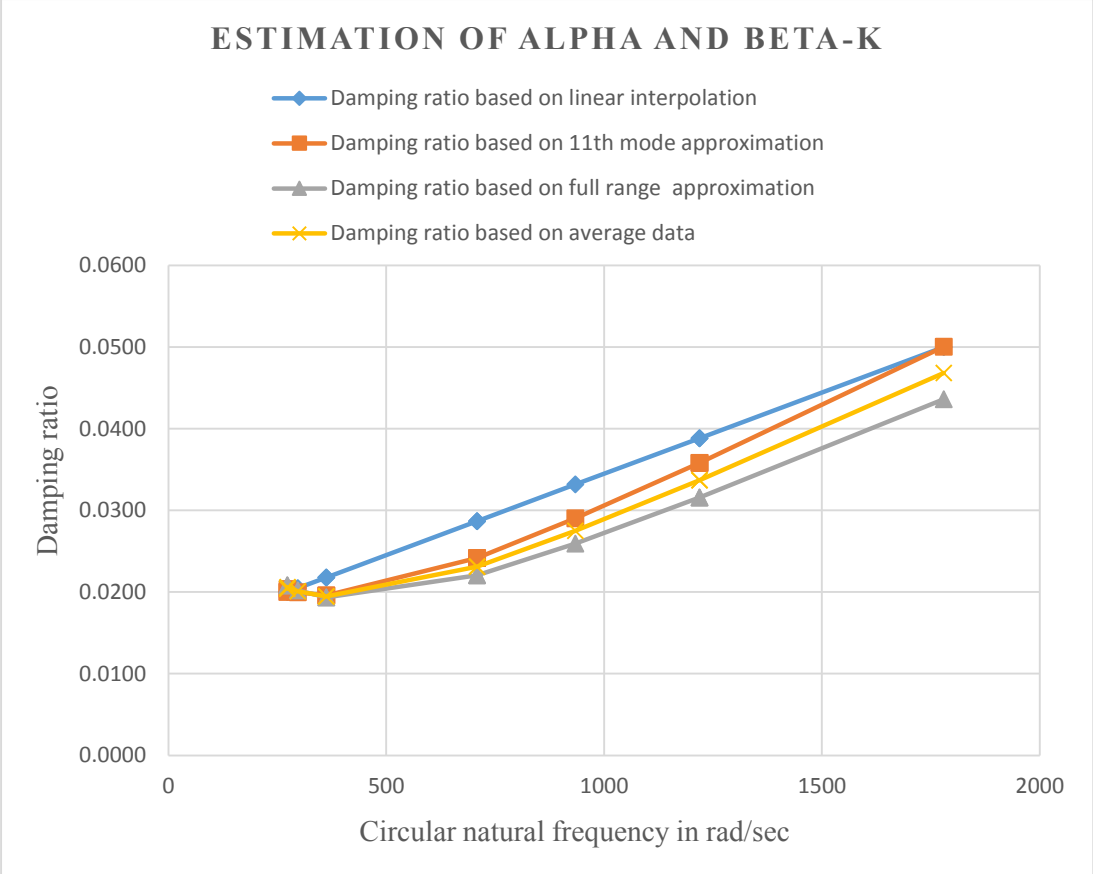

Figure 2.15: Variation of damping ratio with circular natural frequency

It is concluded from above Figure 2.15 that Rayleigh's damping coefficients based on 11th mode approximation are closer to that of the linear approximation and hence they are considered as the input for further dynamic analysis. This data set is also fed to ANSYS to get the damped natural frequencies.

This procedure is used here as it is simple to get the spreadsheet for different damping ratio values and corresponding values of Rayleigh's damping coefficients, which indeed respect the increasing nature of damping ratio as the mode number increases. The obtained values of 'alpha' and 'beta-k' can be fed as the input data for the dynamic analysis to estimate damped natural frequencies.

2.7 Formulation for Orthotropic disc

Formulations presented from Section 2.2 to Section 2.5 are limited to the materials having isotropic property. Nowadays, composite materials have drawn the attention of researchers in many applications due to their many advantageous properties such as light weight and higher stiffness to name a few. This section presents in-plane and out-of-plane vibration analysis of the orthotropic disc.

2.7.1 Modelling strain energy and kinetic energy

In the presented formulation, the principal material coordinate system is used. The axis 1 is aligned with the fiber direction and the axis 2 is in the plane of the layer and also perpendicular to the fiber direction. Let axis 3 be in the direction perpendicular to the layer and also perpendicular to the fiber direction.

Recall the strain energy formulation for isotropic disc described in sub-section 2.1.1, rewriting it with newly defined coordinate system,

$$\Pi_{ortho} = \frac{1}{2}\int_{-\frac{h}{2}}^{\frac{h}{2}}\int_{0}^{2\pi}\int_{R_i}^{R_o}[\sigma_1 \quad \sigma_2 \quad \sigma_3 \quad \sigma_{12} \quad \sigma_{23} \quad \sigma_{13}]\begin{bmatrix}\varepsilon_1\\ \varepsilon_2\\ \varepsilon_3\\ 2\varepsilon_{12}\\ 2\varepsilon_{23}\\ 2\varepsilon_{13}\end{bmatrix} r\,dr\,d\theta\,dz \tag{2.61}$$

For orthotropic disc, stress-strain relationship is as follows:

$$\begin{bmatrix}\sigma_1\\ \sigma_2\\ \sigma_3\\ \sigma_{23}\\ \sigma_{13}\\ \sigma_{12}\end{bmatrix} = \begin{bmatrix}C_{11} & C_{12} & C_{13} & 0 & 0 & 0\\ C_{12} & C_{22} & C_{23} & 0 & 0 & 0\\ C_{13} & C_{23} & C_{33} & 0 & 0 & 0\\ 0 & 0 & 0 & C_{44} & 0 & 0\\ 0 & 0 & 0 & 0 & C_{55} & 0\\ 0 & 0 & 0 & 0 & 0 & C_{66}\end{bmatrix}\begin{bmatrix}\varepsilon_1\\ \varepsilon_2\\ \varepsilon_3\\ 2\varepsilon_{23}\\ 2\varepsilon_{13}\\ 2\varepsilon_{12}\end{bmatrix} \tag{2.62}$$

Furthermore, the strain-displacement relationship is assumed linear. In cylindrical coordinate system,

$$\varepsilon_1 = \frac{\partial u_1}{\partial r} \tag{2.63}$$

$$\varepsilon_2 = \frac{u_1}{r} + \frac{1}{r}\frac{\partial u_2}{\partial \theta} \tag{2.64}$$

$$\varepsilon_3 = \frac{\partial u_3}{\partial z} \tag{2.65}$$

$$\varepsilon_{12} = \frac{1}{2}\left(\frac{1}{r}\frac{\partial u_1}{\partial \theta} + \frac{\partial u_2}{\partial r} - \frac{u_2}{r}\right) \tag{2.66}$$

$$\varepsilon_{13} = \frac{1}{2}\left(\frac{\partial u_1}{\partial z} + \frac{\partial u_3}{\partial r}\right) \tag{2.67}$$

$$\varepsilon_{23} = \frac{1}{2}\left(\frac{1}{r}\frac{\partial u_3}{\partial \theta} + \frac{\partial u_2}{\partial z}\right) \tag{2.68}$$

Substituting Equations (2.63) to (2.68) in Equation (2.61), total strain energy of the orthotropic disc is given by,

$$\begin{aligned}\Pi_{ortho} = \frac{1}{2}\int_{\frac{-h}{2}}^{\frac{h}{2}}\int_0^{2\pi}\int_{R_i}^{R_o} & C_{11}\left(\frac{\partial u_1}{\partial r}\right)^2 + C_{22}\left(\frac{u_1}{r} + \frac{1}{r}\frac{\partial u_2}{\partial \theta}\right)^2 \\ & + C_{33}\left(\frac{\partial u_3}{\partial z}\right)^2 + C_{44}\left(\frac{1}{r}\frac{\partial u_3}{\partial \theta} + \frac{\partial u_2}{\partial z}\right)^2 \\ & + C_{55}\left(\frac{\partial u_1}{\partial z} + \frac{\partial u_3}{\partial r}\right)^2 + C_{66}\left(\frac{1}{r}\frac{\partial u_1}{\partial \theta} + \frac{\partial u_2}{\partial r} - \frac{u_2}{r}\right)^2 \\ & + 2C_{12}\left(\frac{\partial u_1}{\partial r}\right)\left(\frac{u_1}{r} + \frac{1}{r}\frac{\partial u_2}{\partial \theta}\right) + 2C_{13}\left(\frac{\partial u_1}{\partial r}\right)\left(\frac{\partial u_3}{\partial z}\right) \\ & + 2C_{23}\left(\frac{u_1}{r} + \frac{1}{r}\frac{\partial u_2}{\partial \theta}\right)\left(\frac{\partial u_3}{\partial z}\right) r\,dr\,d\theta\,dz\end{aligned} \tag{2.69}$$

Equation (2.69) is derived in non-dimensional form, which is given next:

$$\Pi_{ortho} = \frac{h}{2}\int_{\frac{-1}{2}}^{\frac{1}{2}}\int_{\beta}^{1}\int_{0}^{2\pi} C_{11}\left(\frac{\partial \mathrm{u}_1}{\partial \zeta}\right)^2 + C_{22}\left(\frac{\mathrm{u}_1}{\zeta}+\frac{1}{\zeta}\frac{\partial \mathrm{u}_2}{\partial \theta}\right)^2 + C_{33}\left(\frac{R_o}{h}\frac{\partial \mathrm{u}_3}{\partial \xi}\right)^2 + C_{44}\left(\frac{1}{\zeta}\frac{\partial \mathrm{u}_3}{\partial \theta}+\frac{R_o}{h}\frac{\partial \mathrm{u}_2}{\partial \xi}\right)^2 + C_{55}\left(\frac{R_o}{h}\frac{\partial \mathrm{u}_1}{\partial \xi}+\frac{\partial \mathrm{u}_3}{\partial \zeta}\right)^2 + C_{66}\left(\frac{1}{\zeta}\frac{\partial \mathrm{u}_1}{\partial \theta}+\frac{\partial \mathrm{u}_2}{\partial \zeta}-\frac{\mathrm{u}_2}{\zeta}\right)^2 + 2C_{12}\left(\frac{\partial \mathrm{u}_1}{\partial \zeta}\right)\left(\frac{\mathrm{u}_1}{\zeta}+\frac{1}{\zeta}\frac{\partial \mathrm{u}_2}{\partial \theta}\right) + 2C_{13}\left(\frac{\partial \mathrm{u}_1}{\partial \zeta}\right)\left(\frac{R_o}{h}\frac{\partial \mathrm{u}_3}{\partial \xi}\right) + 2C_{23}\left(\frac{R_o}{h}\right)\left(\frac{\mathrm{u}_1}{\zeta}+\frac{1}{\zeta}\frac{\partial \mathrm{u}_2}{\partial \theta}\right)\left(\frac{\partial \mathrm{u}_3}{\partial \xi}\right)\zeta\, d\theta\, d\zeta\, d\xi \tag{2.70}$$

Similarly, non-dimensional form of total kinetic energy of the orthotropic disc,

$$T_{ortho} = \frac{1}{2}\,\rho h R_o^2 \int_{\frac{-1}{2}}^{\frac{-1}{2}}\int_{\beta}^{1}\int_{0}^{2\pi}\left[\left(\frac{\partial u_1}{\partial t}\right)^2 + \left(\frac{\partial u_2}{\partial t}\right)^2\left(\frac{\partial u_3}{\partial t}\right)^2\right]\zeta\, d\theta\, d\zeta\, d\xi \tag{2.71}$$

Same approach as discussed in Section 2.3.1 and Section 2.3.2 is considered in order to derive the maximum strain energy and the maximum kinetic energy for the orthotropic disc.

2.7.2 In-plane and out-of-plane vibration analysis of orthotropic disc

The deformed shape of pure circumferential mode can be best represented by evaluating Equation (2.50) at n equals to zero. For in-plane vibration analysis of orthotropic disc, an eigenvalue problem can be formulated in the similar manner as explained in sub-section 2.3.3.

Similarly, to calculate the frequency of the lowest out-of-plane mode of the orthotropic disc, Equations (2.43) and (2.45) are evaluated for zero nodal diameter number.

Afterwards, displacement polynomials in radial and transverse directions are substituted in Equation (2.70) and Equation (2.71). Later, Rayleigh-Ritz solutions for the lowest in-plane mode and the lowest out-of-plane mode are compared with finite element solutions to validate the results. Material properties of the Graphite-Polymer composite are given in Table 2.6.

Material properties	Value	Material properties	Value
E_1	155 GPa	G_{12}	4.40 GPa
E_2	12.10 GPa	G_{13}	4.40 GPa
E_3	12.10 GPa	G_{23}	3.20 GPa
v_{12}	0.248	v_{23}	0.458
v_{13}	0.248	$\rho_{ortho} = 1800 \frac{kg}{m^3}$	

Table 2.6: Material properties of the orthotropic disc [43]

The dimensions of the orthotropic disc are taken the same as that of the isotropic disc, described in Section 2.5. The simulation is conducted using SHELL 281 and SHELL 181 elements in ANSYS. SHELL 181 is a four-node element with six degrees of freedom at each node (translations in the X, Y and Z directions and rotations about the X, Y, and Z axes) as shown in the following Figure 2.16. This type of shell element is well suited for analysing thin to moderately thick shell structures. Moreover, SHELL 181 is well-suited for linear, and large rotation and/or large strain nonlinear applications.

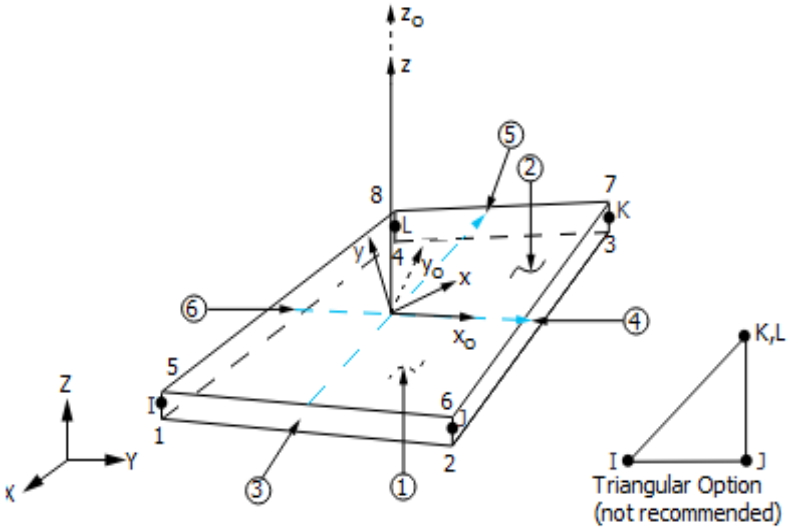

Figure 2.16: Geometry of SHELL 181 [41]

The following Table 2.7 shows the comparison of the lowest circumferential mode and the lowest bending mode natural frequencies of C-F disc made of orthotropic material calculated using Rayleigh-Ritz method and ANSYS.

Lowest in-plane and out-of-plane mode frequencies			
Mode type	Rayleigh-Ritz solution (in Hz)	ANSYS solution using SHELL 281 elements (in Hz)	ANSYS solution using SHELL 181 elements (in Hz)
Circumferential $K = L = 4$	75.95	78.86	74.55
Bending $I = J = P = Q = 3$	39.71	37.00	37.82

Table 2.7: Comparison of natural frequencies for the orthotropic disc

It is observed from above Table 2.7 that the lowest bending mode natural frequency of the disc is less than circumferential mode natural frequency. It is because of the lower stiffness of the orthotropic disc in transverse direction.

2.8 Parametric study

Effect of thickness of the disc on the lowest bending mode natural frequency, the lowest circumferential mode natural frequency and the coupled mode natural frequencies is depicted in the following Table 2.8. It is concluded that the lowest bending mode and the coupled mode natural frequencies increase because of the fact that the stiffness of the disc increases with thickness. The lowest in-plane mode natural frequency is constant with thickness variation. The dimensions and material properties are considered as given in Section 2.5.

Mode set	Ω of 0.2 m thickness disc	Ω of 0.3 m thickness disc
$n = 0$ bending mode	0.2668	0.3919
$n = 0$ circumferential mode	0.61255	0.608
$n = 1$ coupled	0.2494	0.3491
$n = 2$ coupled	0.3132	0.4485
$n = 3$ coupled	0.5992	0.8722

Table 2.8: Variation of non-dimensional frequency parameter with thickness of the disc

Effect of thickness of the disc made of Graphite-Polymer composite material is shown in the following Table 2.9.

Mode type	Outer thickness (in m)	RR solution (Hz)	ANSYS SHELL 281 element (Hz)	ANSYS SHELL 181 element (Hz)
Circumferential $K = L = 4$	0.2	78.84	78.92	74.58
	0.3	75.73	78.91	74.73
Bending $J = P = 7, I = Q = 4$	0.2	46.67	47.27	48.69
	0.3	66.22	65.37	67.42

Table 2.9 : Effect of thickness on in-plane and out-of-plane natural frequencies of Graphite-Polymer composite disc

Note that higher order polynomial is chosen to represent the bending mode shape of a composite disc. These are the minimum number of terms required to make the polynomial mathematically complete. In Equations (2.23), (2.24) and (2.25), chosen upper limits of summation are shown in Table 2.9. Again, in determining the upper limits in Equations (2.23) and (2.25) to represent the deformed shape in bending mode vibrations, the equal number of cross terms in r and z directions (i.e. $J = P = 7$) are chosen to prevent the matrix ill-conditioning.

The variation of non-dimensional frequency parameter $\sqrt{2\omega^2 R_0^2 \frac{\rho(1+\nu)}{E}}$ with Poisson's ratio is shown in the following Table 2.10.

Mode set	Non-dimensional frequency parameter $\sqrt{2\omega^2 R_0^2 \frac{\rho(1+\nu)}{E}}$	
	$\nu = 0.33$	$\nu = 0.4$
$n = 0$ bending mode	0.2083	0.2243
$n = 0$ circumferential mode	0.5945	0.5945
$n = 1$ coupled	0.1745	0.1998
$n = 2$ coupled	0.2243	0.2359
$n = 3$ coupled	0.4476	0.4527

Table 2.10: Variation of non-dimensional frequency parameter with Poisson's ratio of the circular clamped-free disc of uniform thickness

It can be seen from above Table 2.10 that the lowest bending mode natural frequency increases with the Poisson's ratio and the lowest circumferential mode natural frequency decreases with Poisson's ratio. The numerical data shown in above Table 2.10 is non-dimensional. The non-dimensional factors associated with Poisson's ratio of 0.33 and 0.4 are 246.28 and 240.044 respectively (and they should be multiplied with respective frequency parameters shown in above Table 2.10 to calculate natural frequencies).

2.9 Conclusion

In this Chapter, the elastic behaviour of the circular disc of uniform thickness is presented in Section 2.2. In Section 2.3, Rayleigh-Ritz method is presented. The trigonometric functions in circumferential coordinate are employed in Rayleigh-Ritz method. In Sections 2.5 and 2.8, free vibration analyses of the circular disc of uniform thickness made of Structural Steel material and Graphite-Polymer composite material are presented. A summary of observations is as follows:

- For the circular disc made of Graphite-Polymer composite material, the natural frequency of circumferential mode only depends on the shear modulus of the material. The circumferential mode natural frequency almost remains constant with the variation of the disc thickness parameter.
- The lowest bending mode natural frequency increases with the thickness in both isotropic and orthotropic cases.
- For the isotropic disc, the lowest bending mode natural frequency increases with the Poisson's ratio of the material. The natural frequencies of vibration modes of higher nodal diameter numbers increase with Poisson's ratio.
- For the moderately thick discs, it is concluded that, the lowest circumferential mode frequency is higher than the lowest bending mode frequency because of the fact that the circumferential mode vibration involves shearing, in which the sole component of deformation is tangential to the disc middle surface and this behaviour causes the higher stiffness of the disc in circumferential mode vibration compared to the bending mode vibration in which the sole component of displacement present is normal to the disc middle surface (although there exists 'small' radial displacement component as explained in Section 2.5).

- Rayleigh's damping coefficients calculated based on modal mass participation yield more realistic damping characteristic of circular clamped-free disc.

Chapter 3

Three-dimensional in-plane and out-of-plane vibrations of linearly-tapered clamped-free disc

3.1 Introduction

This chapter presents the generalized formulation to investigate the lowest in-plane mode and the lowest out-of-plane mode natural frequencies of the linearly-tapered disc by proposed solution technique which employs conventional Rayleigh-Ritz method with finite-element-like modification. Three-dimensional in-plane and out-of-plane mode vibrations of a circular tapered disc made of isotropic and orthotropic materials are investigated. In all the parametric studies for the orthotropic disc, Graphite-Polymer composite material is considered and for the isotropic disc, Structural Steel material is considered. The material properties of Graphite-Polymer composite material are given in Table 2.6. The clamped-free boundary condition is considered in this Chapter. Effect of linear taper on the lowest circumferential mode and the lowest out-of-plane mode natural frequencies is studied. Rayleigh-Ritz solutions are compared with the results calculated using ANSYS.

As discussed in Section 1.2, the increasing demand for realistic dynamic analysis of thick structural components such as a tapered circular disc in automotive or turbomachinery applications necessitates the requirement for development of robust three-dimensional models and their solution procedures.

Nowadays, finite element solvers are used increasingly for modelling three-dimensional problems. Industrial finite element packages make use of 3-D elements such as tetrahedral, hexahedra etc. One of the major difficulties associated with the use

of such 3-D elements is that one needs a large number of elements to solve the static analysis problem. This fact is quite true for the dynamic analysis also. Again, this makes the finite element solver to solve a large number of simultaneous equations [44]. In this Chapter, this problem is tackled with the presented numerical technique.

The GEnx Commercial Aircraft Engine is used for powering Boeing 747-8 and Boeing 787 Dreamliner. It is the bypass turbofan engine of 21st century consisting of carbon-fiber composite fan blades. GEnx-1B engine offers advantages in terms of weight and delivers up to 15% better specific fuel consumption than its predecessors. This engine has the fan diameter of 111.1 inch and the inner thickness of the blisk is 0.39 m [45]. The later dimension was measured through its CAD drawing. The following Figure 3.1 shows the front view and isometric view of the same.

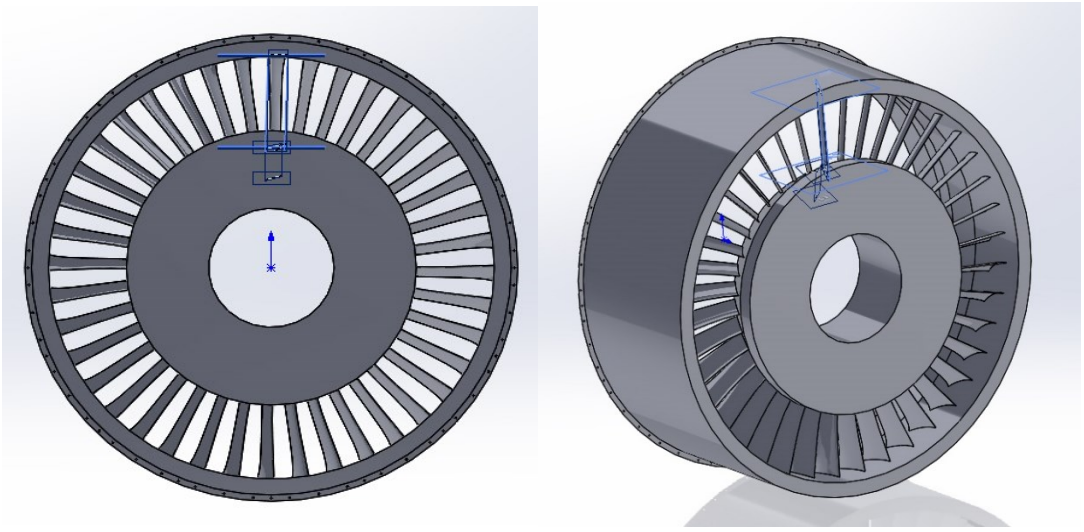

Figure 3.1: CAD geometry of turbofan of GEnx

The above Figure 3.1 shows one of the applications of thick circular annular discs of clamped-free boundary condition. To study the dynamic behaviour of such blisk, it can be modelled as a thick linearly-tapered disc of clamped-free boundary condition. To accurately predict the in-plane and out-of-plane vibration responses of such thick disc, the development of an efficient three-dimensional model is essential.

3.2 Modelling

The basic idea in the finite element method is to solve a complicated problem by replacing it by a simpler one. More specifically, the entire domain of the problem is represented as an assemblage of subdivisions called finite elements. These elements are interconnected at the boundaries of the adjacent elements. These specified joints are called nodes. Generally, we assume the variation of the displacement field (or any other field variable of interest) inside a finite element using a simple approximation function. These functions can be represented as the linear combination of constant coefficients and algebraic displacement terms. By satisfying the boundary condition at a node, such approximating functions can be defined in terms of the values of field variables (here, displacement) at the nodes. To derive the elemental equations, the Lagrange functional can be minimized with respect to each nodal unknown coefficients. Again, the Lagrange functional can be written as the summation of each element contribution. The substitution of assumed displacement polynomial which is indeed a function of unknown nodal value matrix into the minimization of each elemental Lagrange functional leads to the derivation of elemental mass and elemental stiffness matrices [44]. Through the proper assemblage of such elemental mass and elemental stiffness matrices, global stiffness and global mass matrices of the structural system can be calculated. This way finite element method can be summarized as an element wise application of Rayleigh-Ritz method.

Recall the explanation given in sub-section 1.3.1 for the Rayleigh-Ritz method. In this method, an approximate solution to the problem is developed over the entire domain.

In the presented numerical approach, the domain of linearly-tapered disc is divided into subdomains, similar to finite element method. Further, an approximate solution to the problem for each element is developed over the entire domain of linearly-tapered disc, not just over each element as in the case of finite element method. Hence, this approach leads to less number of terms in the approximate functions needed to calculate the natural frequencies that are closer to the exact solutions compared to finite element method.

In the following Figure 3.2, linearly-tapered disc of clamped-free boundary condition is represented in cylindrical coordinate system. R_i and R_o represent the inner radius and outer radius of the disc respectively. The inner and outer thicknesses of the disc are indicated by h_i and h_o.

As shown in Figure 3.2, the linearly-tapered disc is divided into a number of divisions, let it be any positive integer number, in order to model the tapered shape of a non-deformed disc. Midpoint thickness of each division is calculated, and strain energy and kinetic energy are integrated over the respective division, keeping the displacement polynomials global over each division. Later, strain energies and kinetic energies of all divisions are added in order to derive the total strain energy and total kinetic energy of the linearly-tapered disc.

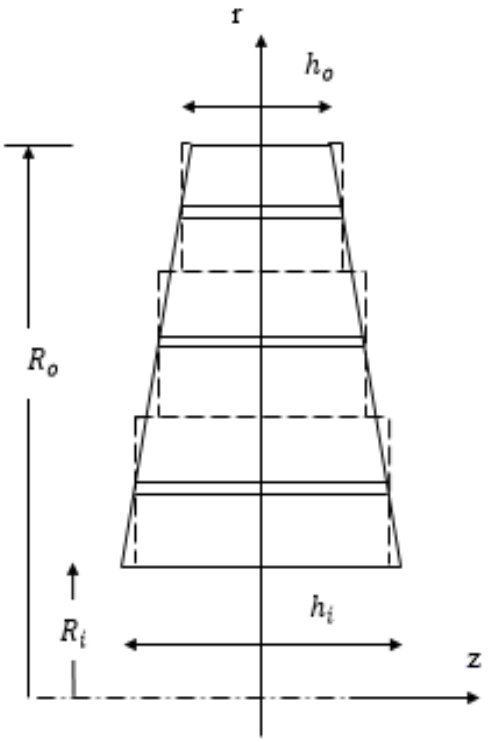

Figure 3.2: Cross-sectional geometry and coordinate system of linearly-tapered disc

3.2.1 Maximum strain energy and maximum kinetic energy

For linearly-tapered disc, total strain energy is derived by adding the strain energy of each division (which is basically derived by integrating it with reference to midpoint thickness and respective radius ratio). It is important to note that thickness term and radius term, according to the respective division, are multiplied inside of the equations of energies unlike the formulation for the case of the uniform-thickness disc. Again, recalling that the non-dimensional term $a = \frac{R_o}{h}$ appears in Equation (2.27), which holds true for the uniform-thickness disc case, here it must be modified for each division.

Maximum strain energy of linearly-tapered disc is calculated by the following Equation (3.1):

$$
\begin{aligned}
&(\pi_{max})_{LT} \\
&= \frac{E}{4(1+v)}\left(\int_{-\frac{1}{2}}^{\frac{1}{2}}\int_{\beta_1}^{1}\int_{0}^{2\pi} h_{mid1}\,(terms\ of\ \Pi_1)\,\zeta d\theta\, d\zeta\, d\xi\right. \\
&+ \int_{-\frac{1}{2}}^{\frac{1}{2}}\int_{\beta_2}^{1}\int_{0}^{2\pi} h_{mid2}\,(terms\ of\ \Pi_2)\,\zeta d\theta\, d\zeta\, d\xi \\
&+ \int_{-\frac{1}{2}}^{\frac{1}{2}}\int_{\beta_3}^{1}\int_{0}^{2\pi} h_{mid3}\,(terms\ of\ \Pi_3)\,\zeta d\theta\, d\zeta\, d\xi \\
&+ \ldots\ldots\ldots \int_{-\frac{1}{2}}^{\frac{1}{2}}\int_{\beta_N}^{1}\int_{0}^{2\pi} h_{midN}\,(terms\ of\ \Pi_N)\,\zeta d\theta\, d\zeta\, d\xi \left.\right)
\end{aligned}
\tag{3.1}
$$

where, $terms\ of\ \Pi_N$ are obtained from Equation (2.26). where, $a_N = \frac{R_{oN}}{h_N}$ and N is the division number.

$$
\begin{aligned}
terms\ of\ \Pi_N = \frac{2v}{1-2v}&\left(\left(\frac{\partial U}{\partial \zeta}\right)\sin n\theta - \frac{n\,V\sin n\theta}{\zeta} + \frac{U\sin n\theta}{\zeta}\right. \\
&\left. + a_N\left(\frac{\partial \mathrm{W}}{\partial \xi}\sin n\theta\right)^2\right) + 2\left(\frac{\partial U}{\partial \zeta}\sin n\theta\right)^2 \\
&+ 2\left(\frac{U\sin n\theta}{\zeta} - \frac{n\,V\sin n\theta}{\zeta}\right)^2 + 2{a_N}^2\left(\frac{\partial \mathrm{W}}{\partial \xi}\sin n\theta\right)^2 \\
&+ \left(\frac{n\,U\cos n\theta}{\zeta} + \frac{\partial V}{\partial \zeta}\cos n\theta - \frac{V\cos n\theta}{\zeta}\right)^2 \\
&+ \left(a_N\frac{\partial \mathrm{V}}{\partial \xi}\cos n\theta + \frac{n\,W\cos n\theta}{\zeta}\right)^2 \\
&+ \left(a_N\frac{\partial \mathrm{U}}{\partial \xi}\sin n\theta + \frac{\partial W}{\partial \zeta}\sin n\theta\right)^2
\end{aligned}
\tag{3.2}
$$

Similarly, the maximum kinetic energy of linearly-tapered disc is expressed by the following equation.

$$
\begin{aligned}
&(T_{max})_{LT} \\
&= \frac{1}{2}\omega^2\rho\left(\int_{-\frac{1}{2}}^{\frac{1}{2}}\int_{\beta_1}^{1}\int_{0}^{2\pi} h_{mid1}R_{o1}^2(terms\ of\ T^*)\,\zeta d\theta\, d\zeta\, d\xi\right. \\
&+ \int_{-\frac{1}{2}}^{\frac{1}{2}}\int_{\beta_2}^{1}\int_{0}^{2\pi} h_{mid2}R_{o2}^2(terms\ of\ T^*)\,\zeta d\theta\, d\zeta\, d\xi \\
&+ \int_{-\frac{1}{2}}^{\frac{1}{2}}\int_{\beta_3}^{1}\int_{0}^{2\pi} h_{mid3}R_{o3}^2(terms\ of\ T^*)\,\zeta d\theta\, d\zeta\, d\xi \\
&\left.+ \cdots\cdots\int_{-\frac{1}{2}}^{\frac{1}{2}}\int_{\beta_N}^{1}\int_{0}^{2\pi} h_{midN}R_{oN}^2(terms\ of\ T^*)\,\zeta d\theta\, d\zeta\, d\xi\right)
\end{aligned}
\tag{3.3}
$$

Here,

$$terms\ of\ T^* = U^2\sin^2 n\theta + V^2\cos^2 n\theta + W^2\sin^2 n\theta \tag{3.4}$$

In Equations (3.1) and (3.3), h_{mid1} is the midpoint thickness of division 1 and h_{mid2} is the midpoint thickness of division 2 and so on. R_{o1} is the outer thickness of division 1, R_{o2} is the outer thickenss of division 2 and so on. In Equations (3.2) and (3.4), n is the nodal diameter number. β_1 represents the radius ratio of division 1, β_2 represents the radius ratio of division 2 and so on.

3.3 Rayleigh-Ritz solution

Rayleigh's quotient for the uniform disc is derived in sub-section 2.3.3. For the linearly-tapered disc, Equation (2.34) is modified as below:

$$(\Omega)^2{}_{LT} = 2\omega^2 \frac{\rho(1+v)}{E} = \frac{\begin{matrix} \int_{-\frac{1}{2}}^{\frac{1}{2}} \int_{\beta_1}^{1} \int_{0}^{2\pi} h_{mid1}(terms\ of\ \Pi_1)\, \zeta d\theta\, d\zeta\, d\xi + \cdots \\ + \int_{-\frac{1}{2}}^{\frac{1}{2}} \int_{\beta_N}^{1} \int_{0}^{2\pi} h_{midN}\ (terms\ of\ \Pi_N)\ \zeta d\theta\, d\zeta\, d\xi \end{matrix}}{\begin{matrix} \int_{-\frac{1}{2}}^{\frac{1}{2}} \int_{\beta_1}^{1} \int_{0}^{2\pi} h_{mid1} R_{o1}^2\ (terms\ of\ T^*)\, \zeta d\theta\, d\zeta\, d\xi + \cdots \\ + \int_{-\frac{1}{2}}^{\frac{1}{2}} \int_{\beta_N}^{1} \int_{0}^{2\pi} h_{midN} R_{oN}^2 (terms\ of\ T^*)\, \zeta d\theta\, d\zeta\, d\xi \end{matrix}} \tag{3.5}$$

Further, $terms\ of\ \Pi$ and $terms\ of\ T^*$ for in-plane mode and out-of-plane mode vibrations are derived from the generalized formulation for the uniform disc, presented in Chapter 2. It is important to note that in Equations (3.1) and (3.3), set (B) functions are employed.

3.3.1 Eigenvalue problem for in-plane vibrations

To calculate the lowest in-plane mode natural frequency of linearly-tapered disc made of isotropic material, terms of maximum strain energy and maximum kinetic energy, represented by Equations (3.2) and (3.4) are modified as follows:

$$terms\ of\ \Pi_N = \left(\frac{\partial V}{\partial \zeta} - \frac{V}{\zeta}\right)^2 + a_N^2 \left(\frac{\partial \mathrm{V}}{\partial \xi}\right)^2 \tag{3.6}$$

$$terms\ of\ T^* = V^2 \tag{3.7}$$

Let this circumferential amplitude V be expressed as the combination of arbitrary coefficients and non-dimensional radius and non-dimensional thickness terms.

$$V = \frac{\zeta(\zeta - \beta)}{(1-\beta)} \sum_{k=0}^{K} \sum_{l=0}^{L} B_{kl}\ \zeta^{k}\ \xi^{l} \tag{3.8}$$

As shown in Equation (3.8), the same shape function is assumed as in the case of the uniform disc case. The advantage of presented approach is that it allows to use lower order polynomial in Equation (3.8). To obtain the best possible approximation of natural frequencies, arbitrary coefficients are adjusted and non-dimensional frequency is made stationary. Minimizing Rayleigh's quotient with respect to arbitrary constants,

$$\frac{\partial (\Omega)^2{}_{LT}}{\partial B_{kl}} = 0 \tag{3.9}$$

The above Equation (3.9) gives the set of $(K+1)(L+1)$ linear algebraic equations in terms of arbitrary coefficients. Upon simplifying, one gets:

$$\frac{\partial N}{\partial B_{kl}} - (\Omega)^2{}_{LT} \frac{\partial D}{\partial B_{kl}} = 0 \tag{3.10}$$

where, N and D are the numerator and the denominator of Equation (3.5).

Equation (3.10) can be rewritten and represented as an eigenvalue problem:

$$\left([K] - (\Omega)^2{}_{LT}[M]\right)\{B_{kl}\} = \{0\} \tag{3.11}$$

To have a non-trivial solution, let the determinant of the augmented matrix be zero in Equation (3.11). MATLAB code is developed to get the non-dimensional frequency parameter $(\Omega)_{LT} = \sqrt{2\omega^2 \frac{\rho(1+\nu)}{E}}$ and subsequently the natural frequency of in-plane mode vibration of the disc made of isotropic material is obtained.

3.3.2 Eigenvalue problem for out-of-plane vibrations

To investigate out-of-plane vibrations of the linearly-tapered disc, Equations (3.2) and (3.4) are recalculated again using set (A) functions expressed as Equations (2.43), (2.44) and (2.45), which hold true for bending mode and coupled modes. Further, these equations are recalculated for $n = 0$ to calculate the lowest bending natural frequency.

For pure transverse mode, the amplitudes in r and z directions are expressed by Equations (2.23) and (2.25) respectively.

3.4 Parametric study on isotropic disc

It is assumed that linearly-tapered disc is made of Structural Steel material. The numerical values of Young's modulus and Poisson's ratio for this material are 200 GPa and 0.3 respectively. The outer radius and inner radius of the linearly-tapered disc are 0.5 m and 0.1 m respectively. The inner thickness of linearly-tapered disc is 0.4 m and kept constant throughout the analysis.

Rayleigh-Ritz solutions are compared with the results calculated using ANSYS. In simulation using ANSYS, SOLID 186 elements are used along with quadratic hexahedral mesh type in order to get accurate results compared to the tetrahedral elements without mid-side nodes. SOLID 186 is a higher-order three-dimensional 20-node element. This element has three translation degrees of freedom per node and it exhibits quadratic displacement behaviour.

3.4.1 In-plane vibrations of linearly-tapered isotropic disc

To study the effect of linear taper on the lowest in-plane mode frequency, consider that the outer thickness of the linearly-tapered disc is varied up to 0.2 m. As shown in the following Figure 3.3, for all of the three radius ratios namely 0.2, 0.25 and 0.3, it is observed that the lowest in-plane mode frequency increases with the decrease of outer thickness.

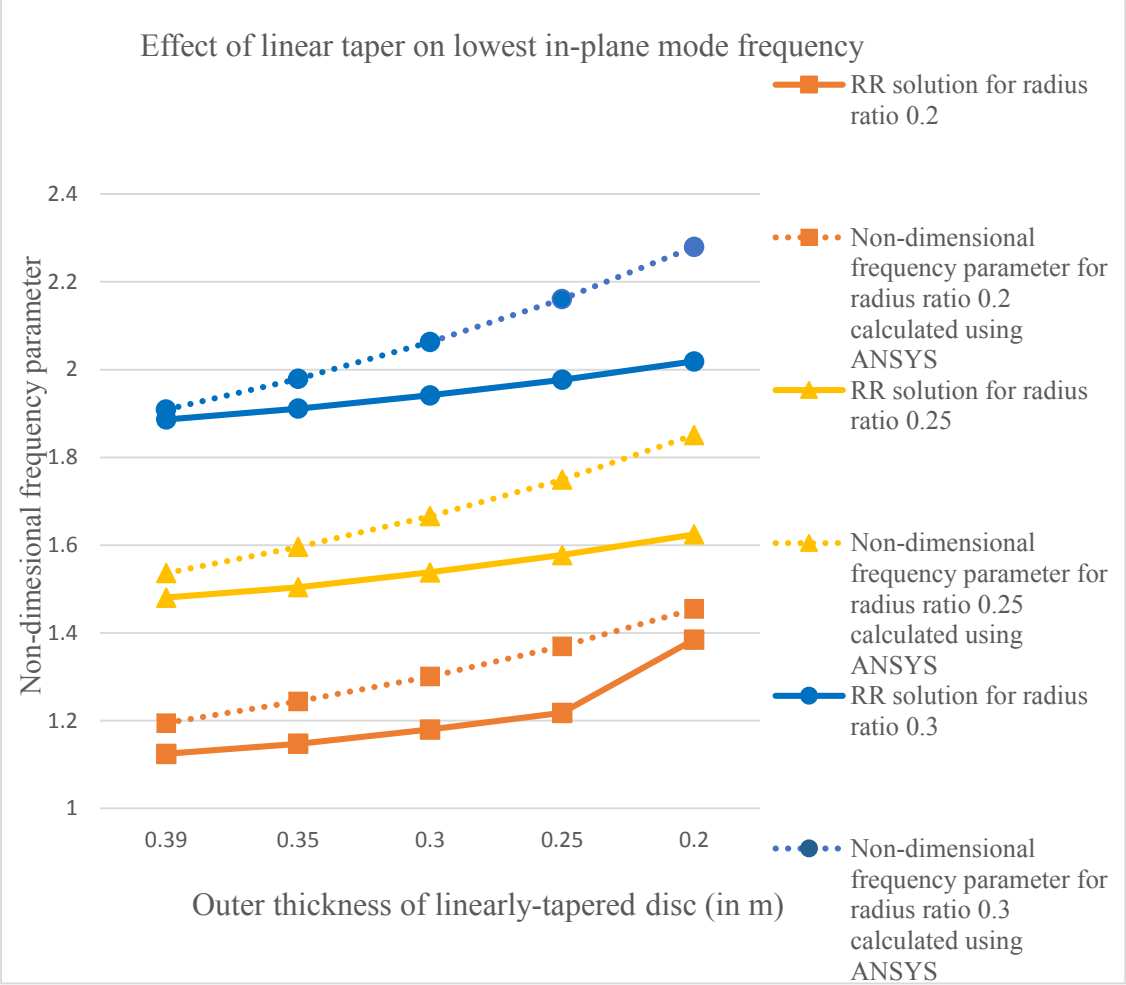

Figure 3.3: Variation of the lowest in-plane mode frequency with outer thickness and radius ratio

As discussed in Section 1.1, in some of the engineering applications of circular tapered discs, it is advisable to study the effect of linear taper on the lowest in-plane mode frequency. Consider the variation of taper angle from infinitesimal taper up to 1 degree of taper. The following Figure 3.4 shows the variation of the lowest in-plane mode frequency with taper angle for radius ratio of 0.3.

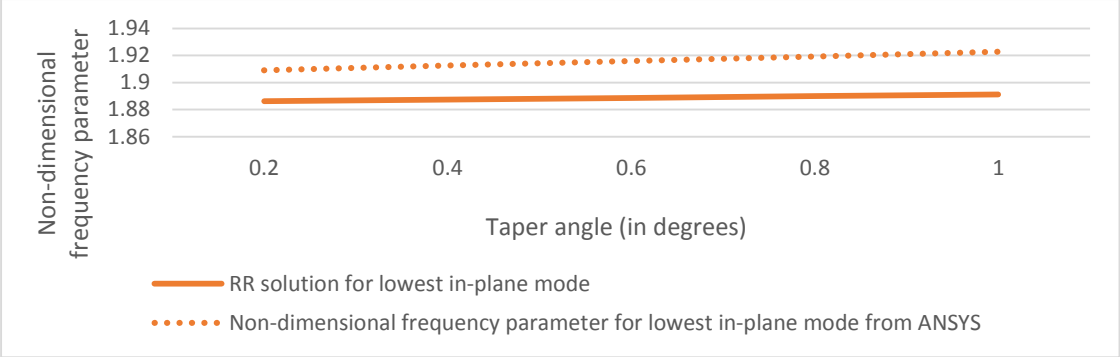

Figure 3.4: Variation of the lowest in-plane mode frequency with taper angle of linearly-tapered isotropic disc for beta value of 0.3

3.4.2 Out-of-plane vibrations of linearly-tapered isotropic disc

The following Figure 3.5 shows the effect of linear taper on the lowest bending mode non-dimensional frequency parameter. This study concludes that the non-dimensional frequency parameter of lowest bending mode increases linearly with taper-angle.

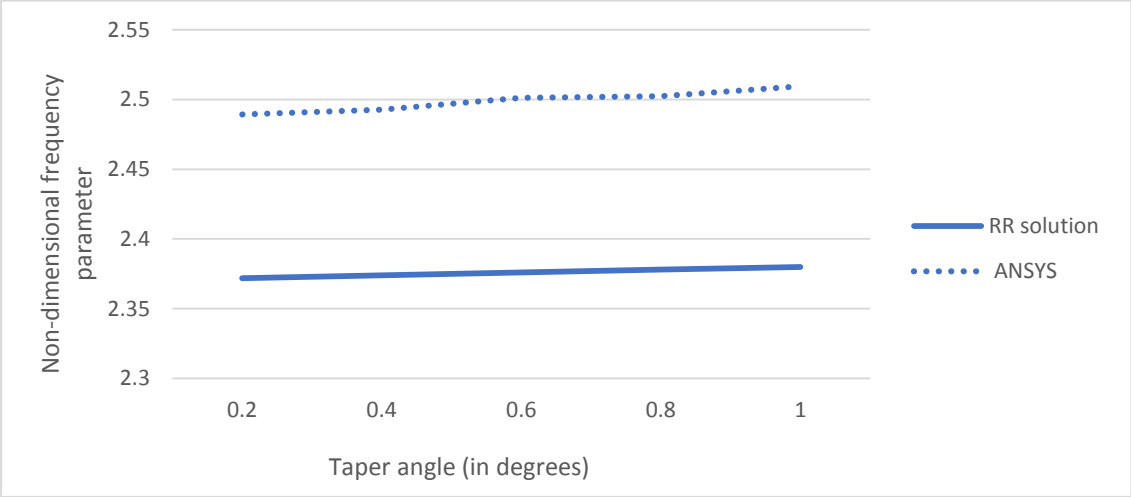

Figure 3.5: Variation of the lowest transverse mode frequency with taper angle of linearly-tapered isotropic disc for beta value of 0.25

Comparison of lowest transverse mode non-dimensional frequency obtained using Rayleigh-Ritz solution and Finite Element solution is made for radius ratio values of 0.2 and 0.25 in the following Figure 3.6.

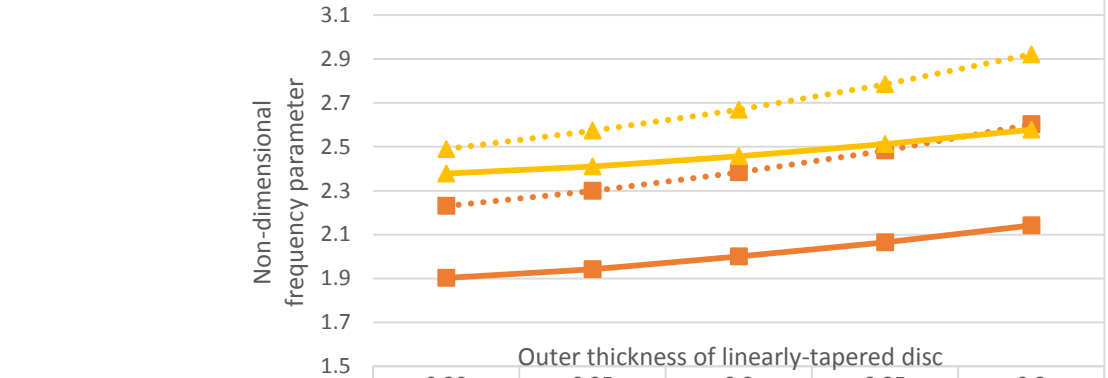

	0.39	0.35	0.3	0.25	0.2
RR solution for radius ratio 0.2	1.902010098	1.942	2	2.0643	2.1423
Non-dimensional frequency parameter for radius ratio 0.2 calculated using ANSYS	2.230830547	2.298738475	2.383346314	2.482706897	2.602519127
RR solution for radius ratio 0.25	2.378	2.410225006	2.456813392	2.511738223	2.578088557
Non-dimensional frequency parameter for radius ratio 0.25 calculated using ANSYS	2.489421737	2.573349796	2.66900336	2.784411788	2.920786699

Figure 3.6: Variation of the lowest transverse mode frequency with linear taper and radius ratio

It is noted from the present three-dimensional analysis that the non-dimensional frequency parameter for the isotropic disc, calculated using ANSYS are higher than that obtained using Rayleigh-Ritz method. Moreover, higher mode vibration analysis can be conducted with acceptable accuracy using presented formulation.

3.5 Vibration analysis of linearly-tapered orthotropic disc

Formulation derived in sub-section 3.2.1 is limited to a linearly-tapered disc of clamped-free boundary condition made of isotropic material. In the present section, the generalized formulation for the orthotropic disc of linearly-varying thickness is

developed to study the effect of linear taper on the lowest in-plane mode and the lowest out-of-plane mode natural frequencies based on the approach discussed in Section 3.2.

For the orthotropic disc, midpoint thickness of each division is calculated. Maximum strain energy and maximum kinetic energy for each division are integrated uniformly over respective division considering the formulation for uniform thickness orthotropic disc case as described in Section 2.7. Material properties of Graphite-Polymer composite as given in Table 2.6, are considered for the present analysis.

3.5.1 In-plane vibrations of linearly-tapered orthotropic disc

To investigate three-dimensional in-plane vibration response, maximum strain energy and maximum kinetic energy of linearly-tapered clamped-free orthotropic disc are calculated as follow:

$$
\begin{aligned}
(\pi_{max})_{LT} = 0.5C_{66}\Bigg(& \int_{-\frac{1}{2}}^{\frac{1}{2}}\int_{\beta_1}^{1}\int_{0}^{2\pi} h_{mid1}\left[\frac{C_{44}}{C_{66}}{a_N}^2\left(\frac{\partial \mathrm{V}}{\partial \xi}\right)^2\right. \\
& \left.+\left(\frac{\partial V}{\partial \zeta}-\frac{V}{\zeta}\right)^2\right]\zeta d\theta\, d\zeta\, d\xi + \cdots \\
& + \int_{-\frac{1}{2}}^{\frac{1}{2}}\int_{\beta_N}^{1}\int_{0}^{2\pi} h_{midN}\left[\frac{C_{44}}{C_{66}}{a_N}^2\left(\frac{\partial \mathrm{V}}{\partial \xi}\right)^2\right. \\
& \left.+\left(\frac{\partial V}{\partial \zeta}-\frac{V}{\zeta}\right)^2\right]\zeta d\theta\, d\zeta\, d\xi\Bigg)
\end{aligned}
\tag{3.12}
$$

$$
(T_{max})_{LT} = \frac{1}{2}\omega^2\rho_o\left(\begin{array}{l}\displaystyle\int_{-\frac{1}{2}}^{\frac{1}{2}}\int_{\beta_1}^{1}\int_{0}^{2\pi} h_{mid1}R_{o1}^2\,V^2\,\zeta d\theta\, d\zeta\, d\xi\ + \cdots \\ \displaystyle + \int_{-\frac{1}{2}}^{\frac{1}{2}}\int_{\beta_N}^{1}\int_{0}^{2\pi} h_{midN}R_{oN}^2 V^2\,\zeta d\theta\, d\zeta\, d\xi\end{array}\right) \tag{3.13}
$$

where, ρ_o is the density of orthotropic material.

From Equations (3.12) and (3.13), the frequency parameter can be obtained as follows:

$$(\Omega)_{LTo} = \sqrt{\frac{\rho_o\, \omega^2}{C_{66}}} \tag{3.14}$$

Again, it is minimized with respect to the arbitrary coefficients to calculate the approximate natural frequency of the lowest in-plane mode. Polynomial described by Equation (3.8) is used here for the three-dimensional in-plane mode vibration analysis of orthotropic disc. MATLAB code is written to solve the eigenvalue problem of a linearly-tapered orthotropic disc having clamped-free boundary condition.

3.5.2 Transverse vibrations of linearly-tapered orthotropic disc

To study three-dimensional out-of-plane vibrations, maximum strain energy and maximum kinetic energy of linearly-tapered clamped-free orthotropic disc are calculated as follow:

$$\begin{aligned}(\pi_{max})_{LT} = \frac{C_{55}}{2}\Bigg(& \int_{-\frac{1}{2}}^{\frac{1}{2}}\int_{\beta_1}^{1}\int_{0}^{2\pi} h_{mid1}[terms\ of\ \Pi_1]_{ortho}\,\zeta d\theta\, d\zeta\, d\xi \\ & + \cdots \\ & + \int_{-\frac{1}{2}}^{\frac{1}{2}}\int_{\beta_N}^{1}\int_{0}^{2\pi} h_{midN}[terms\ of\ \Pi_N]_{ortho}\,\zeta d\theta\, d\zeta\, d\xi\Bigg)\end{aligned} \tag{3.15}$$

$$(T_{max})_{LT} = \frac{1}{2}\omega^2\rho_o\left(\begin{array}{l}\displaystyle\int_{-\frac{1}{2}}^{\frac{1}{2}}\int_{\beta_1}^{1}\int_{0}^{2\pi} h_{mid1}R_{o1}^2\,(U^2+W^2)\,\zeta d\theta\, d\zeta\, d\xi\ + \cdots \\ \displaystyle + \int_{-\frac{1}{2}}^{\frac{1}{2}}\int_{\beta_N}^{1}\int_{0}^{2\pi} h_{midN}R_{oN}^2(U^2+W^2)\,\zeta d\theta\, d\zeta\, d\xi\end{array}\right) \tag{3.16}$$

where,

$$
\begin{aligned}
&[terms\ of\ \Pi_N]_{ortho} \\
&= \frac{C_{11}}{C_{55}}\left(\frac{\partial U}{\partial \zeta}\right)^2 + \frac{C_{22}}{C_{55}}\frac{U^2}{\zeta^2} + \frac{C_{33}}{C_{55}}{a_N}^2\left(\frac{\partial W}{\partial \xi}\right)^2 \\
&+ \left(a_N\frac{\partial U}{\partial \xi} + \frac{\partial W}{\partial \zeta}\right)^2 + 2\frac{C_{12}}{C_{55}}\frac{U}{\zeta}\frac{\partial U}{\partial \zeta} + 2a_N\frac{C_{13}}{C_{55}}\frac{\partial U}{\partial \zeta}\frac{\partial W}{\partial \xi} \\
&+ 2a_N\frac{C_{23}}{C_{55}}\frac{U}{\zeta}\frac{\partial W}{\partial \xi}
\end{aligned}
\tag{3.17}
$$

Equations (3.15) and (3.16) are equated and non-dimensional frequency parameter for the lowest transverse mode can be calculated as follows:

$$
(\Omega)_{LTo} = \sqrt{\frac{\rho_o\,\omega^2}{C_{55}}} \tag{3.18}
$$

This frequency parameter is minimized with respect to the arbitrary coefficients of Equations (2.23) and (2.25). MATLAB code is developed to solve the eigenvalue problem and as a result, the lowest frequency parameter for the lowest transverse mode is reported.

3.6 Parametric study on orthotropic discs

The three-dimensional response of the linearly-tapered disc made of the Graphite-Polymer composite material is studied using the presented approach. The same dimensions of the orthotropic disc are considered as that of the isotropic disc. The inner thickness and outer radius of the disc are kept constant throughout the analysis. Rayleigh-Ritz solutions are compared with results calculated using ANSYS. Effect of taper angle and radius ratio on the lowest in-plane mode and the lowest out-of-plane mode natural frequencies is studied. Moreover, three-dimensional higher mode

vibration analysis for the linearly-tapered disc of orthotropic material also can be conducted with good accuracy with the presented formulation.

The following Figure 3.7 shows the bending mode and circumferential mode vibration of linearly tapered circular disc of beta value of 0.2 (and taper angle of 14.04) and made of Graphite-Polymer composite material. In ANSYS, free vibration analysis was conducted using SOLID 186 elements. For the mentioned disc, the fundamental mode of vibration is the circumferential mode.

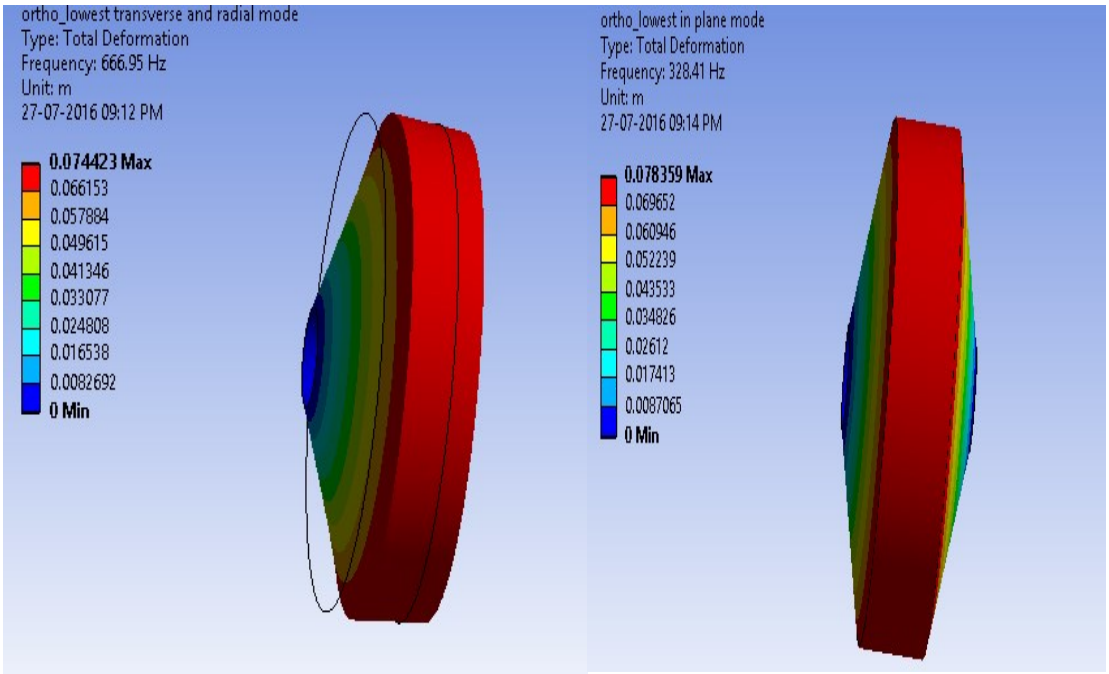

Figure 3.7: The lowest bending and the lowest circumferential mode vibrations of linearly-tapered disc made of Graphite-Polymer composite material having beta value of 0.2

The following Figure 3.8 shows a variation of frequency parameter with outer thickness of the disc and radius ratio. Lower order polynomial in r and z is used along with considering 5, 3 and 2 numbers of divisions for the orthotropic disc of radius ratio 0.2, 0.25 and 0.3 respectively to calculate the lowest in-plane mode frequency.

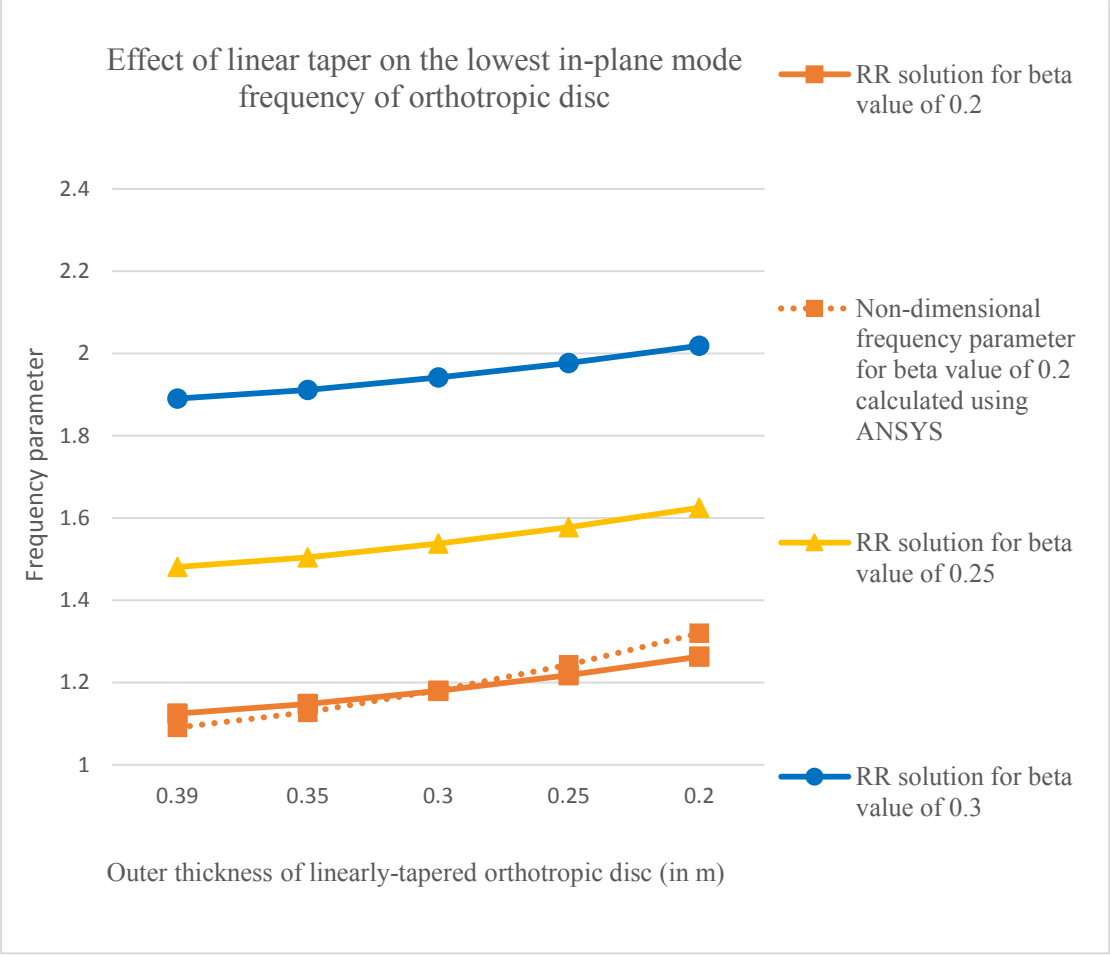

Figure 3.8: Variation of the lowest in-plane mode natural frequency of linearly-tapered orthotropic disc with respect to linear-taper and radius ratio

From above Figure 3.8, it is observed that for the linearly-tapered orthotropic disc, the increase in frequency parameter is non-linear with linear increment of radius ratio. For example, for linearly-tapered disc of outer radius of 0.3, frequency parameters calculated using Rayleigh-Ritz method with finite-element-like modification are 1.1860, 1.538 and 1.9414 for beta values of 0.2, 0.25 and 0.3 respectively.

The variation of the frequency parameters of the lowest in-plane mode with taper angle for different radius ratio values are depicted in the following Figure 3.9. It is observed that for the orthotropic disc, the frequency parameters increase with taper angle and radius ratio.

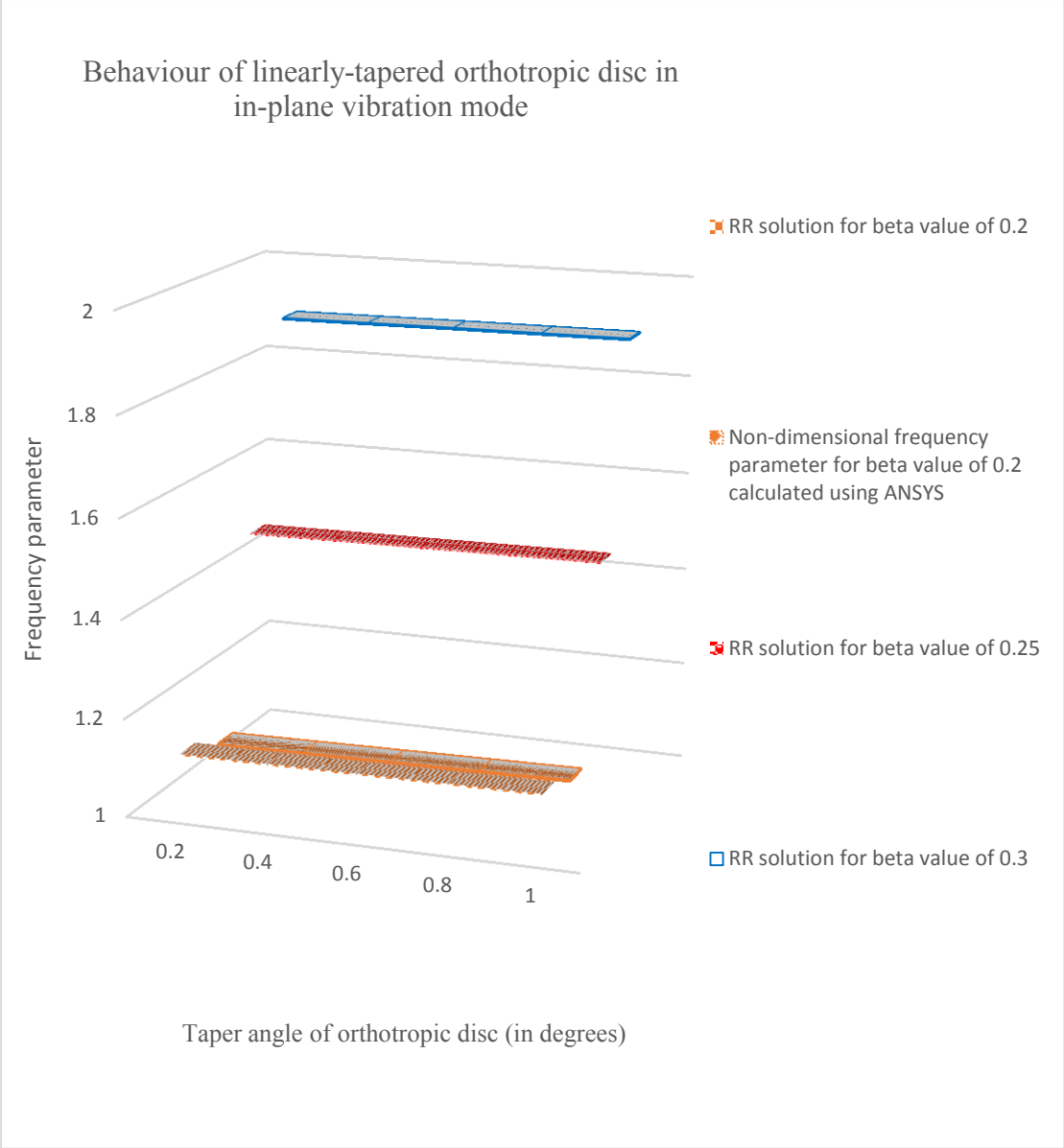

Figure 3.9: Behaviour of orthotropic disc in in-plane vibration mode with respect to taper angle and radius ratio

The natural frequency for the lowest transverse mode of the orthotropic disc is calculated using Rayleigh-Ritz method for the beta value of 0.2 and the variation of natural frequency with outer thickness of the disc is noted in the following Table 3.1. For a disc of radius ratio 0.2, lower order polynomial is considered along with six number of divisions.

Outer thickness (h_o in m)	Taper angle (in degrees)	RR solution (f_3 in Hz)	Finite element solution using ANSYS	% Difference
0.39	0.72	583.4589	573.84	-1.68
0.35	3.58	595.4906	589.29	-1.05
0.3	7.12	612.5969	611.18	-0.23
0.25	10.62	632.5566	636.65	0.64
0.2	14.04	656.1879	666.94	1.61

Table 3.1: Variation of natural frequency of the lowest transverse mode with outer thickness of linearly-tapered orthotropic disc for beta value of 0.2

In Equations (2.23) and (2.25), the upper limit of summation is set to 1 (i.e. four terms in the polynomial are considered) to analyse the three-dimensional out-of-plane vibration response of orthotropic disc having a beta value of 0.25. Here, four number of divisions are considered to determine approximate frequencies.

In above Table 3.1, percentage difference is calculated using the following formula:

$$\% \text{ Difference} = \frac{\text{3D FEA solution} - \text{3D RR solution}}{\text{3D FEA solution}} \tag{3.19}$$

In Table 3.1, taper angle is calculated using the following formula:

$$taper\ angle = 90 - \tan^{-1}\frac{2(R_o - R_i)}{h_i - h_o} \tag{3.20}$$

where, h_i and h_o are the inner and outer thicknesses of the tapered disc and R_i and R_o are the inner and outer radius values of the tapered disc. The following Table 3.2 shows the variation of natural frequency with the outer thickness of the disc.

Outer thickness (h_o in m)	Taper angle (in degrees)	RR solution (f_3 in Hz)	Finite element solution using ANSYS	% Difference
0.39	0.76	666.1490	640.57	-3.99
0.35	3.81	677.2914	658.28	-2.89
0.3	7.59	693.1765	683.25	-1.45
0.25	11.31	711.7809	712.13	0.05
0.2	14.93	733.9158	746.27	1.66

Table 3.2: Variation of natural frequency of lowest transverse mode with outer thickness of linearly-tapered orthotropic disc for beta value of 0.25

Variation of natural frequency of the lowest transverse mode with outer thickness of disc is shown in Table 3.3, which is given below:

Outer thickness (h_o in m)	Taper angle (in degrees)	RR solution (f_3 in Hz)	Finite element solution using ANSYS	% Difference
0.39	0.82	739.5735	715.87	-3.31
0.35	4.09	749.3756	736.27	-1.78
0.3	8.13	763.3466	764.88	0.20
0.25	12.09	779.7100	797.73	2.26
0.2	15.95	800.0	836.31(f_4)	4.34

Table 3.3: Variation of natural frequency of the lowest transverse mode with outer thickness of linearly-tapered orthotropic disc for beta value of 0.3

The following Table 3.4 shows the variation of the natural frequency of the lowest transverse mode with taper angle for beta values of 0.2, 0.25 and 0.3.

Taper angle (in degrees)	RR solution (f_3 in Hz)			Finite element solution using ANSYS (f_3 in Hz)		
	$\beta = 0.2$	$\beta = 0.25$	$\beta = 0.3$	$\beta = 0.2$	$\beta = 0.25$	$\beta = 0.3$
0.2	581.4262	664.2134	737.8186	571.2489	637.4886	712.2384
0.4	582.2225	664.8852	738.3909	572.2691	638.5835	713.4328
0.6	582.9939	665.6069	738.9383	573.2645	639.6783	714.5775
0.8	583.7902	666.2787	739.5355	574.2847	640.7732	715.7719
1	584.6113	666.9755	740.083	575.3049	641.893	716.9414

Table 3.4: Effect of taper angle on natural frequency of lowest transverse mode of linearly-tapered orthotropic disc for beta values of 0.2, 0.25 and 0.3

3.7 Rayleigh's damping for linearly-tapered disc

As discussed in Section 2.6, it is important to calculate the realistic values of Rayleigh's damping coefficients based on the modal mass participation factor. Linearly-tapered disc made of Structural Steel material is considered with beta value of 0.2. The outer thickness and inner thickness are considered as 0.1 m and 0.2 m respectively. Furthermore, the outer radius and inner radius of the disc are considered as 2 m and 0.4 m respectively. Rayleigh's damping coefficients based on linear approximation, significant mode approximation, full range approximation and approximation based on average data are calculated. Numerical values of all four data sets and natural frequencies of linearly-tapered disc that are obtained using ANSYS are tabulated in the following Table 3.5:

Estimation of Rayleigh's damping coefficients for linearly-tapered isotropic disc						
Mode number	Natural frequency from ANSYS (Hz)	Circular Natural frequency from ANSYS (rad/sec)	Damping ratio based on linear interpolation	Damping ratio based on 13th mode approximation	Damping ratio based on full range approximation	Damping ratio based on average data
1	60.641	381.1720	0.0200	0.0200	0.0200	0.0200
2	60.642	381.1783	0.0200	0.0200	0.0200	0.0200
3	63.434	398.7280	0.0203	0.0200	0.0199	0.0199
4	69.628	437.6617	0.0211	0.0200	0.0197	0.0199
5	69.63	437.6743	0.0211	0.0200	0.0197	0.0199
6	112.04	704.2514	0.0263	0.0232	0.0217	0.0225
7	112.04	704.2514	0.0263	0.0232	0.0217	0.0225
8	176.38	1108.6743	0.0341	0.0311	0.0283	0.0297
9	176.38	1108.6743	0.0341	0.0311	0.0283	0.0297
10	181.88	1143.2457	0.0347	0.0319	0.0289	0.0304
11	254.55	1600.0286	0.0436	0.0422	0.0378	0.0400
12	254.55	1600.0286	0.0436	0.0422	0.0378	0.0400
13	307.32	1931.7257	0.0500	0.0500	0.0446	0.0473
14	319.36	2007.4057	0.0515	0.0518	0.0462	0.0490
15	319.36	2007.4057	0.0515	0.0518	0.0462	0.0490
16	344.74	2166.9371	0.0546	0.0556	0.0495	0.0526
17	344.74	2166.9371	0.0546	0.0556	0.0495	0.0526
18	367.11	2307.5486	0.0573	0.0590	0.0525	0.0557
19	367.12	2307.6114	0.0573	0.0590	0.0525	0.0557
20	435.45	2737.1143	0.0656	0.0693	0.0616	0.0655
21	435.45	2737.1143	0.0656	0.0693	0.0616	0.0655
22	446.21	2804.7486	0.0669	0.0710	0.0630	0.0670
23	446.21	2804.7486	0.0669	0.0710	0.0630	0.0670
24	463.52	2913.5543	0.0690	0.0736	0.0653	0.0695
25	463.52	2913.5543	0.0690	0.0736	0.0653	0.0695
26	558.34	3509.5657	0.0805	0.0882	0.0781	0.0832
27	558.34	3509.5657	0.0805	0.0882	0.0781	0.0832
28	597.44	3755.3371	0.0853	0.0942	0.0834	0.0888
29	597.44	3755.3371	0.0853	0.0942	0.0834	0.0888
30	680.53	4277.6171	0.0954	0.1070	0.0947	0.1009
31	680.53	4277.6171	0.0954	0.1070	0.0947	0.1009
32	732.46	4604.0343	0.1017	0.1151	0.1018	0.1084

Table 3.5: Estimation of Rayleigh's damping coefficients for linearly-tapered isotropic disc

The Rayleigh's damping coefficients based on full range approximation are calculated as explained in Section 2.6. The value of Alpha-lt and Beta-klt based on full range approximation are 8.88 and 0.0000438 respectively, which match the best with the datum value calculated based on linear interpolation.

The following Figure 3.10 shows the variation of damping ratio with circular natural frequency of the linearly-tapered circular disc of clamped-free boundary condition.

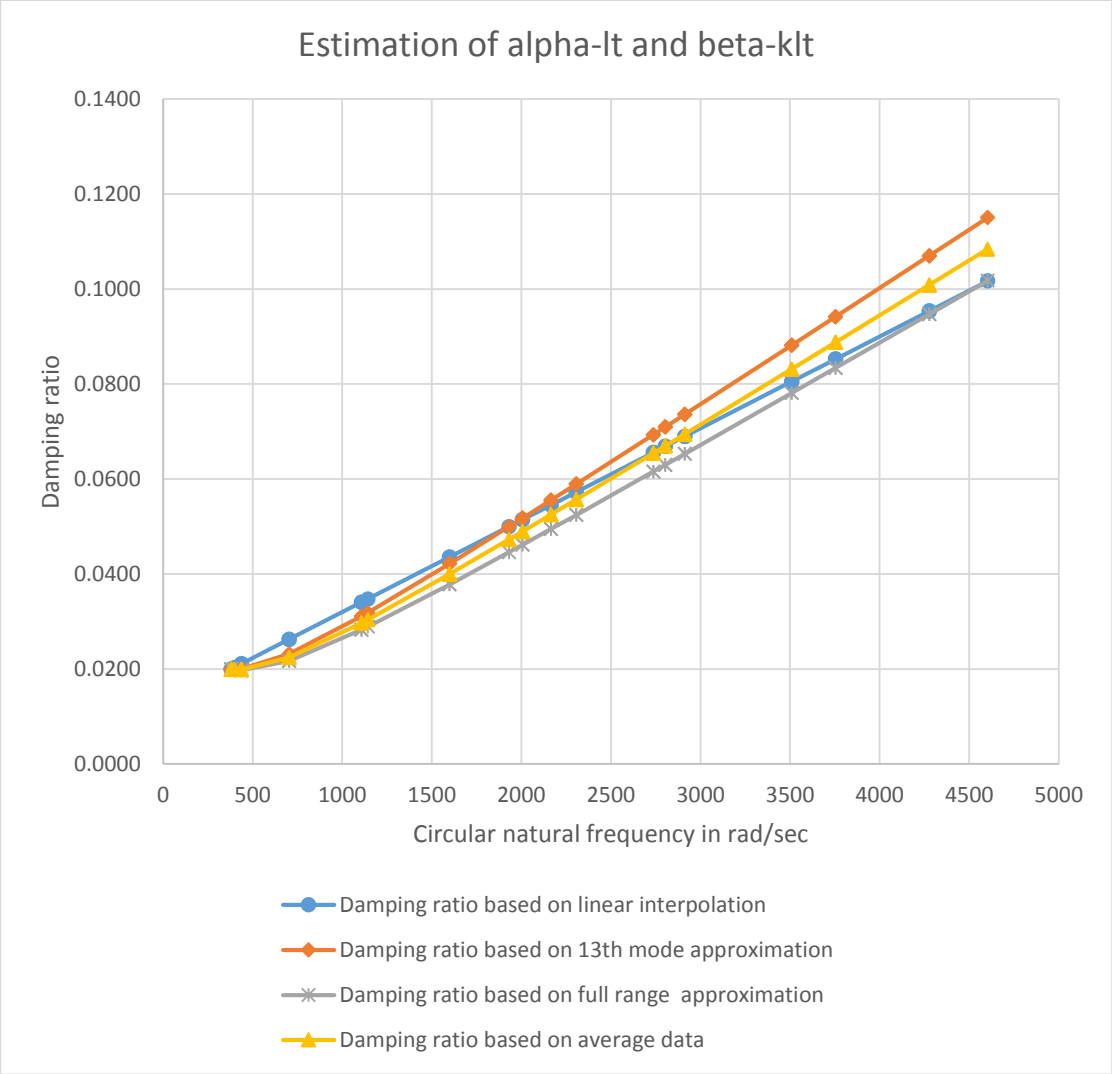

Figure 3.10: Variation of damping ratio with circular natural frequency of linearly-tapered isotropic disc

It is observed from above Figure 3.10 that the damping ratio variation is not significant for the frequency range from 381.1720 rad/sec to 704.2514 rad/sec.

3.8 Conclusion

In this Chapter, free vibration analysis of linearly-tapered circular disc of clamped-free boundary condition has been conducted. Frequency parameters for the discs made of orthotropic and isotropic material have been reported using Rayleigh-Ritz method with finite-element-like modification. For the circular tapered disc made of Graphite-Polymer composite material, the frequency parameters obtained from the presented approach are in good agreement (less than 5% difference is noted) when compared with 3-D finite element solutions using ANSYS. A summary of observations is as follows:

- An efficient and accurate approximate solution for 3-D vibration response of clamped-free isotropic and orthotropic discs has been developed using Rayleigh-Ritz method. Linear strains are considered for the analysis. The presented solution will be useful to check the accuracy of the approximate solutions derived using 2-D approach.
- The presented approach allows one to use the lower order polynomials to calculate the lowest in-plane and the lowest out-of-plane natural frequencies for the linearly-tapered clamped-free circular disc. Moreover, the free-vibration analysis can be conducted using presented formulation for the clamped-clamped and free-clamped boundary conditions considering appropriate constraint functions in displacements polynomials. The clamped-clamped disc has found application as locking device, which locks the connecting machine components

to each other by hydraulic pressure. The free-clamped disc has found application as clamping device (or fixture), which basically holds the machining tool.

- The frequency parameters of the in-plane vibration mode solely depends on shear modulus of the composite material.
- The frequency parameter for the lowest circumferential mode and the lowest bending mode increase with radius ratio.
- The variation of lowest bending mode natural frequency with taper angle is higher when the radius ratio increases.
- For the considerably-thick linearly-tapered disc (with $\frac{R_o}{h_i}$ value of 1.25), it is observed that the fundamental mode of vibration is the circumferential mode. For the thick disc case, the bending stiffness of the structure is higher compared to in-plane stiffness.

Chapter 4

Three-dimensional in-plane and out-of-plane vibrations of non-linearly tapered clamped-free disc

4.1 Introduction

The circular discs of non-linear thickness variation have found applications in turbomachinery. Very specific type of non-linear taper is considered in this Chapter which is defined by the hyperbolic taper. Here, hyperbolic thickness variation along radial direction is represented by the equation $t = \frac{t_1}{r^s}$, where 's' is the taper parameter of the disc. Circular disc with such a thickness variation is often known as Stodola's disc and has wide range of applications as discussed in Chapter 1. It has higher thickness at inner radius and lower thickness at outer radius. In this Chapter, three-dimensional free vibration of Stodola's disc is studied based on the numerical technique developed in the Chapter 3. Parametric study on in-plane and out-of-plane mode natural frequencies of isotropic and orthotropic discs based on the taper parameter of Stodola's disc is conducted. For the parametric studies on orthotropic Stodola's disc and isotropic Stodola's disc, Graphite-Polymer composite material and Structural Steel material are considered respectively. The material properties of Graphite-Polymer composite material are given in Table 2.6. Throughout this Chapter, clamped-free boundary condition is considered.

4.2 Modelling

As shown in the following Figure 4.1, Stodola's disc is divided into a number of divisions to model the non-linear tapered shape of non-deformed Stodola's disc. Similar approach as mentioned in Chapter 3 is developed to study free vibration behaviour of

Stodola's disc. The methodology developed in Chapter 3 to calculate maximum strain energy and maximum kinetic energy for linearly-tapered disc remains the same for the calculation of maximum energies of Stodola's disc.

The clamped-free boundary condition is considered for the Stodola's disc throughout this Chapter.

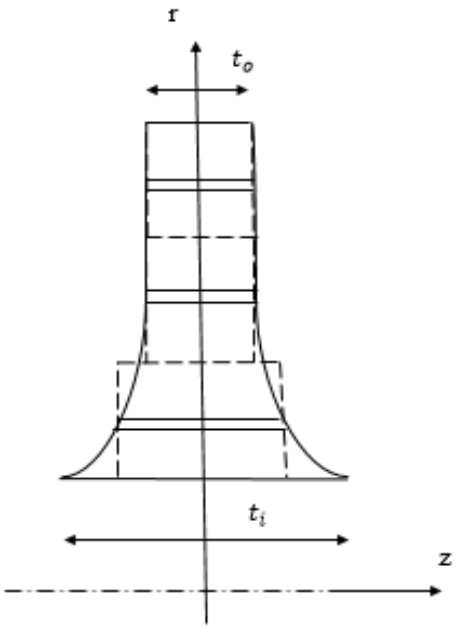

Figure 4.1: Cross-sectional geometry and coordinate system for Stodola's disc

Midpoint thickness of each division is calculated and strain energies and kinetic energies are integrated uniformly over the respective division. Later, strain energies of all divisions are added in order to derive the total strain energy of the tapered disc. The same approach holds true for the derivation of total kinetic energy.

Here, from the geometry, the outer radius of any division M can be calculated as follows:

$$R_{oN} = R_i + M\, l_r \tag{4.1}$$

where M is the number of divisions and l_r is the radial length of each (equal) division. R_i is the inner radius of the Stodola's disc.

Similarly, radius ratio for each division can be calculated using following formula,

$$\beta_N = \frac{R_i + (M-1)\, l_r}{R_i + M\, l_r} \tag{4.2}$$

Midpoint thickness of M^{th} division can be calculated as follows:

$$h_{midM} = \frac{h_{iM} + h_{oM}}{2} \tag{4.3}$$

Here,

$$h_{oM} = \frac{h_i R_i^s}{(R_i + (M-1) l_r)^s} \tag{4.4}$$

Equations (3.1) and (3.3) are modified in accordance with Equation (4.2) and (4.3) to calculate maximum strain energy and maximum kinetic energy of Stodola's disc made of isotropic material and subsequently to study the in-plane and out-of-plane mode vibrations characteristics.

To study the three-dimensional vibrations of Stodola's disc made of a Graphite-Polymer composite material, Equations (3.12) and (3.13) should be modified by considering Equations (4.2) and (4.3).

4.3 Parametric study on isotropic Stodola's discs

It is assumed that the non-linearly tapered disc is made of Structural Steel material. Young's modulus and Poisson's ratio for this material are 200 GPa and 0.3 respectively. Non-dimensional frequency parameters are calculated using Rayleigh-Ritz method with finite-element-like modification and compared with the three-dimensional ANSYS solutions. Three-dimensional in-plane vibration frequencies are noted in following Table 4.1 for different taper parameters of Stodola's disc and for radius ratio of 0.2. The inner thickness of Stodola's disc is 0.4 m and kept constant throughout the analysis.

Taper Parameter 's'	Outer thickness (in m)	RR solution (f_1) in Hz	ANSYS Solution (in Hz)		% Difference from ANSYS (hex mesh) solution
			Hex mesh	Tet mesh	
0.861353	0.1	859.7902	853.45	854.62	-0.74
0.609423	0.15	736.8296	773.25	774.96	4.71
0.430677	0.2	702.7748	719.43	721.48	2.31
0.29203	0.25	677.2498	678.81	680.44	0.23
0.178747	0.3	657.0184	645.88	647.31	-1.72

Table 4.1: Variation of natural frequency of the lowest in-plane mode with taper parameter of Stodola's disc for beta value of 0.2

For non-rotating Stodola's disc, the circumferential in-plane mode is the fundamental mode of vibration. For the disc of beta value of 0.2, three numbers of divisions are considered for the disc of taper parameter value 0.861353 and for rest of the

configurations of non-linear tapers, four numbers of divisions are considered. The lower order shape function has been considered with $K = L = 1$ in Equation (2.24).

In the lowest bending mode, z-direction and r-direction deformations are coupled. The natural frequencies of the lowest bending mode are presented in the following Table 4.2. For the bending mode vibration analysis of Stodola's disc, two numbers of divisions are considered for all the taper parameter values for beta value of 0.2. In Equations (2.23) and (2.25), the values of I, J and P, Q are considered as 2.

Taper Parameter 's'	Outer thickness (in m)	RR solution (f_3) in Hz	ANSYS Solution (in Hz)		% Difference from ANSYS (hex mesh) solution
			Hex Mesh	Tet mesh	
0.861353	0.1	1143.6069	1179.9	1180.5	3.07
0.609423	0.15	1204.9378	1223.5	1224.1	1.52
0.430677	0.2	1180.9205	1221.6	1222.0	3.33
0.29203	0.25	1165.945	1200.5	1200.8	2.88
0.178747	0.3	1154.9725	1171.3	1172.3	1.39

Table 4.2: Variation of natural frequency of the lowest bending mode with taper parameter of Stodola's disc for beta value of 0.2

4.4 Parametric study on orthotropic Stodola's discs

It is assumed that Stodola's disc is made of Graphite-Polymer composite material. Material properties as given in Table 2.6 are considered. Variation of the lowest in-plane mode natural frequency with taper parameter and radius ratio is presented in the following Table 4.3.

Outer thick-ness (in m)	Taper Parameter 's' for $\beta = 0.2$	RR solution (f_1) in Hz $\beta = 0.2$	Taper Parameter 's' for $\beta = 0.25$	RR solution (f_1) in Hz $\beta = 0.25$	Taper Parameter 's' for $\beta = 0.3$	RR solution (f_1) in Hz $\beta = 0.3$
K, L, M	1,1,4 or 5		1,1,3 or 4		1,1,2	
0.1 (M)	0.861353	392.9392 (4)	1	493.7140 (4)	1.151433	-
0.15 (M)	0.609423	368.0136 (4)	0.707519	-	0.814661	513.6337 (2)
0.2 (M)	0.430677	315.8229 (5)	0.5	403.7048 (3)	0.575717	500.4510 (2)
0.25 (M)	0.29203	303.3300 (4)	0.339036	391.5931 (3)	0.390377	490.2533 (2)
0.3 (M)	0.178747	293.4572 (4)	0.207519	381.9056 (3)	0.238944	481.9750 (2)

Table 4.3: Variation of natural frequency of lowest in-plane mode with taper parameter of orthotropic Stodola's disc for beta values of 0.2, 0.25 and 0.3

In above Table 4.3, the second row indicates the numbers of divisions and the order of polynomial considered to conduct the free vibration analysis of the orthotropic

Stodola's disc for beta values of 0.2, 0.25 and 0.3. Recall that beta is the radius ratio of Stodola's disc. M denotes the number of divisions considered for the Stodola's disc in Table 4.3. The number given in parenthesis represents the number of divisions considered in Rayleigh-Ritz formulation with finite-element-like modification. K and L represent the number of terms considered in circumferential direction polynomial.

It is observed from above Table 4.3 that the lowest in-plane mode natural frequency for particular outer thickness increases with radius ratio. The lowest mode natural frequency increases with increases with taper parameter for beta values of 0.2, 0.25 and 0.3.

4.5 Rayleigh's damping for Stodola's disc

Stodola's disc made of Structural Steel material is considered with beta value of 0.2. For Structural Steel material, Young's modulus and Poisson's ratio are taken as 200 GPa and 0.3 respectively. The outer thickness and inner thickness of the disc are considered as 0.1 m and 0.2 m respectively. Furthermore, the inner radius and outer radius of the disc are considered as 0.4 m and 2 m respectively. It is observed from finite element simulation using ANSYS that 90% mass participation occurs within the 13^{th} mode.

Results for all data set as discussed in Section 2.6 are given in the following Table 4.4.

Estimation of Rayleigh's damping coefficients for isotropic Stodola's disc						
Mode number	Natural frequency from ANSYS (Hz)	Circular natural frequency from ANSYS (rad/sec)	Damping ratio based on linear interpolation	Damping ratio based on 13th mode approximation	Damping ratio based on full range approximation	Damping ratio based on average data
1	52.619	330.7480	0.0200	0.0200	0.0200	0.0200
2	52.62	330.7543	0.0200	0.0200	0.0200	0.0200
3	54.522	342.7097	0.0203	0.0200	0.0199	0.0199
4	60.031	377.3377	0.0210	0.0200	0.0197	0.0198
5	60.033	377.3503	0.0210	0.0200	0.0197	0.0198
6	95.561	600.6691	0.0259	0.0227	0.0213	0.0220
7	95.561	600.6691	0.0259	0.0227	0.0213	0.0220
8	152.54	958.8229	0.0336	0.0305	0.0277	0.0291
9	152.54	958.8229	0.0336	0.0305	0.0277	0.0291
10	182.67	1148.2114	0.0378	0.0352	0.0317	0.0335
11	223.99	1407.9371	0.0434	0.0419	0.0374	0.0397
12	223.99	1407.9371	0.0434	0.0419	0.0374	0.0397
13	272.29	1711.5371	0.0500	0.0500	0.0444	0.0472
14	282.99	1778.7943	0.0515	0.0518	0.0460	0.0489
15	283	1778.8571	0.0515	0.0518	0.0460	0.0489
16	307.89	1935.3086	0.0549	0.0560	0.0496	0.0528
17	307.89	1935.3086	0.0549	0.0560	0.0496	0.0528
18	323.84	2035.5657	0.0570	0.0587	0.0520	0.0554
19	323.85	2035.6286	0.0570	0.0587	0.0520	0.0554
20	403.41	2535.7200	0.0679	0.0724	0.0639	0.0682
21	403.41	2535.7200	0.0679	0.0724	0.0639	0.0682
22	406.17	2553.0686	0.0683	0.0729	0.0643	0.0686
23	406.17	2553.0686	0.0683	0.0729	0.0643	0.0686
24	431.86	2714.5486	0.0718	0.0773	0.0682	0.0728
25	431.86	2714.5486	0.0718	0.0773	0.0682	0.0728
26	509.87	3204.8971	0.0824	0.0908	0.0801	0.0855
27	509.87	3204.8971	0.0824	0.0908	0.0801	0.0855
28	523.22	3288.8114	0.0843	0.0932	0.0821	0.0876
29	523.22	3288.8114	0.0843	0.0932	0.0821	0.0876
30	626.67	3939.0686	0.0984	0.1112	0.0979	0.1045
31	626.67	3939.0686	0.0984	0.1112	0.0979	0.1045
32	661.07	4155.2971	0.1031	0.1172	0.1032	0.1102

Table 4.4: Estimation of Rayleigh's damping coefficients for isotropic Stodola's disc

The below Figure 4.2 describes the variation of damping ratio with circular natural frequency of Stodola's disc of clamped-free boundary condition.

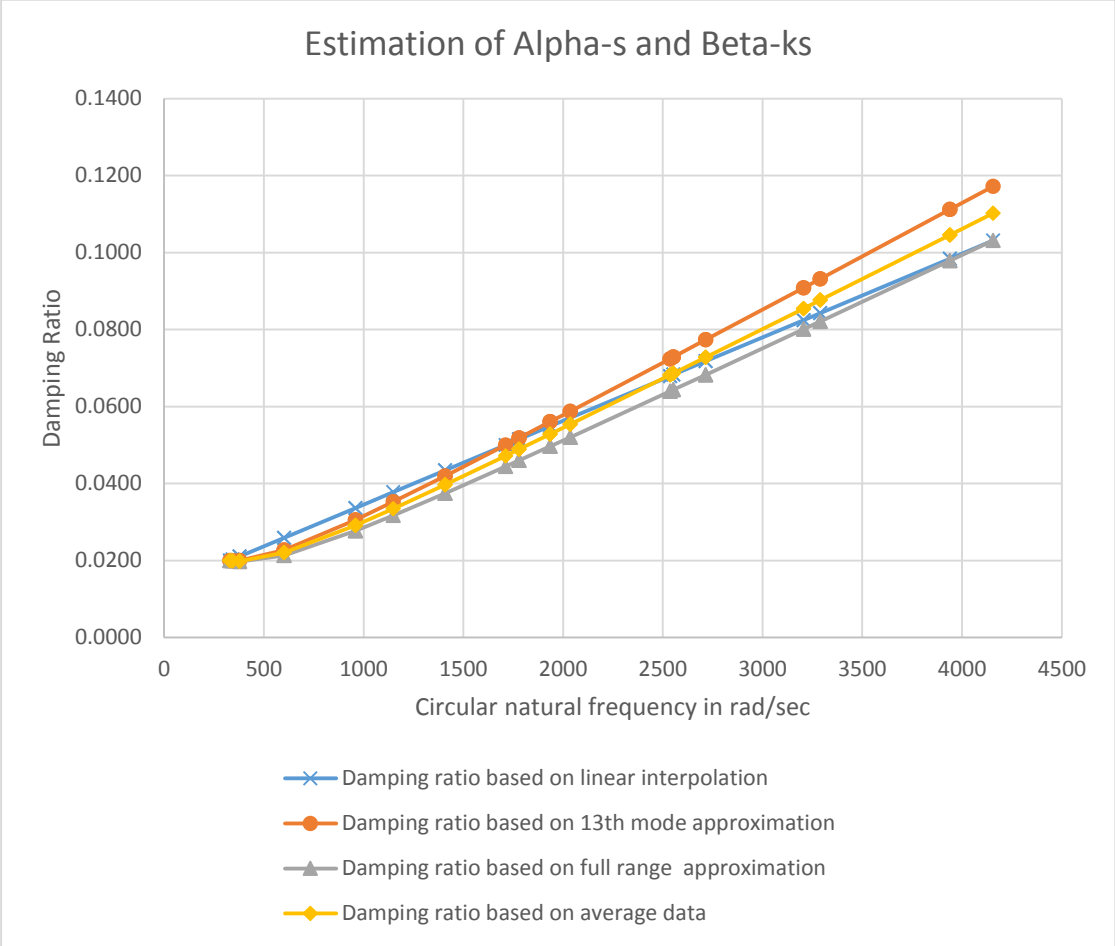

Figure 4.2: Variation of damping ratio with circular natural frequency of isotropic Stodola's disc

The Rayleigh's damping coefficients based on full range approximation are calculated as explained in Section 2.6. The value of Alpha-s and Beta-ks based on full range approximation are 7.85 and 0.0000492 respectively, which match the best with the datum value calculated based on linear interpolation. This data may be considered for the input for further dynamic analysis.

4.6 Conclusion

In this Chapter, free vibration response of the circular Stodola's disc of clamped-free boundary condition is studied using the Rayleigh-Ritz method with finite-element-like modification. This method is already tested on the linearly-tapered circular disc in Chapter 3. The frequency values obtained for the Stodola's disc are in good agreement with the finite element solutions obtained using ANSYS. The maximum percentage difference noted was less than 5%. A summary of observations is as follows:

- Natural frequencies of clamped-free Stodola's disc for each taper parameter increase with the radius ratio.
- The lowest in-plane mode natural frequency increases with the taper parameter of Stodola's disc.
- The lowest bending mode natural frequency of Stodola's disc has parabolic variation with the taper parameter.
- Lowest in-plane mode natural frequency of Stodola's disc made of orthotropic material is lower than that of the linearly-tapered disc of the same outer and inner radius as that of Stodola's disc.
- The fundamental circumferential mode natural frequencies of Stodola's discs made of Graphite-Polymer composite material are less than that of the Stodola's disc made of Structural Steel material and of the same dimensions.
- Vibration analysis for the modes with nodal diameter number one or higher can be conducted with acceptable accuracy using presented formulation.

Chapter 5

Bending mode vibrations of rotating disc of non-linear thickness variation

5.1 Introduction

For the case of rotating structures, it is advisable to get the estimation of the dynamic behaviour of rotating structures in order to prevent the damage due to resonance.

In the present Chapter, out-of-plane vibration responses of the rotating disc of hyperbolic thickness variation is investigated. The effects of non-linear taper on the lowest out-of-plane mode natural frequencies are studied. In the later part of this Chapter, the dynamic behavior of rotating hyperbolic disc made of Graphite-Polymer composite material is investigated using Rayleigh-Ritz method. Rayleigh-Ritz solutions are compared with ANSYS solutions.

As discussed in Chapter 1, tapered rotating discs having clamped-free boundary condition have a wide range of industrial applications such as in automobiles, space structures, and turbomachines. For example, typical gas or steam turbine disc has a larger thickness at inner radius and a smaller thickness at outer radius with hyperbolic thickness variation along radial direction often known as Stodola's disc. Again, it is well established that the rotating disc of hyperbolic thickness variation (i.e. Stodola's disc) has the favorable stress state compared to that of the uniform thickness disc. Hence, this chapter aims to investigate the dynamic behavior of the rotating Stodola's disc.

The present study is based on the consideration of linear strain-displacement relationship. Equations of motion for rotating Stodola's disc are derived using Hamilton's principle. As explained in Chapter 2, exact or closed form solutions for the partial differential equations of non-linearly tapered discs are not known. Hence, Rayleigh-Ritz method is used here to calculate the approximate values of the lowest bending mode natural frequencies.

5.2 Modelling

In the presented approach, the actual thickness variation is taken into account unlike the formulations developed in Chapter 3, where thickness profiles are approximated by considering piecewise uniform thicknesses.

Kirchhoff hypothesis along with linear strains is considered in deriving kinetic energy and strain energy of rotating Stodola's disc. Kirchhoff hypothesis assumes that the normal perpendicular to the middle surface of the plate remains straight and perpendicular and does not extend or contract. This assumption ignores the presence of transverse shear effects. However, the free vibration analysis conducted assuming Kirchhoff hypothesis is expected to give reliable results for thin to moderately thick disc. For higher accuracy, the analysis should be conducted with the assumption of thick plate theories. Displacements of an arbitrary point can be written in terms of displacements of the middle surface. For the cylindrical coordinate system they are written as follows:

$$u_r(r,\theta,z,t) = u(r,\theta,t) - z\,\frac{\partial w(r,\theta,t)}{\partial r}$$
$$u_\theta(r,\theta,z,t) = v(r,\theta,t) - \frac{z}{r}\,\frac{\partial w(r,\theta,t)}{\partial \theta} \tag{5.1}$$

$$u_z(r,\theta,z,t) = w(r,\theta,t)$$

where, u, v and w are the radial, circumferential and transverse displacements respectively, of a point on mid-plane (i.e., $z = 0$) of the disc. u_r, u_θ and u_z are the displacements of an arbitrary point on the disc in r, θ and z directions respectively.

Linear strains as function of displacements in cylindrical coordinate system can be expressed as follows:

$$\varepsilon_{rr} = \frac{\partial u_r}{\partial r} \tag{5.2}$$

$$\varepsilon_{\theta\theta} = \frac{u_r}{r} + \frac{1}{r}\frac{\partial u_\theta}{\partial \theta} \tag{5.3}$$

$$\varepsilon_{r\theta} = \frac{1}{2r}\left(\frac{\partial u_r}{\partial \theta} - u_\theta + r\frac{\partial u_\theta}{\partial r}\right) \tag{5.4}$$

After substituting Equation (5.1) into Equations (5.2), (5.3), and (5.4), linear strains in terms of displacements of the middle surface can be obtained. Further, plane stress assumption is made unlike Chapter 2, in order to simplify calculations for the rotating Stodola's disc. In the presence of manufacturing defect or crack, the transverse shear strain may exist. Hence, transverse shear strain is considered in the present analysis for brevity.

Writing stresses in terms of strains,

$$\sigma_{rr} = Q_{11}\varepsilon_{rr} + Q_{12}\varepsilon_{\theta\theta} \tag{5.5}$$

$$\sigma_{\theta\theta} = Q_{12}\varepsilon_{rr} + Q_{22}\varepsilon_{\theta\theta} \tag{5.6}$$

$$\sigma_{r\theta} = 2Q_{66}\varepsilon_{r\theta} \tag{5.7}$$

where, Q_{ij} are the elements of the reduced stiffness matrix. These elements can be expressed in terms of the engineering properties of orthotropic or isotropic material as follow:

$$Q_{11} = \frac{E_1}{1 - v_{12}v_{21}} \tag{5.8}$$

$$Q_{22} = \frac{E_2}{1 - v_{12}v_{21}} \tag{5.9}$$

$$Q_{12} = \frac{v_{12}E_2}{1 - v_{12}v_{21}} = \frac{v_{21}E_1}{1 - v_{12}v_{21}} \tag{5.10}$$

$$Q_{66} = G_{12} \tag{5.11}$$

Let the thickness variation of the rotating disc along radial direction be expressed as $t = \frac{t_1}{r^s}$. Here, 's' is the taper parameter of the Stodola's disc. Total strain energy of rotating Stodola's disc can be calculated as follow, by integrating the strain energy of infinitesimal volume element over the entire domain of the non-linearly tapered disc.

$$\Pi_{rot} = \frac{1}{2}\int_0^{2\pi}\int_{R_i}^{R_o}\int_{-\frac{c_1}{r^s}}^{\frac{c_1}{r^s}} [\sigma_{rr}\ \sigma_{\theta\theta}\ \sigma_{r\theta}] \begin{bmatrix} \varepsilon_{rr} \\ \varepsilon_{\theta\theta} \\ 2\varepsilon_{r\theta} \end{bmatrix} r dz\, dr\, d\theta \tag{5.12}$$

where, c_1 is the constant defined by $\frac{t_i R_i^s}{2}$ and 's' is the taper parameter of Stodola's disc. R_i and R_o are the inner radius and the outer radius of the Stodola's disc.

Equations (5.5), (5.6) and (5.7) are substituted in Equation (5.12) to derive the total strain energy of rotary disc, which is indeed a function of u, v and w. Now, it is possible to integrate this expression explicitly with respect to z coordinate. MAPLE code is developed to calculate total strain energy of disc under consideration, which is given as follows:

$$\Pi_{rot} = \frac{1}{2}\int_0^{2\pi}\int_{R_i}^{R_o} c_1^3\, L_1 r^{-3s} + c_1(L_2 r^{-s} + L_3 r^{-2-s})\, r dr\, d\theta \tag{5.13}$$

where, L_1, L_2 and L_3 are defined by the following Equations (5.14), (5.15) and (5.16).

$$L_1 = \frac{2}{3}\Bigg(-\frac{1}{2}\Bigg(-Q_{11}\frac{\partial^2 \mathrm{w}}{\partial \mathrm{r}^2} + Q_{12}\Bigg(-\frac{1}{r}\frac{\partial \mathrm{w}}{\partial \mathrm{r}} - \frac{1}{r^2}\frac{\partial^2 \mathrm{w}}{\partial \theta^2}\Bigg)\Bigg)\Bigg(\frac{\partial^2 \mathrm{w}}{\partial \mathrm{r}^2}\Bigg) + \frac{1}{2}\Bigg(-Q_{12}\frac{\partial^2 \mathrm{w}}{\partial \mathrm{r}^2} + Q_{22}\Bigg(-\frac{1}{r}\frac{\partial \mathrm{w}}{\partial \mathrm{r}} - \frac{1}{r^2}\frac{\partial^2 \mathrm{w}}{\partial \theta^2}\Bigg)\Bigg)\Bigg(-\frac{1}{r}\frac{\partial \mathrm{w}}{\partial \mathrm{r}} - \frac{1}{r^2}\frac{\partial^2 \mathrm{w}}{\partial \theta^2}\Bigg) + \frac{2Q_{66}}{r^4}\Bigg(-\frac{\partial^2 \mathrm{w}}{\partial \theta\, \partial \mathrm{r}}r + \frac{\partial \mathrm{w}}{\partial \theta}\Bigg)^2\Bigg) \tag{5.14}$$

$$L_2 = \Bigg(Q_{11}\Bigg(\frac{\partial \mathrm{u}}{\partial \mathrm{r}}\Bigg) + Q_{12}\Bigg(\frac{u}{r} + \frac{1}{r}\frac{\partial \mathrm{v}}{\partial \theta}\Bigg)\Bigg)\Bigg(\frac{\partial \mathrm{u}}{\partial \mathrm{r}}\Bigg) + \Bigg(Q_{12}\frac{\partial \mathrm{u}}{\partial \mathrm{r}} + Q_{22}\Bigg(\frac{u}{r} + \frac{1}{r}\frac{\partial \mathrm{v}}{\partial \theta}\Bigg)\Bigg)\Bigg(\frac{u}{r} + \frac{1}{r}\frac{\partial \mathrm{v}}{\partial \theta}\Bigg) \tag{5.15}$$

$$L_3 = Q_{66}\Bigg(r\frac{\partial \mathrm{v}}{\partial \mathrm{r}} + \frac{\partial \mathrm{u}}{\partial \theta} - v\Bigg)^2 \tag{5.16}$$

For the derivation of kinetic energy of rotating disc, body fixed frame is assumed, which rotates with the rotational speed of the disc. The velocity of a particle in the disc is given as follows [37]:

$$\frac{\partial \mathrm{r}}{\partial \mathrm{t}} = (\dot{\mathrm{u}}_\mathrm{r} - \Omega \mathrm{u}_\theta)\mathrm{e}_\mathrm{r} + [\dot{\mathrm{u}}_\theta + \Omega(\mathrm{r} + \mathrm{u}_\mathrm{r})]\mathrm{e}_\theta + \dot{\mathrm{u}}_\mathrm{z}\mathrm{e}_\mathrm{z} \tag{5.17}$$

where, $\mathrm{e}_\mathrm{r}, \mathrm{e}_\theta$ and e_z are the unit vectors on the body fixed frame in r, θ and z directions respectively. Ω is the angular velocity of the disc rotating about z axis.

The total kinetic energy of the rotating Stodola's disc is derived by integrating the kinetic energy of infinitesimal volume element (which is expressed using Equation (5.17)) over the entire domain of the non-linearly tapered disc. Hence, one gets:

$$\mathrm{T}_{rot} = \frac{1}{2}\rho \int_0^{2\pi} \int_{R_i}^{R_o} \int_{-\frac{c_1}{r^s}}^{\frac{c_1}{r^s}} \left(\frac{\partial \mathrm{u_r}}{\partial \mathrm{t}} - \Omega \mathrm{u_\theta}\right)^2 + \left(\frac{\partial \mathrm{u_\theta}}{\partial \mathrm{t}} + \Omega(\mathrm{r} + \mathrm{u_r})\right)^2 + \left(\frac{\partial \mathrm{u_z}}{\partial \mathrm{t}}\right)^2 r dz\, dr\, d\theta \tag{5.18}$$

Again, $\mathrm{c_1}$ is the constant defined by $\frac{t_i R_i^s}{2}$ and 's' is the taper parameter of Stodola's disc. R_i and R_o are the inner radius and the outer radius of the Stodola's disc.

Equation (5.18) can be rewritten as follows:

$$\mathrm{T}_{rot} = \frac{1}{2}\,\rho \int_0^{2\pi} \int_{R_i}^{R_o} \int_{-\frac{c_1}{2}}^{\frac{c_1}{2}} (T_1 + T_2 + T_3)\; r dz\, dr\, d\theta \tag{5.19}$$

where,

$$T_1 = \left(\frac{\partial \mathrm{u_r}}{\partial \mathrm{t}}\right)^2 + \left(\frac{\partial \mathrm{u_\theta}}{\partial \mathrm{t}}\right)^2 + \left(\frac{\partial \mathrm{u_z}}{\partial \mathrm{t}}\right)^2 \tag{5.20}$$

$$T_2 = -2\Omega \mathrm{u_\theta} \frac{\partial \mathrm{u_r}}{\partial \mathrm{t}} + 2\Omega(\mathrm{r} + \mathrm{u_r}) \frac{\partial \mathrm{u_\theta}}{\partial \mathrm{t}} \tag{5.21}$$

$$T_3 = \Omega^2 \mathrm{u_\theta^2} + \Omega^2 (r + \mathrm{u_r})^2 \tag{5.22}$$

Equation (5.20) represents the terms of the kinetic energy associated with the kinetic energy of stationary disc. Equation (5.21) shows the Coriolis terms, which are responsible for the gyroscopic effect. The final Equation (5.22) represents the terms that generate centrifugal forces, which are ultimately responsible for the centrifugal stiffening effect.

Again, after substituting Equation (5.1) into Equation (5.19) and integrating resultant equation with respect to the z-coordinate, total kinetic energy expression becomes:

$$\mathrm{T}_{rot} = \frac{1}{2}\int_0^{2\pi}\int_{R_i}^{R_o} \rho\,(D_1 c_1^3 r^{-3s} + D_2 c_1 r^{-s})\, r\,dr\,d\theta \tag{5.23}$$

where,

$$D_1 = \frac{2}{3r^2}\left(\left(r\frac{\partial^2 \mathrm{w}}{\partial \mathrm{t}\,\partial \mathrm{r}} - \Omega\frac{\partial \mathrm{w}}{\partial \theta}\right)^2 + \left(r\Omega\frac{\partial \mathrm{w}}{\partial \mathrm{r}} + \frac{\partial^2 \mathrm{w}}{\partial \theta\,\partial \mathrm{t}}\right)^2\right) \tag{5.24}$$

and

$$D_2 = 2\left(-\Omega v + \frac{\partial \mathrm{u}}{\partial \mathrm{t}}\right)^2 + 2\left(\Omega \mathrm{u} + \Omega \mathrm{r} + \frac{\partial v}{\partial \mathrm{t}}\right)^2 + 2\left(\frac{\partial \mathrm{w}}{\partial \mathrm{t}}\right)^2 \tag{5.25}$$

In Equation (5.25), terms multiplied with the square of rotating speed and contain no derivatives of displacements are centrifugal rotational terms. They modify the stiffness of the structure. The Coriolis terms are neglected in the present study.

5.3 Equations of motion

The presented dynamic system has three generalized coordinates and let then be the displacements of a point on the mid-plane surface of the disc. Hence, kinetic energy and strain energy derived in Section 5.2 can be described as the function of these generalized coordinates namely u, v and w. Equations (5.13) and (5.23) can be summarized as follows:

$$T_{rot} = T_{rot}(u, v, w, \dot{u}, \dot{v}, \dot{w}) \tag{5.26}$$

$$\Pi_{rot} = \Pi_{rot}(u, v, w) \tag{5.27}$$

Lagrangian functional for rotating Stodola's disc is written from above Equations (5.26) and (5.27), which is given below:

$$L = T_{rot} - \Pi_{rot} \tag{5.28}$$

It is clear from Equation (5.28) that Lagrangian functional for the considered dynamics problem depends on both the generalized coordinates and the generalized velocities.

$$L = L(u, v, w, \dot{u}, \dot{v}, \dot{w}) \tag{5.29}$$

Here, it should be noted that any suitable quantities can be used for generalized coordinates and hence the Hamilton formulation is invariant to the coordinate system used to express the Lagrangian.

Hamilton's principle states that the variation of integral of Lagrangian functional from time $t_1$to t_2 is zero if the variations of the displacements are zero at time t_1 and t_2.

$$I = \delta \int_{t_1}^{t_2} L(u, v, w, \dot{u}, \dot{v}, \dot{w}) dt = 0 \tag{5.30}$$

In other words, the motion of the system in given time interval will be such that the action integral in Equation (5.30) gets maximized or minimized.

Applying variational operator inside of Equation (5.30), the following equation is obtained.

$$\int_{t_1}^{t_2} \left[\left(\frac{\partial L}{\partial u} - \frac{d}{dt}\frac{\partial L}{\partial \dot{u}} \right) \delta u + \left(\frac{\partial L}{\partial v} - \frac{d}{dt}\frac{\partial L}{\partial \dot{v}} \right) \delta v + \left(\frac{\partial L}{\partial w} - \frac{d}{dt}\frac{\partial L}{\partial \dot{w}} \right) \delta w \right] dt = 0 \tag{5.31}$$

From Hamilton's principle, $\delta u(t_1) = \delta u(t_2) = 0,\ \delta v(t_1) = \delta v(t_2) = 0$ and $\delta w(t_1) = \delta w(t_2) = 0$. Integration by parts of Equation (5.31) gives the following three equations, known as Euler-Lagrange equations:

$$\frac{\partial L}{\partial u} - \frac{d}{dt}\frac{\partial L}{\partial \dot{u}} = 0 \tag{5.32}$$

$$\frac{\partial L}{\partial v} - \frac{d}{dt}\frac{\partial L}{\partial \dot{v}} = 0 \tag{5.33}$$

$$\frac{\partial L}{\partial w} - \frac{d}{dt}\frac{\partial L}{\partial \dot{w}} = 0 \tag{5.34}$$

In the present analysis, Equations of motion are derived using MAPLE by Euler-Lagrange equations. They are given below:

$$\begin{aligned}
&\rho\left(r^{1-s}\,\frac{d\Omega}{dt}\,v + 2r^{1-s}\Omega\frac{d\,v}{dt} - r^{1-s}\frac{\partial^2 \mathrm{u}}{\partial \mathrm{t}^2} + r^{1-s}\Omega^2 u + r^{2-s}\Omega^2\right) \\
&\qquad = -r^{-s}(1-s)Q_{11}\frac{\partial u}{\partial r} - r^{1-s}Q_{11}\frac{\partial^2 \mathrm{u}}{\partial \mathrm{r}^2} \\
&\qquad + ur^{-s-1}(Q_{22} + sQ_{12}) - Q_{66}r^{-s-1}\frac{\partial^2 \mathrm{u}}{\partial \theta^2} \\
&\qquad + r^{-s-1}\frac{\partial v}{\partial \theta}(Q_{22} + Q_{66} + sQ_{12}) - r^{-s}\frac{\partial^2 v}{\partial \theta \partial r}(Q_{66} \\
&\qquad + Q_{12})
\end{aligned} \tag{5.35}$$

$$\begin{aligned}
&\rho\left(-r^{1-s}\,\frac{d\Omega}{dt}\,(u+r) - 2r^{1-s}\Omega\frac{\partial u}{\partial t} - r^{1-s}\frac{\partial^2 v}{\partial \mathrm{t}^2} + r^{1-s}\Omega^2 v\right) \\
&\qquad = \; -Q_{22}r^{-s-1}\frac{\partial^2 v}{\partial \theta^2} - Q_{66}r^{-s}\frac{\partial v}{\partial r}(1-s) \\
&\qquad - r^{1-s}Q_{66}\frac{\partial^2 v}{\partial \mathrm{r}^2} - Q_{66}vr^{-s-1}s(s-1) \\
&\qquad - r^{-s-1}\frac{\partial u}{\partial \theta}(Q_{22} + (1-s)Q_{66}) - r^{-s}\frac{\partial^2 u}{\partial \theta\,\partial \mathrm{r}}(Q_{12} \\
&\qquad + Q_{66})
\end{aligned} \tag{5.36}$$

$$\rho\left(\frac{2}{3}r^{-3s}(1-3s)c_1^3\frac{\partial^3 w}{\partial \mathrm{t}^2\,\partial \mathrm{r}}+\frac{2}{3}r^{1-3s}c_1^3\frac{\partial^4 w}{\partial \mathrm{t}^2\,\partial \mathrm{r}^2}+2sr^{-1-3s}c_1^3\,\frac{d\Omega}{dt}\frac{\partial w}{\partial \theta}+4s\Omega c_1^3 r^{-1-3s}\frac{\partial^2 w}{\partial\theta\partial t}\right.$$

$$-\frac{2}{3}c_1^3\Omega^2 r^{-1-3s}\frac{\partial^2 w}{\partial\theta^2}-\frac{2}{3}c_1^3\Omega^2 r^{-3s}(1-3s)\frac{\partial w}{\partial r}-\frac{2}{3}c_1^3\Omega^2 r^{1-3s}\frac{\partial^2 w}{\partial \mathrm{r}^2}$$

$$\left.+\frac{2}{3}r^{1-3s}c_1^3\frac{\partial^4 w}{\partial \mathrm{t}^2\,\partial\theta^2}-2c_1 r^{1-s}\frac{\partial^2 w}{\partial \mathrm{t}^2}\right)$$

$$=-c_1 r^{-1-s}(Q_{12}+2Q_{66})\left(\frac{\partial w}{\partial\theta}\right)^2\frac{\partial^2 w}{\partial \mathrm{r}^2}--c_1 r^{-1-s}(Q_{12}+Q_{66})\left(\frac{\partial w}{\partial \mathrm{r}}\right)^2\frac{\partial^2 w}{\partial\theta^2}$$

$$-2Q_{66}c_1 r^{-s}\left(2\frac{\partial w}{\partial \mathrm{r}}\frac{\partial^2 w}{\partial\theta\partial r}\right)-2Q_{12}c_1 r^{-s}u\frac{\partial^2 w}{\partial \mathrm{r}^2}$$

$$+\ r^{-1-3s}c_1^3\left(6s^2Q_{11}-2Q_{12}-\frac{2}{3}Q_{22}-2Q_{11}\right)\frac{\partial^2 w}{\partial \mathrm{r}^2}-3Q_{11}c_1 r^{1-s}\left(\frac{\partial w}{\partial \mathrm{r}}\right)^2\frac{\partial^2 w}{\partial \mathrm{r}^2}$$

$$-sc_1^3 r^{-3-3s}\left(2.67Q_{12}+8Q_{66}+\frac{2.67}{s}Q_{66}\right)\frac{\partial^3 w}{\partial\theta^2\partial r}$$

$$+\ sc_1^3 r^{-3s}\left(\frac{1.33Q_{12}}{s}-4Q_{11}\right)\frac{\partial^3 w}{\partial \mathrm{r}^3}+Q_{66}(8s+2.67))\frac{\partial^2 w}{\partial\theta^2}+Q_{12}(\frac{1}{3}+s)\,)\frac{\partial w}{\partial \mathrm{r}}$$

$$+Q_{11}c_1 r^{-s}s(s-1)\ \ \left(\frac{\partial w}{\partial \mathrm{r}}\right)^3+\frac{2}{3}c_1^3 r^{-3-3s}(r^4\frac{\partial^4 w}{\partial \mathrm{r}^4}Q_{11}+Q_{22}\frac{\partial^4 w}{\partial\theta^4})$$

$$+c_1^3 r^{-1-3s}(2.67Q_{66}+1.33Q_{12})\frac{\partial^4 w}{\partial\theta^2\partial r^2} \tag{5.37}$$

Note that the presented linear in-plane Equations of motion namely Equations (5.35) and (5.36) are uncoupled with transverse deformation. This coupling is observed if the analysis is conducted considering non-linear Von-Karman strains. These non-linear Equations of motion based on non-linear Von-Karman strain-displacement relationships are given in Appendix B.

5.4 Bending mode vibrations of rotating Stodola's disc

The lowest out-of-plane mode for the rotating Stodola's disc is the transverse mode or it can be named as the bending mode. Transverse vibrations of the rotating Stodola's discs rotating about its axis at constant angular speed are studied. It is clear from the above equations of motion of the transverse vibration that they are not coupled with displacements of other two directions. Hence, the lowest bending mode can be treated independently. Higher out-of-plane modes are coupled in terms of displacements and can be grouped based on the nodal diameters (i.e. n equals to 1, 2...).

The circumferential symmetry of the circular Stodola's disc about the circumferential coordinate is considered. Mid-plane transverse direction displacement of the rotating Stodola's disc can be written in terms of the assumed shape functions, which is as follows:

$$w(r,\theta,\mathrm{t}) = W(r)\ \cos n\theta\ \sin \omega t \tag{5.38}$$

where, W represents the amplitude of vibration in transverse direction.

For the lowest bending mode ($n = 0$), let the amplitude be expressed by the following polynomial:

$$W(r) = \ n_z \sum_{i=1}^{I} C_i\ r^{i-1} \tag{5.39}$$

where I is the maximum number of terms in the polynomial. The constraint function n_z for the clamped-free annular disc in Equation (5.39) is $\frac{r}{R_0}$, which is multiplied with each term. This constraint function is necessary to impose necessary boundary condition to the disc. For the free-fixed boundary condition, it takes the form of $\frac{r}{R_0} - 1$.

5.4.1 Maximum strain energy and maximum kinetic energy for bending mode

Equation (5.38) is substituted in Equations (5.13) and (5.23) to derive maximum strain energy and maximum kinetic energy of the rotating disc. Hence, one gets:

$$(\Pi_{rot})_{max} = \int_0^{2\pi}\int_{R_i}^{R_o} c_1^3 r^{-1-3s}\left(\frac{1}{3}rQ_{11}\left(\frac{d^2W}{dr^2}\right)^2 + \frac{2}{3}Q_{12}\left(\frac{d^2W}{dr^2}\right)\left(\frac{dW}{dr}\right) + \frac{1}{3r}Q_{22}\left(\frac{dW}{dr}\right)^2\right) r\,dr\,d\theta \tag{5.40}$$

$$(\mathrm{T}_{rot})_{max} = \rho\, c_1 \int_0^{2\pi}\int_{R_i}^{R_o}\left(\frac{1}{3}r^{1-3s}c_1^2\Omega^2\left(\frac{dW}{dr}\right)^2 + \Omega^2\mathrm{r}^{3-\mathrm{s}} + \mathrm{r}^{1-\mathrm{s}}W^2\omega^2\right) r\,dr\,d\theta \tag{5.41}$$

Kinetic energy of rotating disc can be seen as the kinetic energy of stationary disc plus the kinetic energy due to rotational effect. Hence, they are maximized independently to get the maximum kinetic energy of the rotating Stodola's disc.

To maximize the energies, it should be noted that maximum values of $\sin^2 \omega t$ and $\cos^2 \omega t$ are considered while deriving Equations (5.40) and (5.41). In Equation (5.41), terms $\frac{1}{3}\rho\, r^{2-3s}c_1^3\Omega^2\left(\frac{dW}{dr}\right)^2$ and $\rho\, c_1\Omega^2\mathrm{r}^{3-\mathrm{s}}$ describe the work done in bending due to the centrifugal force generated due to rotational effect, hence these terms should be added to the maximum strain energy equation. This centrifugal effect generated due to rotation modifies the stiffness of structure. Based on this fact, Equations (5.40) and (5.41) are modified and rewritten as follows:

$$(\Pi_{rot})_{max}$$

$$= \int_0^{2\pi}\int_{R_i}^{R_o} c_1^3 r^{-1-3s}\left(\frac{1}{3}rQ_{11}\left(\frac{d^2W}{dr^2}\right)^2 + \frac{2}{3}Q_{12}\left(\frac{d^2W}{dr^2}\right)\left(\frac{dW}{dr}\right)\right. \tag{5.42}$$

$$\left. + \frac{1}{3r}Q_{22}\left(\frac{dW}{dr}\right)^2\right) + \frac{1}{3}\rho\, r^{2-3s}c_1^3\Omega^2\left(\frac{dW}{dr}\right)^2 + \rho\, c_1\Omega^2 \mathrm{r}^{3-\mathrm{s}}\, rdr\, d\theta$$

$$(\mathrm{T}_{rot})_{max} = \rho\, c_1 \int_0^{2\pi}\int_{R_i}^{R_o} (\mathrm{r}^{1-\mathrm{s}}W^2\omega^2)\, rdr\, d\theta \tag{5.43}$$

5.4.2 Solution using Rayleigh-Ritz method

Equation (5.42) shows that the maximum strain energy of the rotating disc for the lowest bending mode is independent of the shear modulus of the composite material.

As described in Section 2.3.3, Rayleigh's quotient is calculated by comparing maximum strain energy and maximum kinetic energy of the rotating Stodola's disc. From Equations (5.42) and (5.43):

$$(\Pi_{rot})_{max} = \omega^2(\mathrm{T}_{rot}{}^*)_{max} \tag{5.44}$$

$$(\mathrm{T}_{rot}{}^*)_{max} = \rho\, c_1 \int_0^{2\pi}\int_{R_i}^{R_o} \mathrm{r}^{1-\mathrm{s}}W^2\, rdr\, d\theta \tag{5.45}$$

$$\omega^2 = \frac{(\Pi_{rot})_{max}}{(\mathrm{T}_{rot}{}^*)_{max}} \tag{5.46}$$

The transverse direction amplitude that appears in Equation (5.38) can be approximated by taking a finite number of functions, which satisfy the geometric boundary conditions multiplied with the arbitrary coefficients as developed in Equation (5.39). As we are taking a finite number of terms in Equation (5.39), we are imposing certain limitations on representing possible transverse deformation shape of the disc. Hence, Equation (5.46) yields higher frequency than that of the exact solution. To make a better

approximation to estimate the natural frequency of the lowest bending mode, Rayleigh's quotient with respect to the arbitrary coefficients is minimized. Hence, one gets:

$$\frac{\partial \omega^2}{\partial C_i} = 0 \tag{5.47}$$

From Equations (5.46) and (5.47),

$$\frac{\partial (\Pi_{rot})_{max}}{\partial C_i} - \omega^2 \frac{\partial (\mathrm{T}_{rot}{}^{*})_{max}}{\partial C_i} = 0 \tag{5.48}$$

Equation (5.48) gives the set equations which are homogeneous and linear in $C_1, C_2, C_{3,}$ .... The number of equation obtained from Equation (5.48) is equal to the number of coefficients in Equation (5.39). These equations can be rewritten in the matrix form as follows:

$$([K] - \omega^2[M])[\{C_i\}] = 0 \tag{5.49}$$

where, $\{C_i\}$ is the column vector consisting of coefficients. To have non-zero solution, the determinant of augmented matrix, which consists of the coefficients $C_1, C_2, C_{3,}$ ...must be zero. MAPLE code is developed to calculate the bending mode natural frequency ($\omega_i, i = 1,2, ...$) of rotating Stodola's disc.

5.4.3 Solution using Finite element method (using ANSYS)

It is important to consider the pre-stressed effectes generated due to rotation of the Stodola's disc. It is believed that this effect modifies the overall stiffness of the structure. Hence, the pre-stressed modal analysis is performed from a linear based analysis. SOLID 186 elements are considered for the pre-stressed modal analysis. SOLID 186 element is a higher-order 3-D, 20-node element. It has quadratic

displacement behaviour and is well suited to model structures with irregular meshes. The element has three degrees of freedom at each node that are translation one. Moreover, the SOLID186 element has stress stiffening and large deflection capabilities.

Large deflection option is turned off during the simulation. The inclusion of large deflection effects means that ANSYS accounts for changes in the stiffness due to the change in the shape of the disc.

5.4.4 Example

Consider that the outer radius and the inner radius of Stodola's disc are 0.5m and 0.1m respectively. The inner thickness of the disc is 0.4m and taper parameter of Stodola's disc is taken as 0.861353(i.e. outer thickness of the disc becomes 0.1 m). Modulus of elasticity and Poisson's ratio for Structural Steel material are 200 GPa and 0.3 respectively. The clamped-free boundary condition is considered in the analysis. Consider that the disc is rotating at a constant angular speed of 100 rad/sec.

Four terms are considered in Equation (5.39). Comparison of the two solution methods explained in sub-sections 5.4.2 and 5.4.3 are given in Table 5.1 as follows:

Solution method	Lowest bending mode natural frequency f_3 (Hz)
RR solution	1195.6283
Finite element solution using ANSYS (f_3)	1194.1
% Difference	-0.128

Table 5.1: Comparison of lowest transverse mode natural frequency of Stodola's disc rotating at constant angular velocity of 100 rad/sec and beta value of 0.2

5.5 Parametric study

The effect of rotational speed on the lowest transverse mode natural frequency is studied. Note that the Stodola's disc of taper parameter value 0.861353 has an outer thickness of 0.1 m and hyperbolic thickness variation along the radial direction. Such a disc of taper parameter value 0.861353 can be considered as moderately thick disc and Kirchhoff hypothesis is expected to give closer results. Four number of terms are considered in the Rayleigh-Ritz polynomial for this disc of outer thickness value 0.1 m. Parametric study with respect to rotational speed is conducted and presented in Table 5.2 as follows:

5.5.1 Effect of rotational speed on lowest bending mode natural frequency

Rotational speed (Ω) in rad/sec	RR solution in Hz	Finite element solution in Hz (using ANSYS) (f_3)	% Difference
100	1195.6283	1194.1	-0.128
200	1195.8516	1194.3	-0.13
300	1196.2168	1194.6	-0.135
400	1196.7137	1195.0	-0.143
500	1197.3296	1195.6	-0.145
600	1198.0489	1196.2	-0.155
700	1198.8555	1197.0	-0.155
800	1199.7322	1197.9	-0.153
900	1200.6625	1198.9	-0.147
1000	1201.6304	1200.1	-0.128
1499	1206.5828	1207.5	0.076
2000	1211.0613	1217.8	0.553
2499	1214.7147	1230.7	1.3

Table 5.2: Variation of bending mode natural frequency with rotational speed for the isotropic Stodola's disc having radius ratio of 0.2

From above Table 5.2, it is concluded that effect of rotational speed on the natural frequency of the lowest transverse mode (i.e. bending mode) is not significant for the lower rotating speeds. As the gyroscopic couple is neglected in the present analysis, there are no forward-whirl and backword-whirl frequencies obtained. Hence, increase in the natural frequency with an increase in rotational speed is solely due to increasing the stiffness due to centrifugal forces. At higher rotating speed, the gyroscopic effect should be considered to accurately predict the critical speeds of rotating structures.

For orthotropic disc, material properties presented in Table 2.6 are considered. Geometry of Stodola's disc made of orthotropic material is considered to the same as that of isotropic Stodola's disc analysis presented in sub-section 5.5.1. The effect of rotational speed on lowest bending mode is studied. The following Table 5.3 shows the variation of f_4 (in ANSYS) of orthotropic Stodola's disc rotating at constant rotational speed for each case.

Rotational speed (Ω) in rad/sec	Rotational speed (Ω) in rpm	RR solution in Hz	Finite element solution in Hz (using ANSYS) (f_4)
100	954.93	665.7915	638.62
200	1909.86	666.1405	639.01
300	2864.79	666.6692	639.65
400	3819.72	667.3167	640.56
500	4774.65	668.0253	641.72
600	5729.58	668.7432	643.13
700	6684.51	669.4392	644.8
800	7639.44	670.0922	646.71
900	8594.37	670.6931	648.86
1000	9549.30	671.2411	651.25
1499	14314.40	673.3061	666.58

Table 5.3: Variation of bending mode natural frequency with rotational speed for the orthotropic Stodola's disc having radius ratio of 0.2

5.5.2 Effect of taper parameter on the lowest bending mode natural frequency

The following Figure 5.1 shows the variation of lowest bending mode natural frequencies of rotating Stodola's disc with taper parameters. Consider three values of taper parameters S1, S2 and S3 as 0.861353, 0.609423 and 0.430677 respectively. These values of taper parameters generate the Stodola's discs of outer thicknesses 0.1, 0.15 and 0.2 m respectively. Stodola's disc made of Structural Steel material is considered here. It is observed that the lowest bending mode natural frequency is inversely proportional to the taper parameter value of the disc.

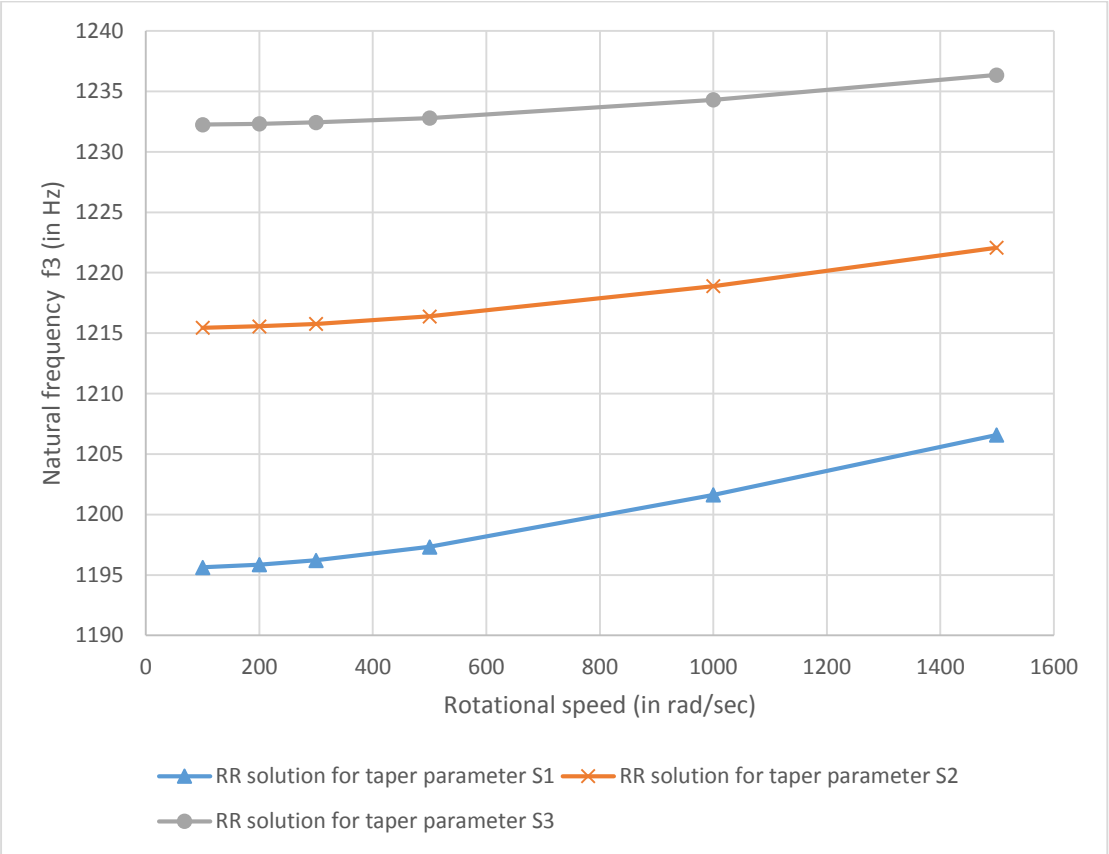

Figure 5.1: Variation of natural frequency f_3 of Stodola's disc with taper parameter and rotational speed for beta value of 0.2

It is not advisable to study the free vibration response of the discs with lower values of taper parameter using presented formulation as these generate considerable thickness

in the transverse direction. The ignorance of transverse shear deformation makes the present formulation inadequate for the thick discs. It is clear from Table 5.2 that, Rayleigh-Ritz solutions for rotating discs are in good agreement with the three-dimensional ANSYS solution.

5.5.3 Effect of degree of orthotropy on natural frequency

A parametric study based on the degree of orthotropy is conducted in this section. Degree of orthotropy ($\bar{n}$) can be defined as the ratio of Young's Modulus of material in radial direction to Young's Modulus in circumferential direction. The value of this ratio of taken from 0.1 to 10. Recall that the elements of material stiffness matrix consists of Equations (5.8) to (5.11):

$$Q_{ij} = \begin{bmatrix} \frac{E_1}{1-v_{12}v_{21}} & \frac{v_{21}E_1}{1-v_{12}v_{21}} & 0 \\ \frac{v_{21}E_1}{1-v_{12}v_{21}} & \frac{E_2}{1-v_{12}v_{21}} & 0 \\ 0 & 0 & G_{12} \end{bmatrix} \tag{5.50}$$

Upon simplifying,

$$Q_{ij} = \frac{E_1}{1-v_{12}v_{21}} \begin{bmatrix} 1 & v_{21} & 0 \\ v_{21} & \frac{E_2}{E_1} & 0 \\ 0 & 0 & \frac{G_{12}(1-v_{12}v_{21})}{E_1} \end{bmatrix} \tag{5.51}$$

Substituting $\frac{E_1}{E_2} = \bar{n}$ in above Equation (5.51), one gets:

$$Q_{ij} = \frac{E_1}{1-\bar{n}v_{21}^2} \begin{bmatrix} 1 & v_{21} & 0 \\ v_{21} & \frac{1}{\bar{n}} & 0 \\ 0 & 0 & \frac{G_{12}(1-\bar{n}v_{21}^2)}{E_1} \end{bmatrix} \tag{5.52}$$

The maximum energies given by Equations (5.42) and (5.43) are modified considering the stiffness elements of Equation (5.52). The variation of frequency factor $\Omega_{rot} = \omega \sqrt{\frac{\rho\,(1-\bar{n}v_{21}^2)}{E_1}}$ for the bending mode with the degree of orthotropy is studied. Consider the Stodola's disc having radius ratio of 0.2 and taper parameter value of 0.861353. To study the sole effect of degree of orthotropy on the lowest bending mode natural frequency, the rotational speed of Stodola's disc is kept at zero for this analysis. The following Figure (5.2) shows the stated behaviour of the disc.

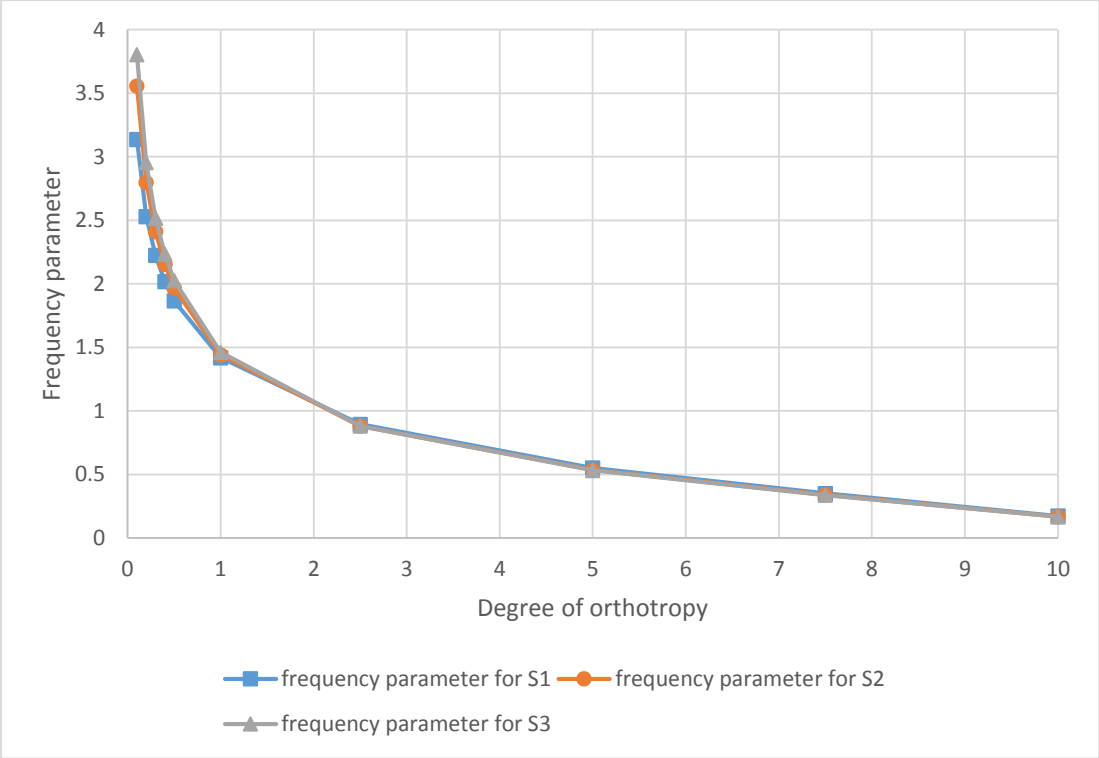

Figure 5.2: Variation of frequency parameter with the degree of orthotropy for Stodola's disc of beta value of 0.2 and v_{21} = 0.3

It is concluded from above Figure 5.2 that the bending mode natural frequency for each taper parameter of Stodola's disc decreases due to the decrease in bending stiffness with the degree of orthotropy.

5.6 Conclusion

In this Chapter, the effect of rotational speed on the lowest bending mode natural frequency is studied based on the linear analysis. Transverse shear effects have been neglected in the analysis to simplify the mathematical calculations. The clamped-free boundary condition has been considered throughout this Chapter. Rayleigh-Ritz method has been employed to calculate the lowest bending mode natural frequency. Moreover, the effect of degree of orthotropy on bending mode natural frequency is studied. A summary of observations is given next:

- Rayleigh's quotient for the rotating Stodola's disc is calculated for the first time considering the work done by centrifugal forces due to rotational effect. Accordingly, the total strain energy of the Stodola's disc was modified.
- Overall stiffness of the disc increases and as a result the bending mode natural frequency increases with the rotational speed.
- It is observed that at lower rotating speeds, the increase in the bending mode natural frequency is not significant.
- The bending mode natural frequency of rotating Stodola's disc decreases with increase of taper parameter of Stodola's disc.

Chapter 6 Conclusion and future work

6.1 Major Contributions

The major contributions of present study are as follow:

1) The free-vibration response of uniform thickness disc of clamped-free boundary condition made of orthotropic material is studied based on the three-dimensional elasticity theory.
2) Effect of damping on natural frequency of the uniform-thickness disc is studied considering the modal mass participation factor. This procedure leads to better prediction of damped natural frequency as it accounts for the variable nature of damping ratios as mode increases.
3) The novel numerical approach based on the classical Rayleigh-Ritz method with finite-element-like modification is developed to study the free vibration response of linearly-tapered discs and non-linearly tapered discs of clamped-free boundary condition and made of isotropic and orthotropic materials.
4) Transverse mode vibrations of rotating Stodola's disc are investigated using Rayleigh-Ritz method. Kirchoff hypothesis is considered to reduce the complexity of the problem. The Rayleigh-Ritz solution is validated with three-dimensional finite element solution. Moreover, the effect of rotational speed on the lowest bending mode natural frequency is studied for Stodola's disc of clamped-free boundary condition. The effect of degree of orthotropy on lowest bending mode natural frequency is presented for rotating Stodola's disc.
5) The effects of taper angle and taper parameter of linearly-tapered disc and non-linearly-tapered discs on lowest circumferential mode and bending mode natural frequencies are studied respectively.

6.2 Conclusions

The principal conclusions of the present study are as follow:

1) For the uniform-thickness disc made of Graphite-Polymer Composite material, the circumferential mode natural frequency only depends on the shear modulus of the material. Further, it is observed that circumferential mode natural frequency of circular disc is higher than that of the lowest bending mode natural frequency. This is because of the fact that the circumferential mode involves pure shearing and the sole component of displacement present is in the tangential direction of the disc middle surface. This concludes the higher stiffness of the disc in circumferential mode vibration compared to bending mode vibration. Furthermore, the spacing between these two frequencies is considerably less in the uniform thickness disc made of Graphite-Polymer composite material compared to the disc made of Structural Steel material.
2) It is concluded from the present study that the lowest bending mode natural frequency increases with Poisson's ratio. Natural frequencies of modes with one or higher nodal diameter number increase with Poisson's ratio. The circumferential mode natural frequency decreases slightly with increase in Poisson's ratio. This is because of reduction of shear modulus and subsequently due to the reduction of stiffness of the disc in circumferential direction.
3) The Rayleigh-Ritz method with finite-element-like modification allows the use of lower order polynomial to calculate the lowest in-plane mode and the lowest out-of-plane mode natural frequencies of linearly-tapered circular disc and Stodola's disc of clamped-free boundary condition.

4) For linearly-tapered disc of clamped-free boundary condition, the variation of lowest bending mode natural frequency is higher at higher radius ratios.
5) The lowest in-plane mode natural frequency increases with taper parameter of Stodola's disc. Whereas, the lowest bending mode natural frequency has parabolic variation with taper parameter of Stodola's disc of clamped-free boundary condition.
6) The natural frequencies of in-plane mode and out-of-plane mode vibrations increase with taper angle and radius ratio in the case of linearly-tapered isotropic or orthotropic disc of clamped-free boundary condition.
7) The lowest bending mode natural frequency of Stodola's disc of clamped-free boundary condition increases with the rotational speed because of the fact that stiffness of the structure increases due to the centrifugal forces generated due to rotation.
8) The effect of degree of orthotropy on the lowest bending mode natural frequency is significant at lower values of Young's modulus ratio of orthotropic material.

6.3 Future recommendations

1) The present work can be extended to study the forced vibration response of the stationary and rotating circular discs.
2) The present work is based on the consideration of linear strains. Von-Karman strain non-linearity can be considered for non-linear analysis.
3) Coriolis effect may be considered to predict the three-dimensional dynamic response of Stodola's disc rotating at high rotational speeds.
4) In practical applications, the thickness of rotating discs is much beyond the limits of thin plate theory. In such cases, FSDT (First order shear deformation theory) or higher order shear deformation theory can be considered to have better accuracy in determining free vibration response of moderately thick discs.

Appendix A

Non-linear equations of motion for orthotropic Stodola's disc rotating at constant speed are as follows:

$$\rho\left(r^{1-s}\,\frac{d\Omega}{dt}\,v + 2r^{1-s}\Omega\frac{d\,v}{dt} - r^{1-s}\frac{\partial^2 \mathrm{u}}{\partial \mathrm{t}^2} + r^{1-s}\Omega^2 u + r^{2-s}\Omega^2\right)$$

$$= -r^{-s}(1-s)Q_{11}\frac{\partial u}{\partial r} - r^{1-s}Q_{11}\frac{\partial^2 \mathrm{u}}{\partial \mathrm{r}^2}$$

$$+ ur^{-s-1}(Q_{22} + sQ_{12}) - Q_{66}r^{-s-1}\frac{\partial^2 \mathrm{u}}{\partial \theta^2}$$

$$- r^{-s-1}\frac{\partial w}{\partial \theta}\frac{\partial^2 \mathrm{w}}{\partial \theta \partial r}(Q_{66} + Q_{12})$$

$$- 2Q_{66}r^{-s-1}\frac{\partial w}{\partial \mathrm{r}}\frac{\partial^2 \mathrm{w}}{\partial \theta^2}$$

$$+ \frac{1}{2}r^{-s}\left(\frac{\partial w}{\partial \mathrm{r}}\right)^2(Q_{12} - (1-s)Q_{11})$$

$$- r^{1-s}Q_{11}\frac{\partial w}{\partial \mathrm{r}}\frac{\partial^2 \mathrm{w}}{\partial r^2}$$

$$+ \frac{1}{2}r^{-s-2}\left(\frac{\partial w}{\partial \theta}\right)^2(Q_{22} + (s+1)Q_{12})$$

$$+ r^{-s-1}\frac{\partial v}{\partial \theta}(Q_{22} + Q_{66} + sQ_{12})$$

$$- r^{-s}\frac{\partial^2 v}{\partial \theta \partial r}(Q_{66} + Q_{12})$$

$$\rho\left(-r^{1-s}\,\frac{d\Omega}{dt}\,(u+r)-2r^{1-s}\Omega\frac{\partial u}{\partial t}-r^{1-s}\frac{\partial^2 v}{\partial \mathrm{t}^2}+r^{1-s}\Omega^2 v\right)$$

$$=\;-Q_{22}r^{-s-1}\frac{\partial^2 v}{\partial \theta^2}-Q_{66}r^{-s}\frac{\partial v}{\partial r}(1-s)-r^{1-s}Q_{66}\frac{\partial^2 v}{\partial \mathrm{r}^2}$$

$$-Q_{66}vr^{-s-1}(s-1)-Q_{66}r^{-s-1}\frac{\partial w}{\partial r}\frac{\partial w}{\partial \theta}(1-s)-Q_{66}r^{-s}\frac{\partial w}{\partial \theta}\frac{\partial^2 w}{\partial \mathrm{r}^2}$$

$$-r^{-s}\frac{\partial w}{\partial r}\frac{\partial^2 w}{\partial \theta\,\partial r}(Q_{12}+Q_{66})-r^{-s-1}\frac{\partial u}{\partial \theta}(Q_{22}+(1-s)Q_{66})$$

$$-Q_{22}r^{-s-2}\frac{\partial w}{\partial \theta}\frac{\partial^2 w}{\partial \theta^2}-r^{-s}\frac{\partial^2 u}{\partial \theta\,\partial \mathrm{r}}(Q_{12}+Q_{66})$$

$$\rho\left(\frac{2}{3}r^{-3s}(1-3s)c_1^3\frac{\partial^3 w}{\partial t^2\,\partial r}+\frac{2}{3}r^{1-3s}c_1^3\frac{\partial^4 w}{\partial t^2\,\partial r^2}+2sr^{-1-3s}c_1^3\,\frac{d\Omega}{dt}\frac{\partial w}{\partial\theta}+4s\Omega c_1^3 r^{-1-3s}\frac{\partial^2 w}{\partial\theta\partial t}\right.$$

$$-\frac{2}{3}c_1^3\Omega^2 r^{-1-3s}\frac{\partial^2 w}{\partial\theta^2}-\frac{2}{3}c_1^3\Omega^2 r^{-3s}(1-3s)\frac{\partial w}{\partial r}-\frac{2}{3}c_1^3\Omega^2 r^{1-3s}\frac{\partial^2 w}{\partial r^2}$$

$$\left.+\frac{2}{3}r^{1-3s}c_1^3\frac{\partial^4 w}{\partial t^2\,\partial\theta^2}-2c_1 r^{1-s}\frac{\partial^2 w}{\partial t^2}\right)$$

$$=-c_1 r^{-1-s}(Q_{12}+2Q_{66})\left(\frac{\partial w}{\partial\theta}\right)^2\frac{\partial^2 w}{\partial r^2}--c_1 r^{-1-s}(Q_{12}+Q_{66})\left(\frac{\partial w}{\partial r}\right)^2\frac{\partial^2 w}{\partial\theta^2}$$

$$-2c_1 r^{-s}(Q_{12}+Q_{66})\frac{\partial w}{\partial r}\frac{\partial^2 v}{\partial\theta\partial r}-2Q_{66}c_1 r^{-s}\left(\frac{\partial w}{\partial\theta}\frac{\partial^2 v}{\partial r^2}+2\frac{\partial w}{\partial r}\frac{\partial^2 w}{\partial\theta\partial r}\right)$$

$$-2Q_{12}c_1 r^{-s}u\frac{\partial^2 w}{\partial r^2}-r^{-1-3s}c_1^3\left(\left(6s^2Q_{11}-2Q_{12}-\frac{2}{3}Q_{22}-2Q_{11}\right)\frac{\partial^2 w}{\partial r^2}\right)$$

$$-2Q_{12}c_1 r^{-s}\frac{\partial v}{\partial\theta}\frac{\partial^2 w}{\partial r^2}-2Q_{22}c_1 r^{-2-s}u\frac{\partial^2 w}{\partial\theta^2}-2Q_{22}c_1 r^{-s-2}\left(\frac{\partial w}{\partial\theta}\frac{\partial^2 v}{\partial\theta^2}+\frac{\partial v}{\partial\theta}\frac{\partial^2 w}{\partial\theta^2}\right)$$

$$-2Q_{11}c_1 r^{1-s}\left(\frac{\partial w}{\partial r}\frac{\partial^2 u}{\partial r^2}+\frac{\partial u}{\partial r}\frac{\partial^2 w}{\partial r^2}\right)-c_1 r^{-1-s}(Q_{12}+Q_{66})-2Q_{12}c_1 r^{-1-s}\frac{\partial u}{\partial r}\frac{\partial^2 w}{\partial\theta^2}$$

$$-2Q_{66}c_1 r^{-1-s}\left(\frac{\partial w}{\partial r}\frac{\partial^2 u}{\partial\theta^2}+2\frac{\partial u}{\partial\theta}\frac{\partial^2 w}{\partial\theta\partial r}-2v\frac{\partial^2 w}{\partial\theta\partial r}\right)3Q_{22}c_1 r^{-3-s}\left(\frac{\partial w}{\partial\theta}\right)^2\frac{\partial^2 w}{\partial\theta^2}$$

$$-3Q_{11}c_1 r^{1-s}\left(\frac{\partial w}{\partial r}\right)^2\frac{\partial^2 w}{\partial r^2}-sc_1^3 r^{-3-3s}\left(2.67Q_{12}+8Q_{66}+\frac{2.67}{s}Q_{66}\right)\frac{\partial^3 w}{\partial\theta^2\partial r}$$

$$+sc_1^3 r^{-3s}\left(\frac{1.33Q_{12}}{s}-4Q_{11}\right)\frac{\partial^3 w}{\partial r^3}$$

$$+c_1^3 r^{-3-3s}\left(Q_{12}(6s^2+6s+1.33)+Q_{22}(2s+1.33)+Q_{66}(8s+2.67)\right)\frac{\partial^2 w}{\partial\theta^2}$$

$$-(8Q_{66}+4Q_{12})c_1 r^{-1-s}\frac{\partial^2 w}{\partial\theta\partial r}\frac{\partial w}{\partial r}\frac{\partial w}{\partial\theta}+c_1 r^{-2-s}(s+1)(Q_{12}+2Q_{66})\frac{\partial w}{\partial r}\left(\frac{\partial w}{\partial\theta}\right)^2$$

$$+2Q_{66}c_1(1+s)r^{-1-s}\frac{\partial w}{\partial\theta}\frac{\partial v}{\partial r}+2c_1 r^{-1-s}(sQ_{12}+Q_{66})\frac{\partial v}{\partial\theta}\frac{\partial w}{\partial r}$$

$$+2c_1 r^{-s}(Q_{11}(s-1)-Q_{12})\frac{\partial u}{\partial r}\frac{\partial w}{\partial r}+2c_1 r^{-2-s}(Q_{66}(s+1)-Q_{22})\frac{\partial w}{\partial\theta}\frac{\partial u}{\partial\theta}$$

$$-\ 2Q_{66}c_1 r^{-2-s}(1+s)v\frac{\partial w}{\partial\theta}+2c_1^3 r^{-2-3s}(Q_{12}\left(\frac{r^{2s+1}}{c_1^2}su+s+3s^2\right)+Q_{12}(\frac{1}{3}$$

$$+s)\,)\frac{\partial w}{\partial r}+Q_{11}c_1 r^{-s}s(s-1)\left(\frac{\partial w}{\partial r}\right)^3+\frac{2}{3}c_1^3 r^{-3-3s}(r^4\frac{\partial^4 w}{\partial r^4}Q_{11}+Q_{22}\frac{\partial^4 w}{\partial\theta^4})$$

$$+c_1^3 r^{-1-3s}(2.67Q_{66}+\ 1.33Q_{12})\frac{\partial^4 w}{\partial\theta^2\partial r^2}$$

Appendix B

- Three-dimensional Rayleigh-Ritz solution for the uniform-thickness disc of clamped-free boundary condition is presented in Chapter 2. Presented results are validated by comparing them to the Rayleigh-Ritz solution obtained using series comprising of orthogonally-generated polynomial functions derived by Kim and Dickinson [22] and the 2D exact solution [46].

  In this example, the uniform-thickness disc of clamped-free boundary condition made of Structural Steel material is considered. The values for Young's modulus and Poisson's ratio are considered as 200 GPa and 0.3 respectively for this material. Density is considered as 7850 kg/m^3. Beta value of the disc is considered as 0.1, which is the ratio of inner radius to outer radius of the disc. Thickness of the disc is taken as 0.15 m. The inner radius and outer radius of the circular annular disc are taken as 0.2 m and 2 m. The following Table B.1 shows the comparison of presented results with Rayleigh-Ritz solution obtained using series comprising of orthogonally-generated polynomial functions derived by Kim and Dickinson.

Solution method	Beta value	Numbers of nodal diameter and nodal circle (n, s)				
		(0,0)	(1,0)	(2,0)	(3,0)	(4,0)
Present	0.1	41.2609	30.1554	48.7213	110.6195	193.5625
polynomial		$I = Q = 3$, $J = P = 4$	$I = K = Q = 4$ and $J = L = P = 2$			
Kim & Dickinson [22]		38.6330	31.7256	51.2819	113.5071	199.064
2D Exact [46]		38.5619	28.6252	51.2336	113.0421	-
Polynomial	0.5	$I = Q = 3$, $J = P = 3$	$I = J = K = L = P = Q = 3$			
Present		119.1250	125.5368	136.4365	168.4583	229.4701
Kim & Dickinson [22]		118.7307	121.1556	134.046	169.2168	233.3408
2D Exact [46]		118.5119	121.2468	134.0096	168.6512	-

Table B. 1: Comparison of natural frequencies of uniform-thickness annular C-F disc

In above Table B.1, (n, s) represents the nodal diameter number and nodal circle number respectively. For zero nodal diameter number and zero nodal circle value, the results are compared with that of literature for the lowest transverse mode vibration. The boundary condition taken at inner radius is clamped and at outer radius the boundary condition considered is free. It is shown that the presented data are in good agreement with the 2D exact solutions for natural frequencies of transversely vibrating uniform annular plates derived using Bessel's functions by Vogel and Skinner [46]. Three-dimensional Rayleigh-Ritz solution for clamped-free circular annular disc, presented in this thesis may be useful to validate the results obtained using 2-D plate theories.

- The natural frequency results obtained using Rayleigh-Ritz method with finite-element-like modification are presented in Chapter 3. Validation is conducted by comparing the natural frequencies of linearly-tapered disc of small taper angle with that of uniform-thickness disc of comparable thickness.

Consider the linearly-tapered disc of clamped-free boundary condition and made of the same material as that of the uniform-thickness disc, considered for the validation in above Table B.1. The linearly-tapered disc with small taper angle of 0.1592 degree is considered with beta value of 0.1. This way, outer thickness of the linearly-tapered disc becomes 0.14 m. Thicknesses of uniform-thickness disc are considered as 0.15 m and 0.14 m.

The following Table B.2 shows the comparison of natural frequency results of linearly-tapered disc with small taper angle with the results of uniform-thickness circular annular disc of clamped-free boundary condition.

Mode type	Linearly-tapered disc with taper angle of 0.1592 degree ($h_i = 0.14$)	Number of divisions	Uniform-thickness disc of $h = 0.15$	Uniform-thickness disc of $h = 0.14$
Lowest circumferential mode natural frequency (in Hz)	72.9074 $K = L = 1$	5	71.4508 $K = L = 4$	74.3620 $K = L = 4$
Lowest bending mode natural frequency (in Hz)	39.8818 $I = J = 2,$ $P = Q = 2$	61	41.2609 $I = Q = 3,$ $J = P = 4$	38.6090 $I = Q = 3,$ $J = P = 4$

Table B. 2: Comparison of natural frequencies of linearly-tapered annular C-F disc

From above Table B.2, it is concluded that the natural frequencies of the lowest in-plane mode and the lowest out-of-plane mode vibration changes slightly with small taper angle. Here, for the disc with thicknesses 0.14 m and 0.15 m, it is observed that the circumferential mode natural frequency is higher than that of the frequency of vibration in lowest bending mode.

Appendix C

- The selection of number of divisions considered in Chapter 3 to calculate natural frequencies of in-plane and out-of-plane vibration modes of linearly-tapered disc is described below:

  Results presented in Figure 3.3, Figure 3.6, Figure 3.8, Table 3.1, Table 3.2 and Table 3.3 are calculated considering the following number of divisions and the order of polynomial.

Results	Mode type	Beta value	Number of divisions	Order of polynomial
Figure 3.3	In-plane	0.2	5	$K = L = 1$
		0.25	3	
		0.3	2	
Figure 3.6	Out-of-plane	0.2	3	$I = Q = 1$ and $J = P = 2$
		0.25	2	
Figure 3.8	In-plane	0.2	5	$K = L = 1$
		0.25	3	
		0.3	2	
Table 3.1	Out-of-plane	0.2	6	$I = Q = 1$ and $J = P = 2$
Table 3.2	Out-of-plane	0.25	4	
Table 3.3	Out-of-plane	0.3	3	

Table C. 3: Selection of number of divisions to calculate the natural frequencies of linearly-tapered disc

- The selection of number of divisions considered in Chapter 4 to calculate natural frequencies of in-plane and out-of-plane vibration modes of Stodola's disc is as follows:

  Results presented in Table 4.1 and Table 4.2 are calculated considering the following number of divisions and the order of polynomial.

Results	Mode type	Beta value	Taper parameter	Number of divisions	Order of polynomial
Table 4.1	In-plane	0.2	-	4	$K = L = 1$
Table 4.2	Out-of-plane	0.2	0.861353	3	$I = Q = 2$ and $J = P = 2$
			0.609423	2	
			0.430677	2	
			0.29203	2	
			0.178747	2	

Table C. 4: Selection of number of divisions to calculate the natural frequencies of Stodola's disc

Bibliography

[1] J. Obuchowski, A. Wylomanska, and R. Zimroz, "Vibration Engineering and Technology of Machinery," *Mech. Mach. Sci.*, vol. 23, pp. 401–410, 2015.

[2] D. J. Thompson and C. J. C. Jones, "A Review of the Modelling of Wheel/Rail Noise Generation," *J. Sound Vib.*, vol. 231, no. 3, pp. 519–536, 2000.

[3] "http://www.walter-tools.com/en-gb/industry_solutions/aerospace/engine/pages/turbine_disk.aspx." .

[4] "https://www.performanceonline.com/1937-42-ford-car-disc-brake-conversion-kits/." .

[5] W. Weaver, S. P. Timoshenko, and D. H. Young, *Vibration Problems in Engineering*. John Wiley & Sons, 1990.

[6] A. Love, *A treatise on the Mathematical Theory of Elasticity*. New York: Dover Publications, 1944.

[7] H. Deresiewicz and R. Mindlin, "Axially symmetric flexural vibrations of a circular disk," *Am. Soc. Mech. Eng. J. Appl. Mech.*, vol. 22, pp. 86–88, 1955.

[8] V. Kunukkasseril and S. Venkatesan, "Free Vibration of Layered Circular Plates," *J. Sound Vib.*, vol. 60, no. 4, pp. 511–534, 1978.

[9] P. Guruswamy and T. Y. Yang, "A sector finite element for dynamic analysis of thick plates," *J. Sound Vib.*, vol. 62, no. 4, pp. 505–516, 1979.

[10] T. Irie, G. Yamada, and K. Takagi, "Natural Frequencies of Thick Annular Plates," *J. Appl. Mech.*, vol. 49, no. September 1982, pp. 633–638, 2016.

[11] K. M. Liew, Y. Xiang, C. M. Wang, and S. Kitipornchai, "Flexural Vibration of Shear Deformable Circular and Annular Plates on Ring Supports," *Comput. Methods Appl.*

Mech. Eng., vol. 110, pp. 301–315, 1993.

[12] J. So and A. W. Leissa, "Three-Dimensional Vibrations of Thick Circular and Annular Plates," *J. Sound Vib.*, vol. 209, no. 1, pp. 15–41, 1998.

[13] J. Kang, "Free vibration analysis of shallow spherical dome by three-dimensional Ritz method," *J. Vib. Control*, pp. 1–14, 2014.

[14] D. Zhou, F. T. K. Au, Y. K. Cheung, and S. H. Lo, "Three-dimensional vibration analysis of circular and annular plates via the Chebyshev–Ritz method," *Int. J. Solids Struct.*, vol. 40, no. 12, pp. 3089–3105, 2003.

[15] C. Il Park, "Frequency Equation for the In-plane Vibration of a Clamped Circular Plate," *J. Sound Vib.*, vol. 313, no. 1–2, pp. 325–333, 2008.

[16] S. Bashmal, R. Bhat, and S. Rakheja, "In-plane free vibration analysis of an annular disk with point elastic support," *Shock Vib.*, vol. 18, pp. 627–640, 2011.

[17] S. Bashmal, R. Bhat, and S. Rakheja, "In-plane free vibration of circular annular disks," *J. Sound Vib.*, vol. 322, no. 1–2, pp. 216–226, 2009.

[18] C. H. Huang and Y. . Chen, "Vibration Analysis for Piezoceramic Circular Plates with V-Notches Part 1:Theory," *J. Mech.*, vol. 30, no. 6, pp. 603–609, 2014.

[19] C. Sridhar and K. P. Rao, "Large Deformation Finite Element Analysis of Laminated Circular Composite plates," *Comput. Struct.*, vol. 54, no. 1, pp. 59–64, 1995.

[20] K. Gupta, S. . Singh, V. Tiwari, S. Takkar, R. Dev, and A. Rai, "Vibration Analysis of Fiber Reinforced Composite Discs," in *9th IFToMM International Conference on Rotor Dynamics, Mechanisms and Machine Science*, 2015, vol. 21, no. July, pp. 1665–1675.

[21] Q. Wang, D. Shi, Q. Liang, and F. Ahad, “A Unified Solution for Free In-plane Vibration of Orthotropic Circular, Annular and Sector Plates with General Boundary Conditions,” *Appl. Math. Model.*, vol. 40, pp. 9228–9253, 2016.

[22] C. S. Kim and S. M. Dickinson, “On the Lateral Vibration of Thin Annular and Circular Composite Plates Subject to Certain Complicating Effects,” *J. Sound Vib.*, vol. 130, no. 3, pp. 363–377, 1989.

[23] C. Prasad, R. K. Jain, and S. R. Soni, “Axisymmetric vibrations of circular plates of linearly varying thickness,” *J. Appl. Math. Phys.*, vol. 23, no. 6, pp. 941–948, 1972.

[24] U. S. Gupta and R. LaL, “Vibrations and Buckling of Parabolically Tapered Circular Plates,” *Indian J.ournal pure Appl. Math.*, vol. 10, no. 3, pp. 347–356, 1979.

[25] S. R. Soni and C. L. Amba-rao, “Axisymmetric Vibrations of Annular Plates of Variable Thickness,” *J. Sound Vib.*, vol. 38, no. 4, pp. 465–473, 1975.

[26] J. Kirkhope and G. J. Wilson, “Vibration and stress analysis of thin rotating discs using annular finite elements,” *J. Sound Vib.*, vol. 44, no. 4, pp. 461–474, 1976.

[27] C. A. Mota Soares and M. Petyt, “Finite Element Dynamic Analysis of Practical Discs,” *J. Sound Vib.*, vol. 61, no. 4, pp. 547–560, 1978.

[28] T. A. Lenox and H. D. Conway, “An exact, closed form, solution for the flexural vibration of a thin annular plate having a parabolic thickness variation,” *J. Sound Vib.*, vol. 68, no. 2, pp. 231–239, 1980.

[29] J. N. Reddy and C. L. Haung, “Nonlinear axisymmetric bending of annular plates with varying thickness,” *Int. J. Solids Struct.*, vol. 17, no. 8, pp. 811–825, 1981.

[30] B. Singh and V. Saxena, “Axisymmetric Vibration of a Circular Plate with Double Linear Variable Thickness,” *J. Sound Vib.*, vol. 179, no. 5, pp. 879–897, 1995.

[31] W. H. Duan, S. T. Quek, and Q. Wang, “Generalized hypergeometric function solutions for transverse vibration of a class of non-uniform annular plates,” *J. Sound Vib.*, vol. 287, no. 4–5, pp. 785–807, 2005.

[32] U. S. Gupta, R. Lal, and S. Sharma, “Vibration analysis of non-homogeneous circular plate of nonlinear thickness variation by differential quadrature method,” *J. Sound Vib.*, vol. 298, no. 4–5, pp. 892–906, 2006.

[33] D. Sheen and K. . Viswanathan, “Free Vibration of Layered Circular Cylindrical Shells of Variable Thickness Using Spline Function Approximation,” *Indian J. Eng. Mater. Sci.*, vol. 16, no. December, pp. 433–448, 2009.

[34] H. Lamb and R. V. Southwell, “The Vibrations of a Spinning Disk,” *Proc. R. Soc. London*, vol. 99, no. 699, pp. 272–280, 2016.

[35] J. Nowinski, “Nonlinear Transverse Vibrations of a Spinning Disk,” *Trans. ASME*, pp. 72–78, 1964.

[36] Y. C. S. Barasch, “On the Vibration of a Rotating Disk,” *Am. Soc. Mech. Eng. Appl. Mech.*, vol. 39, pp. 1143–1144, 1972.

[37] N. Baddour, “A Modelling and Vibration Analysis of Spinning Disks,” University of Toronto, 2001.

[38] A. Khoshnood and M. A. Jalali, “Normal oscillatory modes of rotating orthotropic disks,” *J. Sound Vib.*, vol. 314, no. 1–2, pp. 147–160, 2008.

[39] H. R. Hamidzadeh, “In-plane free vibration and stability of rotating annular discs,” *Proc. Inst. Mech. Eng. Part K J. Multi-body Dyn.*, vol. 216, no. 4, pp. 371–380, 2002.

[40] S. Dousti and M. Abbas Jalali, “In-Plane and Transverse Eigenmodes of High-Speed Rotating Composite Disks,” *J. Appl. Mech.*, vol. 80, no. 011019, pp. 1–7, 2012.

[41] ANSYS Inc., “ANSYS Mechanical APDL Element Reference,” 2013.

[42] I. Chowdhury and S. P. Dasgupta, “Computation of Rayleigh Damping Coefficients for Large Systems,” *Electron. J. Geotech. Eng.*, vol. 8, no. 0, 2003.

[43] M. Hyer, “Stress analysis of fiber-reinforced composite materials.” 1998.

[44] S. S. Rao, *The Finite Element Method in Engineering*, Third Edit. Butterworth-Heinemann publications, 1999.

[45] “http://www.geaviation.com/commercial/engines/genx/.” .

[46] S. M. Vogel and D. W. Skinner, “Natural Frequencies of Transversely Vibrating Uniform Annular Plates,” *J. Appl. Mech.*, no. 2010, pp. 926–931, 1965.